INFORMATION TO USERS

This manuscript has been reproduced from the microfilm master. UMI films the text directly from the original or copy submitted. Thus, some thesis and dissertation copies are in typewriter face, while others may be from any type of computer printer.

The quality of this reproduction is dependent upon the quality of the copy submitted. Broken or indistinct print, colored or poor quality illustrations and photographs, print bleedthrough, substandard margins, and improper alignment can adversely affect reproduction.

In the unlikely event that the author did not send UMI a complete manuscript and there are missing pages, these will be noted. Also, if unauthorized copyright material had to be removed, a note will indicate the deletion.

Oversize materials (e.g., maps, drawings, charts) are reproduced by sectioning the original, beginning at the upper left-hand corner and continuing from left to right in equal sections with small overlaps. Each original is also photographed in one exposure and is included in reduced form at the back of the book.

Photographs included in the original manuscript have been reproduced xerographically in this copy. Higher quality 6" x 9" black and white photographic prints are available for any photographs or illustrations appearing in this copy for an additional charge. Contact UMI directly to order.

UMI

A Bell & Howell Information Company
300 North Zeeb Road, Ann Arbor MI 48106-1346 USA
313/761-4700 800/521-0600

GLOBAL MICROMOTION OF NONCEMENTED COMPONENTS USED IN TOTAL HIP ARTHROPLASTY

by

Frank Charles Barich

A thesis submitted in partial fulfillment of the requirements for the
Doctor of Philosophy
degree in Biomedical Engineering
in the Graduate College of
The University of Iowa

May 1998

Thesis supervisor: Professor Thomas D. Brown

Graduate College
The University of Iowa
Iowa City, Iowa

CERTIFICATE OF APPROVAL

PH.D. THESIS

This is to certify that the Ph.D. thesis of

Frank Charles Barich

has been approved by the Examining Committee for the thesis requirement for the Doctor of Philosophy degree in Biomedical Engineering at the May 1998 graduation.

Thesis committee:

Thesis supervisor

Member

Member

Member

Member

To my wife Mara whose encouragement, strength, and eye on the big picture enabled me to complete this project.

"A little Consideration, a little Thought for Others, makes all the difference."

A. A. Milne

ACKNOWLEDGMENTS

I would like to acknowledge Drs. Thomas D. Brown and John J. Callaghan whose efforts provided the genesis of this project. I also want to thank Dr. Richard A. Brand and Prof. James G. Andrews for their unwavering support and encouragement.

I am grateful for the financial support, acetabulum prostheses and surgical equipment provided by DePuy, Inc. and for the femoral prostheses and surgical equipment provided by BIOMET, Inc. I am also grateful for institutional support of the Department of Orthopaedic Surgery.

I would also like to thank my fellow students from the University of Iowa Orthopaedics Biomechanics Laboratory for their friendship and support - especially Jim Rudert, Rhonda Aper, Scott Shaver, Scott Steffensmeier, Jason Otto, Michael Bottlang, Christian Puttlitz- and Doug Adams.

I must also recognize my sons Devin, Peter, and Colin. Thanks for understanding when dad had to go back into the lab and for the smiles and hugs when he came home.

ABSTRACT

Short term results of cemented total hip arthroplasty are very good. However, long term results remain less successful. Noncemented prostheses indicate biological fixation may provide the solution to long term clinical difficulties. Prediction of clinical performance of noncemented prostheses rests in part in predicting bone ingrowth. Prediction of bone ingrowth from *in vitro* tests requires two criteria be met: First, apply three-dimensional load patterns that adequately match the load patterns observed *in vivo*, and second determine three-dimensional micromotion over the entire surface of the porous-coated region of the prosthesis. In an attempt to better understand *in vivo* processes and predict bone ingrowth, testing procedures were developed for both the femur and the acetabulum to simulate hip loading for level walking and stair climbing, and to determine the relative motion between the prosthesis and bone over the entire prosthesis during these activities. The procedures were then employed to study various fixation techniques for both femoral and acetabular components. Present data suggest that to achieve sufficient fixation conducive to bone ingrowth in the porous-coated region for the femoral prosthesis studied, a tight proximal fit must be achieved. The quality of distal fit exhibited minimal effect on the stability of the femoral prosthesis. The acetabular data indicate that two central screws are the best configuration for cup stability.

TABLE OF CONTENTS

LIST OF TABLES

LIST OF FIGURES

CHAPTER 1

INTRODUCTION

The aims of total hip arthroplasty (THA) are to relieve pain, correct deformity, and reduce disability. Cemented arthroplasties have been very successful in the short and intermediate term. However, long term clinical results (greater than eight years) have been substantially worse. This has led to a great deal of research aimed at improving long term performance.

Clinical success of THA increased greatly with the introduction of low friction components and cemented fixation by Sir John Charnley in the late 1950's. Fixation of most prostheses used prior to that time was achieved by interference fit. Charnley (1960) proposed the use of an acrylic cement to increase the contact area, hence providing better load transfer between the prosthesis and the bone. Success of cement fixation was far superior to that of earlier techniques, and for the next twenty years polymethylmethacrylate (PMMA) was used almost exclusively for THA component fixation.

Even with the use of cement fixation, long term results have been less than optimal. Failure of THA is generally defined by radiographic loosening or by revision. Radiographic evaluation is based on the amount of radiolucency around a component and/or component migration (DeLee and Charnley, 1976; Engh et al., 1990b; Gruen et al., 1979; Harris et al., 1982). Femoral radiographic loosening rates are generally less than 10% during the first eight years (Engh et al., 1990b; Schulte et al., 1993; Sugano et al., 1995). After ten years the femoral radiographic loosening rate ranges from 20% to 40% (Beckenbaugh and Ilstrup, 1978; Nuemann et al., 1994; Ranawat et al., 1984; Rockborn

and Olsson, 1993, Schulte et al., 1993; Sutherland et al., 1982; Stauffer, 1982, Wroblewski, 1986). Acetabular radiographic loosening rates are comparable to those of femoral components, with long-term rates ranging from 13% to 30% (Nuemann et al., 1994, Ranawat et al., 1984, Schulte et al., 1993, Sugano et al., 1995, Sutherland et al., 1982, Stauffer, 1982, Wroblewski, 1986).

While radiographic loosening rates are high, some investigators use revision as the end point to determine the success of THA. Because radiographic loosening does not always indicate the need for revision surgery (Neumann et al., 1993; Nilsson et al., 1993), reported revision rates (due to either component loosening) are lower than radiographic loosening rates. Ranawat (1984) reported a 10% revision rate and Sutherland (1982) only 7.4% after ten years. Reported twenty year rates are less than 11% (Schulte et al., 1993; Neumann et al., 1993).

As the success of cemented THA increased and its clinical application spread, the procedure was extended to younger and more active patients, which heightened demands for improved long-term performance. Generally, both radiographic and revision results are worse for young patients (Johnsson et al., 1993; Morscher, 1992). In a five-year follow-up study, Chandler et al. (1981) reported radiographic loosening for at least one component in 57% of patients under thirty years of age. For patients under twenty years of age, Torchia et al. (1997) reported radiographic loosening of 20% for femoral components and 60% for acetabular components after 15 years. Revision rates (for either component) of 9% at seven years and 25% at twenty years have been reported by Collis (1984) and Joshi et al. (1992), respectively. In a sixteen to twenty-two year study, Sullivan et al. (1994) observed a better revision rate of 2% for femoral components and 13% for acetabular components.

The need to improve long-term clinical results led to the development of improved cementing techniques. These began with the use of intramedullary plugs and cement guns to provide pressurization of the cement, the so-called second generation techniques. They were followed by centrifugation or vacuum mixing, irrigation and drying of the intramedullary canal, and improved prosthesis designs, the so-called third generation techniques (Mohler et al., 1995). These new techniques have reduced both radiographic loosening and revision rates in studies from five to seven years for femoral components (Goetz et al., 1994; Oishi et al., 1994; Russotti et al., 1988; Dall et al., 1992; Cornell and Ranawat, 1986; Harris and Maloney, 1989; Mohler et al., 1995). A recent study by Madey et al. (1997) reported only a 5% revision rate due to aseptic loosening of either the femoral or acetabular component after a minimum follow up of fifteen years. Improved cementing techniques have not been successful for all patient types. Mohler et al. (1995) reported debonding of 29 femoral components at an average of five years after surgery for heavy (87 kg) and active (level 4 of definition by Johnson et al., 1990) patients. For patients under 30 years of age with juvenile rheumatoid arthritis, Chmell et al. (1997) reported a femoral revision rate of 18% after 13 years, and an acetabular revision rate of 35% after 12 years. In addition, studies by Mulroy and Harris (1990) and Ballard et al. (1994) indicate that improved cementing techniques do not have as much of an effect on acetabular components as on femoral components.

With increasing recognition of long-term failure rates, and despite the promise of improved cementing techniques, investigators presumed that elimination of cement in favor of fixation of prostheses directly to bone (i.e. "biological fixation") might provide more durable implant constructs. Biological fixation (where stability of the implant is due to tissue growth into the surface of the prosthesis) results in a bone-to-prosthesis interface that is self-maintaining and that theoretically could eliminate prosthesis

loosening for the lifetime of the patient. In contrast, the passive nature of cement fixation and inherent mechanical drawbacks of PMMA (e.g. brittleness and low fatigue strength - Engh and Bobyn, 1985) suggest the duration of successful cement fixation is independent of the patient's lifespan.

Clinical results of biological fixation of noncemented components with metallic porous coatings have been promising. The remarkable long-term results reported by Engh et al. (1994), a 1.5% revision rate for femoral stems and a 2.2% rate for acetabular cups at 15 years, are as good as the results of any other type of fixation method (a second acetabulum design in this study had a 7.5% revision rate). Other shorter term studies also show acceptable loosening rates (Boehler et al., 1993; Callaghan et al., 1988; Havelin et al., 1994; Heekin et al., 1993; Kim and Kim, 1992; Martell et al., 1993; Mont et al., 1993). Two more recent studies both reported no revisions of porous-coated acetabular components fixed with screws at a follow-up of 5-10 years (Latimer and Lachiewicz, 1996; Tompkins et al., 1997). Attempting to improve on noncemented performance several investigators have coated components with hydroxyapatite. Results of these studies show that hydroxyapatite coatings may increase bone ingrowth (Dalton et al., 1995; Tisdel et al., 1994). However, the short-term clinical results have not shown any difference between porous-coated components and those with an additional hydroxyapatite coating (D'Antonio et al., 1996; Geesink and Hoefnagels, 1995; Kärrholm et al., 1994b; Rothman et al., 1996).

Regardless of fixation technique, clinical results indicate that new techniques or designs require long-term study (a minimum of ten years) to show useful improvements. The paradox is that this places large numbers of patients at greater risk of poor results in the meantime. There is, therefore, a need for accurate prediction of clinical performance from *in vitro* testing.

An accepted fundamental principle for biological fixation is: prevention of excessive motion between the bone and the prosthesis is essential to achieve bone ingrowth. The objective of this study is to develop a method to characterize relative motion over the entire prosthesis for femoral and acetabular components used in THA, under time-variant, three-dimensional, quasi-physiologic loads simulating those present during level walking and stair climbing. In addition, the method will be used to determine the effect of initial fixation parameters under direct control of the operating surgeon on relative motion between the prosthesis and bone.

1.1 Definition of Micromotion

Relative motion between the prosthesis and bone falls into two categories: recoverable motion and non-recoverable motion (Figure 1). Recoverable motion, often termed

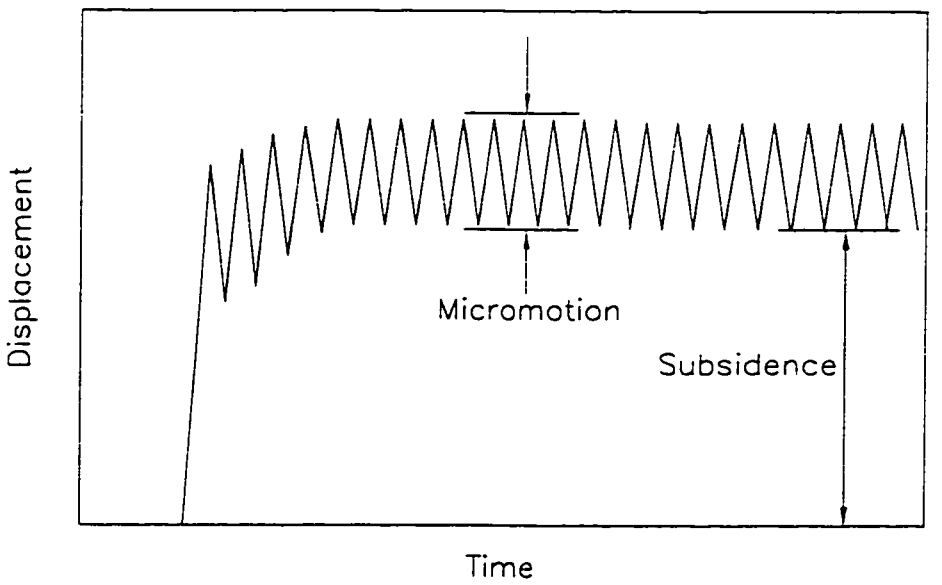

Figure 1. Schematic representation of component displacement during cyclic loading.

micromotion, is an effect of elastic deformation. Adjacent points at the bone/prosthesis interface move with respect to each other as loads are applied, then return to their original position after the loads are removed. Micromotion is most commonly thought of in respect to cyclic loading, e.g. during different types of gait. Short-term non-recoverable motion, termed subsidence, is the displacement of the prosthesis from its initial position immediately post-operatively, to the position occupied after removal of all loads. Subsidence is herein defined to mean three-dimensional "seating" of the femoral or acetabular prosthesis into the prepared bony bed, as opposed to one-dimensional motion along the axis of the femur, which is another common definition. Migration defines non-recoverable motion occurring over the course of several years and does not affect initial bone ingrowth, thus it is not discussed here.

1.2 Initial Fixation

Biological fixation, and subsequently clinical success of noncemented THA prostheses, is directly affected by the initial fixation of the prosthesis. To enhance biological fixation, relative motion and bone-to-prosthesis gaps should be minimized (Cameron et al., 1973, 1976). Good initial fixation reduces relative motion and bone-to-prosthesis gaps by increasing bone-to-prosthesis apposition (surface contact). Subsequently, the likelihood of stable fixation via bone ingrowth is increased.

Studies of the effect of femoral design on initial fixation have addressed a broad spectrum of stem design parameters: stem size, i.e., length, diameter, and shape (Bechtold et al., 1988; Callaghan et al., 1992; Holmberg et al., 1986; Engh and Bobyn, 1988); component material (Otani et al., 1991; Rohlmann et al., 1987; Cheal et al., 1991; Lewis et al., 1993; Ramamurti et al., 1993; Morscher and Dick, 1983); location of porous coating (Natarajan et al., 1991; Keaveny and Bartel, 1993; Engh and Bobyn, 1988); and

surgical technique affecting collar support and the amount of surface apposition or fit (Sugiyama et al., 1992; Markolf et al., 1980; Jasty et al., 1988; Whiteside et al., 1989b).

Acetabular fixation studies similarly address a number of design features and/or fixation techniques: threaded components (i.e. self-locking), components with pegs or spikes, adjuvant fixation with screws, and press-fit. Most current studies focus on press-fit, pegs, spikes, or screw fixation because of the poor short-term results threaded cups have shown (Engh et al., 1990a; Harper et al., 1995; Tooke et al., 1988). Press-fit is a term used for a method of achieving initial fixation for both femoral and acetabular components, and means an interference fit. On the acetabular side, surgeons often quantify the amount of interference. For example, a 2 mm press-fit indicates that the last reamer used to prepare the acetabulum is 2 mm smaller in diameter than the prosthesis to be implanted. "On-line" reaming means that the last reamer used has the same nominal diameter as the prosthesis.

1.3 Purpose of Study

Optimal initial fixation, on the femoral side, would theoretically be achieved by an exact anatomical fit, both proximally and distally. Proximal fit is defined as apposition of the prosthesis to cortical bone in the calcar region, and distal fit is the complete filling of the diaphysis with the prosthesis stem. Clinical and experimental evidence suggest that distal fit is important in resisting torsional loads (Engh et al., 1987; Noble et al., 1989; Sugiyama et al., 1992; Whiteside et al., 1989). Recently, good proximal fill (a term they use which more closely approximates the term of "fit" in this thesis) has been shown to reduce vertical and rotational motion of the prosthesis (Dujardin et al., 1996). Clinically it is not always possible to achieve an optimum fit both proximally and distally. The first purpose of this study is to clarify the most favorable fit

condition (proximal vs. distal), in terms of minimizing micromotion and subsidence, when presented with a less than optimal anatomical situation clinically.

Recent data reveal undesirable sequellae of screw and press-fit fixation of noncemented acetabular components. Clinical observations indicate that screw holes may be a pathway for polyethylene wear debris (Bauer et al., 1993), which is a major cause of aseptic loosening of acetabular components (Horowitz et al., 1993; Kim et al., 1994; Schmalzried et al., 1992c). Elimination of the screw holes by using press-fit cups would remove this pathway. However, press-fit cups have been shown to crack a large percentage of acetabulae (Kim et al., 1995b; MacKenzie et al., 1994). In addition, both press-fit and on-line reamed cups have been reported to leave large gaps between the cup and the bone (Kim et al., 1995a). Attempts to minimize the potentially adverse effects of each type of acetabular component fixation include reducing the number of screws used, the magnitude of press-fit (e.g. from 4 mm to 2 mm), and cup-to-bone gap width. The second purpose of this study is to compare various screw fixation configurations as they relate to micromotion and cup-to-bone gaps of on-line reamed acetabular components.

CHAPTER 2

REVIEW OF LITERATURE

The ultimate goal of *in vitro* testing of THA prostheses is to predict clinical performance. To predict clinical performance of noncemented components one must predict bony ingrowth. To predict the amount of bony ingrowth, a researcher ideally must understand the biological mechanisms of ingrowth and their constraints, reproduce the mechanical environment in which ingrowth occurs, and measure the critical parameters affecting ingrowth.

2.1 Biological Fixation

The greatest theoretical advantage of biological fixation is that the prosthesis is held in place by a dynamic, adaptable material, namely bone. Optimal fixation occurs when there is bone ingrowth into the prosthesis. Adequate fixation can also be achieved by a combination of bony and fibrous ingrowth (Cook et al., 1988b; Engh et al., 1987; Pilliar et al., 1986), but bony fixation produces better clinical results (Engh et al., 1987). If the initial fixation of the prosthesis is inadequate and excessive motion persists, bone will fail to grow into the porous coating. In addition, if the load transfer deviates too greatly from normal, the remodeling process will remove bone, thus increasing the potential for component failure.

Biological fixation is achieved when the tissue surrounding the prosthesis holds it in place. To facilitate ingrowth, a porous coating is applied to the surface of the prosthesis. A variety of materials, including polymers, ceramics, and metals, have been investigated. The brittle nature of ceramics and the deformation characteristics of

polymers have led to the widespread use of metals (Galante, 1985). The most common metals used for this purpose are titanium and cobalt chromium alloys. These are generally sintered to the prosthesis surface, in the form of beadlets or short wires which form a fiber mesh.

The process of ingrowth occurs in several stages: inflammatory, repair, and remodeling. Initially, an inflammatory response to surgery is observed. This is followed by the formation of woven bone in the porous coating, beginning approximately one week after surgery. As the woven bone develops, osteoblasts produce osteoid, which eventually mineralizes. At four to six weeks initial remodeling of woven bone into lamellar bone is observed (Galante, 1985). Based on canine interface shear strength studies, stabilization of the prostheses occurs between three and twelve weeks (Cameron et al., 1976; Bobyn et al., 1981). In humans, the remodeling process continues for at least one year (Engh et al., 1987; Pidhorz et al., 1993) and may continue for several years (Engh et al., 1992) until an equilibrium state is achieved. The role of the mechanical environment in each of these three stages is poorly understood, but evidence suggests it most affects the latter two stages.

In order for mature lamellar bone to develop within the porous surface of THA prostheses, there are three overriding requirements:

1) Appropriate pore size.

2) Sufficiently narrow gap between the bone and the prosthesis.

3) Sufficiently small relative motion between the bone and the prosthesis.

Failure to satisfy any of these requirements will inhibit the development of osseous tissue, resulting in either fibrous ingrowth or a smooth encapsulating membrane (Haddad et al., 1987).

Many studies have been performed in an attempt to determine the optimum pore

size for ingrowth (Bobyn et al., 1980; Cameron et al., 1976; Collier, 1988, Galante et al., 1971, 1983; Haddad et al., 1987; Harris et al., 1983; Hedley et al., 1983). The accepted pore size for ingrowth ranges from 50 μm to 400 μm (Bobyn and Engh, 1983). Prostheses with porous layers matching these pore sizes have proved effective in humans (Pilliar, 1983). Additional studies using mechanical strength of fixation (rather than the amount of ingrowth) to determine the optimum pore size have indicated that a minimum of 250 μm is required for Haversian remodeling (Galante, 1985).

Bone-to-cup affects bone ingrowth. Cameron et al. (1976) observed that bone can bridge a gap up to 1.5 mm in dog femurs. In a recent study, also using dog femurs, Dalton et al. (1995) observed some ingrowth with a 2 mm gap but it was only 50% of the amount with a gap of 0.5 mm. Both studies reported the time to firmly fix a prosthesis increases with gap width. In humans Hofman et al. (1993) observed fibrous ingrowth for gaps between 50 μm and 500μm. The effect of apposition bone type remains unclear. Bobyn et al. (1981) reported improved bone quality with apposition to cortical bone. In contrast, Dalton et al. (1995) reported no difference between cancellous and cortical apposition for gaps less than 1 mm but increased ingrowth for gaps larger than 1 mm with apposition to cancellous versus cortical bone.

Micromotion affects the amount and type of ingrowth. One of the earliest studies of the effect of micromotion concluded that ingrowth will occur in the presence of micromovement, but not macromovement, and thus recommended that some form of mechanical fixation be used as initial supplementary fixation (Cameron et al., 1973).

The upper limit of micromotion compatible with bone ingrowth is not known. To quantify the magnitude of micromotion that allows ingrowth, Pilliar et al. (1986) applied known displacements to porous-coated implants. They observed bone ingrowth for relative motion less than 28 μm. Motion up to 150 μm resulted in prosthesis fixation by

mature well-ordered fibrous tissue. Engh et al. (1992) examined fourteen retrieved femurs with radiographic evidence indicating tissue integration, thirteen with bone ingrowth and one with fibrous ingrowth. Loads of 445 N axially and 22.4 N-m torsionally about the stem were applied to simulate physiologic loads for level walking and stair climbing. Maximum relative motion in porous coated areas with bone ingrowth was 40 μm (resultant of two components of motion). The one case where no bone ingrowth was observed had 150 μm of micromotion. Whiteside et al. (1993) observed 30 to 44 μm of micromotion in three retrieved specimens with noncemented prostheses. Whiteside et al., applied loads ranging from 245 to 1960 N axially and 4.9 to 22.5 N-m torsionally. In a similar study of cemented components, Maloney et al. (1989) reported maximum axial micromotion of 40 μm for radiographically and clinically fixed prostheses. An effective spinal load of 1100 N was applied to the femurs in single-limb stance and stair-climbing (30° of hip flexion) positions. Transverse micromotion averaged 25 μm, with only one specimen exhibiting more than 40 μm of motion. Maloney et al., also observed bone ingrowth into the cement mantle. Burke et al. (1991) applied known torsional displacements to titanium pins in canine femoral condyles. They observed bone ingrowth at 40 μm of micromotion and fibrous fixation at 150 μm of micromotion. In a recent study Bragdon et al. (1996) applied known bone/pin interface motion and observed fixation by ingrowth of bone, bone and fibrous tissue, and fibrous tissue alone, at 20 μm, 40 μm and 150 μm of micromotion, respectively. These studies suggest that micromotion greater than 50 μm reduces bone ingrowth but tissue ingrowth still occurs up to 150 μm.

In vivo studies indicate early relative motion between the prosthesis and bone is predictive of clinical outcome. Using Roentgen stereophotogrammetric analysis (RSA) Green et al. (1983) measured micromotion of femoral components up to 30 months post-

operatively. Five of seven components exhibiting micromotion at one month required revision surgery within two years. Using RSA to measure subsidence Kärrholm et al. (1994a) and Ryd et al. (1995) observed that early relative motion is predictive of prosthesis loosening for THA femoral components and total knee arthroplasty tibial components respectively. Kärrholm et al. reported that subsidence more than 0.33 mm at six months combined with total subsidence of more than 0.85 mm increased the risk of revision. They also noted subsidence greater than 1.2 mm at two years increased the probability of revision by 50%. Ryd et al. reported RSA subsidence data between one and two years can indicate "at risk" tibial components with a predictive power of 85%. Freeman and Plante-Bordeneuve (1993) measured subsidence rate with standard post-operative radiographs. They reported that a migration rate of 1.22 mm/year is a strong indication revision will be required by eight years. These clinical studies indicate the strong effect early micromotion has on the outcome of THA.

2.2 *In vivo* Motion

In vivo studies using RSA confirm that relative motions between the femur and prosthesis are three-dimensional. Mjöberg et al. (1984) reported three-dimensional displacements for cemented THA components when loaded in distraction, compression, external and internal rotation. The lower limit of displacements in components exhibiting instability varied depending on the applied loads: 0.5 mm to 0.8 mm along the transversal-axis; 0.4 mm to 0.7 mm along the frontal-axis; 0.2 mm to 2.3 mm along the sagittal-axis. Nistor et al. (1991) observed three-dimensional motion in terms of internal rotation and axial migration. Three years post-operatively they observed average internal rotation of 7.4° and average subsidence of 2.44 mm. Recently, Thanner et al. (1996) observed rotational migration of noncemented components about three axes. Anterior-posterior tilt ranged from -0.8° to 0.7°, retro/anteversion ranged from -1.6° to 3.9°, and

valgus/varus angulation from -0.7° to 0.4°. The fact that components rotate with respect to the bone indicates that micromotion will vary over the surface of the component.

In vitro studies suggest that micromotion of acetabular components is also three-dimensional. Kamaric et al. (1996b) and Pfleiderer et al. (1996) reported different magnitudes and directions of micromotion at sites around the acetabulum. Mjöberg et al. (1984) reported motion of the acetabular component *in vivo*, but in only one direction.

Studies suggest that the magnitude of micromotion, but not the direction or type (i.e. anterior-posterior vs. medial-lateral or shear vs. tension), dictates whether bony ingrowth occurs. Many studies report approximately the same magnitude of micromotion (Pilliar et al., 1986, Engh et al., 1992, Maloney et al., 1989, Burke et al., 1991, Bragdon et al., 1996, Whiteside et al., 1993) for which bone ingrowth occurs. However, the type of displacement varied between tests. Pilliar et al., applied a ±20 N load, which induced displacements that were a combination of shear deformation at the implant-bone interface and cantilever bending of the surrounding bone; Burke et al., and Bragdon et al., applied rotational displacement to pins placed in canine femurs; Engh et al., Maloney et al., and Whiteside et al., measured micromotion in retrieved human specimens, where the initial relative motion was three-dimensional. Relative motion consisted of interface shear, cantilever bending, and three-dimensional translation but the resultant magnitude of micromotion under which bone ingrowth occurred was relatively consistent. This indicates that the magnitude, not the type of micromotion, is the critical feature regarding bone ingrowth.

2.3 *In vivo* Loads

To replicate *in vivo* loads one must first know the loads acting on the hip. The first attempt at direct measurement of the bony contact force across the joint was reported by Rydell (1966). Six months after implantation, access was gained to subcutaneous

leads connected to strain gages mounted on an implanted prosthesis. The contact forces during gait had peak values of three times body weight (BW). English and Kilvington (1979) reported similar values with an instrumented hip prosthesis.

Several studies report estimated hip joint forces (Brand et al., 1994; Calderale et al., 1987; Crowninshield et al., 1978; Paul, 1976; Röhrle et al., 1984; Seireg and Arvikar, 1975). These studies used data from external measurements (usually force plates) and muscle force estimates as input into mathematical models. The analytical investigations generally predicted higher joint forces than did direct measurements, especially for the second half of the stance phase of level walking gait.

A new generation of instrumented components have been used to directly measure the three-dimensional forces acting on the femoral component. Kotzar et al. (1991) used instrumented femoral components implanted in two patients to measure forces during level walking and stair climbing. Peak values of the resultant hip joint contact force (hereafter referred to as the joint reaction force or JRF) reached 2.8 BW for normal gait and 2.6 BW for stair climbing. Bergman et al. (1993) also used instrumented femoral components to measure loads up to 30 months after implantation in two patients. The peak resultant JRF during normal gait was 2.8 BW at 1 km/hr, and increased to 4.8 BW at 5 km/hr for one patient. The second patient experienced a peak JRF of 4.1 BW at a walking speed of 3 km/hr. Out-of-plane forces created torques ranging from 24 N-m to 40 N-m about the stem of the prosthesis for both patients.

In addition to more accurately reporting the JRF, these newer instrumented components also show the time-varying relationship between coronal plane forces, namely medial-lateral (ML) and superior-inferior (SI) forces, and anterior-posterior (AP) forces. The relationship is non-linear during level walking and stair climbing (Kotzar et al., 1995). This is significant in femoral loading because coronal plane forces contribute

to torsional resistance by wedging the prosthesis into the diaphysis. It may also be important when loading acetabulae because changes in the JRF vector direction change the strain patterns in the pelvis.

The way in which the JRF is applied (i.e. by muscle forces and specimen support) is also important because local strains in the bone affect the magnitude of micromotion (Paul, 1996). Resistance to micromotion and load transfer depend initially on the contact between the bone and prosthesis (via friction). Strains in the bone effect the nature of the contact between the bone and prosthesis, and subsequently, micromotion. Hazelwood et al. (1996) cited the significance of abductor muscle forces in the development of femoral strain patterns. Support of specimens that significantly changes the stiffness or load path also alters strain patterns and subsequently affects micromotion measurements.

Lastly, the dynamic nature of gait loads may play an important role. The deformation of viscoelastic materials (including bone) depends on the rate as well as the magnitude of applied loads.

2.4 *In vitro* Micromotion Studies

Previous studies of initial fixation of THA prostheses provide *in vitro* comparisons (either by intent or through inherent limitations of the test methods) rather than prediction of clinical performance. Tests intended for *in vitro* comparison typically have utilized load-to-failure as the outcome measure and consequently results could not be translated to relative clinical performance. A second genre of tests utilized micromotion to predict *in vivo* performance. These tests were limited in their objective by the difficulty in replicating the *in vivo* loading environment *in vitro* and the complicated nature of measuring the small displacements between the prosthesis and bone.

2.4.1 Femoral Studies

Due to the complex nature of the *in vivo* loads acting across the hip, most previous studies simplified the loads applied *in vitro*. These early tests simulated either coronal plane forces or torsion about the stem. In addition, most previous studies reported motion at only a few locations on the prosthesis. In the following discussion two-dimensional load indicates a test setup which generates force components in both the ML and SI directions. By definition, three-dimensional load indicates a force component acting on the prosthesis in the AP direction or the stem torque created by such a force, in addition to a two-dimensional applied load.

To determine the effectiveness of his method of cement fixation, Charnley and Kettlewell (1965) performed the first quantitative micromotion test. They compared micromotion between cemented components and noncemented components under steady axial compressive loads. The only measurement reported was axial displacement at the tip of the prosthesis. Displacement was measured with a dial gage clamped to the bone, with motion at the tip transmitted by a pivoted lever attached to the prosthesis through a hole drilled into the specimen. Micromotion was reported as "slip per 100 lbs (445 N) of load". Cemented prostheses were significantly more stable, exhibiting only 5 μm/100 lbs, compared to 1140 μm/100 lbs for noncemented prostheses. This test indicated a significant difference between cemented and noncemented femoral prostheses. However, the applied loads were not physiological and motion was only measured in one direction at one point, so the clinical relevance was limited.

Investigators gradually developed more sophisticated specimen loading methods, i.e. two-dimensional. Markholf et al. (1980), Whiteside et al. (1988) and Whiteside and Easley (1989) applied uni-directional loads but oriented the specimen to simulate coronal plane forces during single leg stance, a slight improvement on Charnley and Kettlewell's

(1965) loading technique. Displacements (measured with linear variable differential transformers, LVDT's) were recorded in one direction only, at one, two, or three locations.

Early tests studying the torsional stability of femoral components applied torsion about the stem but ignored coronal plane forces (Bechtold et al., 1988; Gustilo et al., 1989; Nunn et al., 1989; Phillips et al., 1991; Sugiyama et al., 1989, 1992). Applied loads consisted of either pure torque or a force acting in the posterior direction. Noncemented femoral components resist torsion initially by friction between the prosthesis and the bone. An axial load "wedges" the prosthesis into the femur and thus increases torsional resistance. Also, the majority of these tests potted the specimen in PMMA well above the femoral condyles, significantly altering the pattern of load transfer from that observed *in vivo*. In a study comparing the torsional stability of two stem designs, Whiteside et al. (1994) accounted for the wedge effect by applying a constant axial load while applying a variable torsional load regimen.

Several groups recognized the importance of three-dimensional loads. Walker et al. (1987) applied coronal forces with one actuator and posteriorly directed forces with a second actuator. However, only static loads were applied. The measurement technique was also more developed, recording three orthogonal displacements at each of two locations and prosthesis rotation about two axes measured using eddy current transducers.

Schneider et al. (1989a,b) applied the first dynamic three-dimensional loading. Axial and torsional loads were applied synchronously at a frequency of 0.5 Hz. The axial loads had amplitudes of one, two, three, and four BW. The torsional amplitude was 8 N-m throughout the test. Micromotion was measured with a custom device incorporating a strain gage in two directions at each of two locations. Stem rotation and subsidence were also measured. Though dynamic, the loads were not as physiologic as those of Walker et

al. (1987), because Schneider et al.,'s loading fixture applied the axial load in the direction of the stem, and applied the torsional load around the same axis.

To better replicate coronal plane forces several studies incorporated a loading fixture to simulate the pelvis. The simulated pelvis incorporates a strap to approximate the abductor muscle group and offsets the femur from the center of gravity (i.e. the loading axis). The strap and offset enables ML and SI force components to be generated by applying a uni-directional force through the center of gravity. Use of the simulated pelvis does not eliminate the possibility of applying three-dimensional loads. AP loads can be applied via weights and pulleys (Callaghan et al., 1992) or by rotating the assembly (Burke et al., 1991). Studies using this apparatus applied only static loads and therefore could not replicate *in vivo* load waveforms.

As loading techniques improved, so did the appreciation that a complete knowledge of the three-dimensional motion of prostheses is necessary to accurately predict micromotion patterns (Buhler et al., 1995; Gilbert et al., 1992; Kamaric et al., 1996; Noble et al., 1995; Pfleiderer et al., 1996). Gilbert et al. (1992) developed a technique, based on the assumption of rigid-body motion, to completely determine the motion of any and all points on a femoral prosthesis. In this method an array of seven LVDT's measures the necessary displacements. Six of the LVDT's measure three-dimensional motion at two points. The seventh LVDT is used to determine the rigid-body rotation about the axis passing through the two points. The displacements are incorporated into a software package to calculate the motion of all points on the device during cyclic loading, and subsequently to determine the direction and magnitude of the migration and micromotion of the prosthesis.

Assuming rigid-body motion of the bone and prosthesis to calculate micromotion at any point on the prosthesis is not universally accepted. Hayes et al. (1992) developed a

technique to measure translational and rotational micromotion in one plane of a femoral prosthesis. Moving the displacement measurement jig would have enabled calculations of rigid-body motion, but they stated that bony compliance would have created errors on the order of hundreds of microns. Bühler et al. (1995) developed a similar but more sophisticated technique which allows the precise measurement of the isolated three-dimensional interfacial motion at different points along the femoral shaft. They measured displacement at three sites along the shaft (proximal end, middle, and distal tip using a laser diode sensor) and calculated the micromotion in a transverse plane at the level of the measurements. Bühler recorded a sufficient number of displacements to apply rigid-body motion kinematics. But they chose not to do so, stating that strains in the bone and prosthesis would lead to unacceptable errors.

2.4.2 Acetabular Studies

Studies of the initial fixation of acetabular components developed in a manner similar to femoral component studies. Early tests focused on load to failure, and were followed by studies investigating the effects of different fixation techniques on micromotion and bone-to-prosthesis gaps. As with femoral studies, applied loads in acetabulum studies were greatly simplified from *in vivo* loads. In several studies replication of physiologic loads was not even attempted. This, coupled with displacement measurements at only a few sites, restricts these studies to *in vitro* comparisons between fixation techniques and greatly limits the prediction of clinical performance.

Early acetabular component studies examined the effects of press-fit, screw, and spike fixation on torsional stability (Clarke et al., 1991; Curtis et al., 1992; Lachiewicz et al., 1989). These early studies embedded the acetabulum completely in PMMA or a similar acrylic, making the most compliant area of the pelvis extremely rigid. Takedani et al. (1991) improved on these studies by supporting the acetabulum locally with dental

cement at the ischium, ilium, and pubic bones. Failure was defined as motion presumably inhibiting bone ingrowth, generally two degrees of rotation. More remarkable than the method of specimen support is the magnitude of applied torques. The reported minimum applied torque causing failure was 8.8 N-m (Curtis et al., 1992), with most specimens resisting 20 N-m or more. *In vivo* torque values reported in the literature range from 0.9 N-m to 1.5 N-m (Andersson et al., 1972; Ma et al., 1983), an order of magnitude less than torques applied *in vitro*.

Acetabular micromotion studies have examined the effects of screw location, screw tightness, acetabular bony defects, and implant size on the initial stability of porous-coated implants. Stiehl et al. (1991) applied 980 N to specimens for 100,000 cycles. However, like the early torsional studies, the acetabulum was completely embedded in PMMA. Tests were also performed where pelvis support was accomplished by potting the iliac crest (Hadjari et al., 1994; Kwong et al., 1994; Perona et al., 1992). This method of support allowed more natural deflection of the acetabulum. Won et al. (1995) advanced the realism of specimen support further by using an intact pelvis and supporting it at only two points (bolt connections to the test fixture at the superior aspect of each ilium). All of these studies measured micromotion at the rim of the cup using LVDT's. Only two measured micromotion in three directions (Kwong et al., 1994 at one location; Stiehl et al., 1991 at each of two locations), the remainder measuring micromotion in one direction at each of three locations (Hadjari et al., 1994; Perona et al.; 1992, Won et al., 1995). Only Kwong et al. (1994) measured micromotion at a location other than cup rim; they measured three directional motion at the dome of cup.

Two recent studies suggest but do not document the potential importance of measuring micromotion in three-dimensions and at several points on the prosthesis. Kamaric et al. (1996b) mounted whole pelves with ischial and iliac supports to allow free

deflection under applied loads. They measured micromotion with proximity transducers in three directions at the dome of the cup, at the acetabular notch, and at the floor of the acetabulum. Pfleiderer et al. (1996) employed a much more complex loading fixture that used cables representing the three glutei and the ischio-crural muscles to counterbalance the applied load. Pfleiderer et al., also measured micromotion in three dimensions at each of three locations using custom built three-dimensional strain gage sensors. Both studies reported point to point variations in the magnitude and direction of observed micromotion. The data also indicated tilting of the cups. The observed variation of three-dimensional micromotion over the cup suggests that site-specific micromotion measurements are not necessarily indicative of global micromotion patterns.

Bone-to-prosthesis gaps have been studied because they affect the amount of bony ingrowth (Cameron et al., 1976; Dalton et al., 1995; Hofman et al., 1993). The expanded use of press-fit acetabular fixation has increased the importance of determining the effect of this type of fixation on initial bone-to-prosthesis gaps. The initial apposition of cup to acetabulum for three different designs (hemispherical with three spikes, threaded, and without adjuvant fixation) was evaluated by Schwartz et al. (1993). All components were 1 mm press-fit. Even though implantation was carefully performed in a controlled environment, gaps still existed for all components. The effect of the severity of press-fit (from on-line reaming to 4 mm press-fit) on bone-to-prosthesis gaps and acetabular fracture was investigated by MacKenzie et al. (1994) and Kim et al. (1995a,b). Gaps were observed for all magnitudes of press-fit, with press-fits greater than 2 mm producing fractures during insertion 60% of the time.

2.5 Noncemented Component Studies

Early micromotion tests, while perhaps effective for relative rankings of prostheses, have, in retrospect, not served well for predicting the amount of bony

ingrowth. Most previous studies reported micromotion much less than 100 μm, suggesting that bone ingrowth would be found routinely in most of the porous-coated region. However, almost without exception, retrieval studies have failed to show consistent amounts of bony ingrowth. Various investigations report ingrowth in terms of either area fraction or volume fraction. Area fraction is defined as the (global scale) area of ingrowth divided by the (global scale) available surface area of the porous-coated region. Volume fraction is the volume of bone ingrowth divided by the available volume within the porous coating. While canine studies have reported area fractions up to 53% (Harris et al., 1983), Cook et al. (1988a) retrieved 22 femoral and 14 human acetabular components with a maximum of 10% volume fraction. More recent acetabulum retrieval studies reported series average volume fractions of 21% and 4% (Pidhorz et al., 1993 and Sumner et al., 1993, respectively). Engh et al. (1993) reported a series average area fraction of 32% with a range from 3% to 84%. Volume fraction was comparable to other studies at 14%. Engh et al., did observe a volume fraction of 48% if only the areas with bone ingrowth were used. All studies reported 20-30% of components with no ingrowth, yet all of the hips from all studies were stable at the time of death. This may be due to the relatively short follow-up time, an average of four years.

Possible reasons that previous *in vitro* studies fail to accurately predict bony ingrowth include failure to reproduce the *in vivo* mechanical environment, i.e. application of non-physiologic loads and insufficient measurement of critical parameters, i.e. micromotion. Non-physiologic load application resulted from use of two-dimensional loads, improper specimen support, no spatial variation in the JRF vector, and arbitrary load magnitudes (not scaled to body weight). Micromotion description may have been insufficient because it was reported at only a few sites and often in only one or two directions.

In an attempt to better understand *in vivo* micromotion processes for the purpose of predicting bone ingrowth, testing procedures were developed for both the femur and the acetabulum. The testing procedures emphasized improved simulation of hip loading for level walking and stair climbing, and collection of sufficient displacement data to estimate the relative motion between the prosthesis and bone over the entire prosthesis during these activities.

2.5.1 Hip Loading

To improve the clinical realism of *in vitro* micromotion experiments, more accurate loading seems appropriate. This is feasible now for two reasons. First, the three-dimensional time-variant nature of the loads across the hip is now reasonably well established from *in vivo* data (Bergmann et al., 1993; Kotzar et al., 1991). Second, programmable dual-actuator servo-hydraulic materials testing machines allow application of temporally- and directionally-variant three-dimensional loads.

Several studies suggest that torsional loading may be more critical to femoral prosthesis loosening than is axial loading (Whiteside et al., 1994; Jasty et al., 1994, Sugiyama et al., 1992). During testing of femora with noncemented components retrieved at autopsy, Engh et al. (1992) observed slightly larger magnitudes of micromotion during simulated stair climbing than for single leg stance. In a similar study with cemented components, Maloney et al. (1989) observed an average increase of 300% in transverse micromotion during stair climbing compared to single leg stance. Stair climbing generates a large posterior force component of femoral head loading, which in turn creates large torques about the prosthesis shaft. Level walking, however, is also of clinical interest due to the much larger number of loading cycles and the generally higher resultant joint force magnitudes involved. Consequently, loads from both activities were considered in this study.

2.5.2 Displacement Measurement

To increase the accuracy of predicting bone ingrowth *in vivo*, measurement of micromotion should be made at enough sites to determine the three-dimensional micromotion over the entire surface of the prosthesis. The test procedures developed include measurement of micromotion at a sufficient number of sites to allow calculation of micromotion over the entire surface of the prosthesis using the assumption of rigid-body kinematics.

CHAPTER 3

MATERIALS AND METHODS

The three major aspects of the experimental procedures are prosthesis implantation, development of a test setup to apply three-dimensional quasi-physiologic loading, and calculation of the relative interfacial motion between the prosthesis and the bone (micromotion).

3.1 Experimental Procedure for the Femur

3.1.1 Prosthesis Implantation

Nineteen fresh frozen cadaver specimens, five pairs and nine single legs, average age 52 years, were implanted with the anatomically shaped femoral component of the Ranawat/Burstein Uncemented THA System (BIOMET Inc., Warsaw, IN). This femoral prosthesis was chosen because its shape is designed to allow good fit both proximally and distally (Figure 2). The Ranawat/Burstein femoral implant is made from a cobalt-chromium alloy, has 15 degrees of anteversion, a stem with a circular cross-section, and a sintered bead porous coating over the proximal third.

The standard procedure for implanting this system uses templates and pre-surgical radiographs to size the femoral prosthesis, reamers to prepare the diaphysis (the shaft of the femur), and a combination of broaches and rasps to prepare the metaphysis (Figure 3). The prosthesis is sized by overlaying templates on an AP radiograph of the femur. The template is positioned by placing a reference line on the template along the osteotomy line. The surgeon then assesses the proper size (quantified by the manufacturer as parameters of height and width) of the proximal portion of the prosthesis. The proper

diameter of the prosthesis stem is determined by measuring the inner cortical diameter 10 cm below the lesser trochanter. After properly sizing the prosthesis the surgeon prepares the femur, first the diaphyseal canal then the metaphysis. Canal reaming begins with a 9.0 mm reamer, then progresses in 0.5 mm increments until the desired diameter (that indicated by the template sizing) is reached. Metaphysis preparation begins with progressive broaching. Broaching always starts with the smallest broach and progresses with increasing broach size until the proper size (as indicated by the template sizing) is reached. The last step in preparing the metaphysis consists of impacting a rasp, with the same height and width as the prosthesis, until it is fully seated. The femoral prosthesis is impacted into the femur after removal of the rasp.

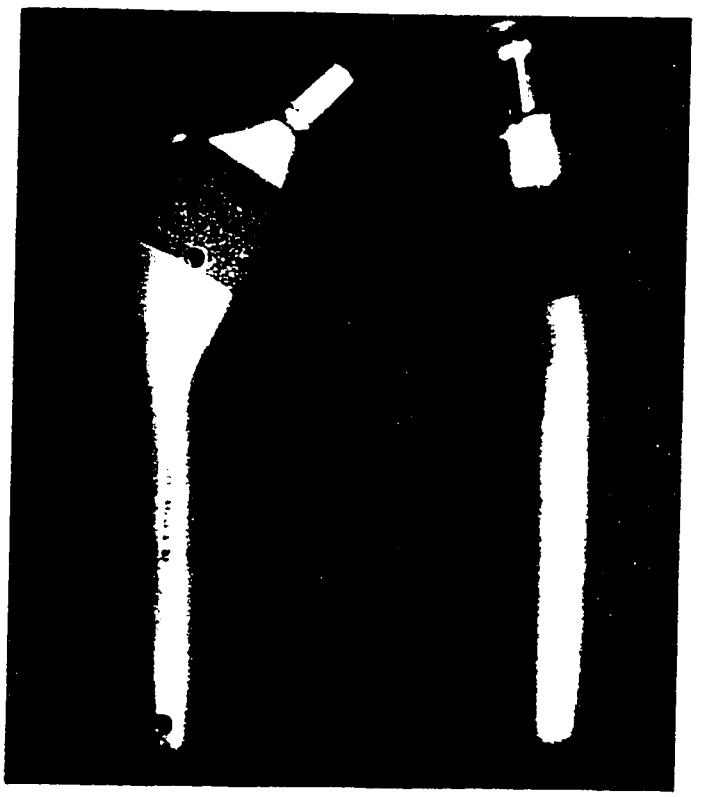

Figure 2. Ranawat/Burstein anatomically shaped femoral prosthesis.

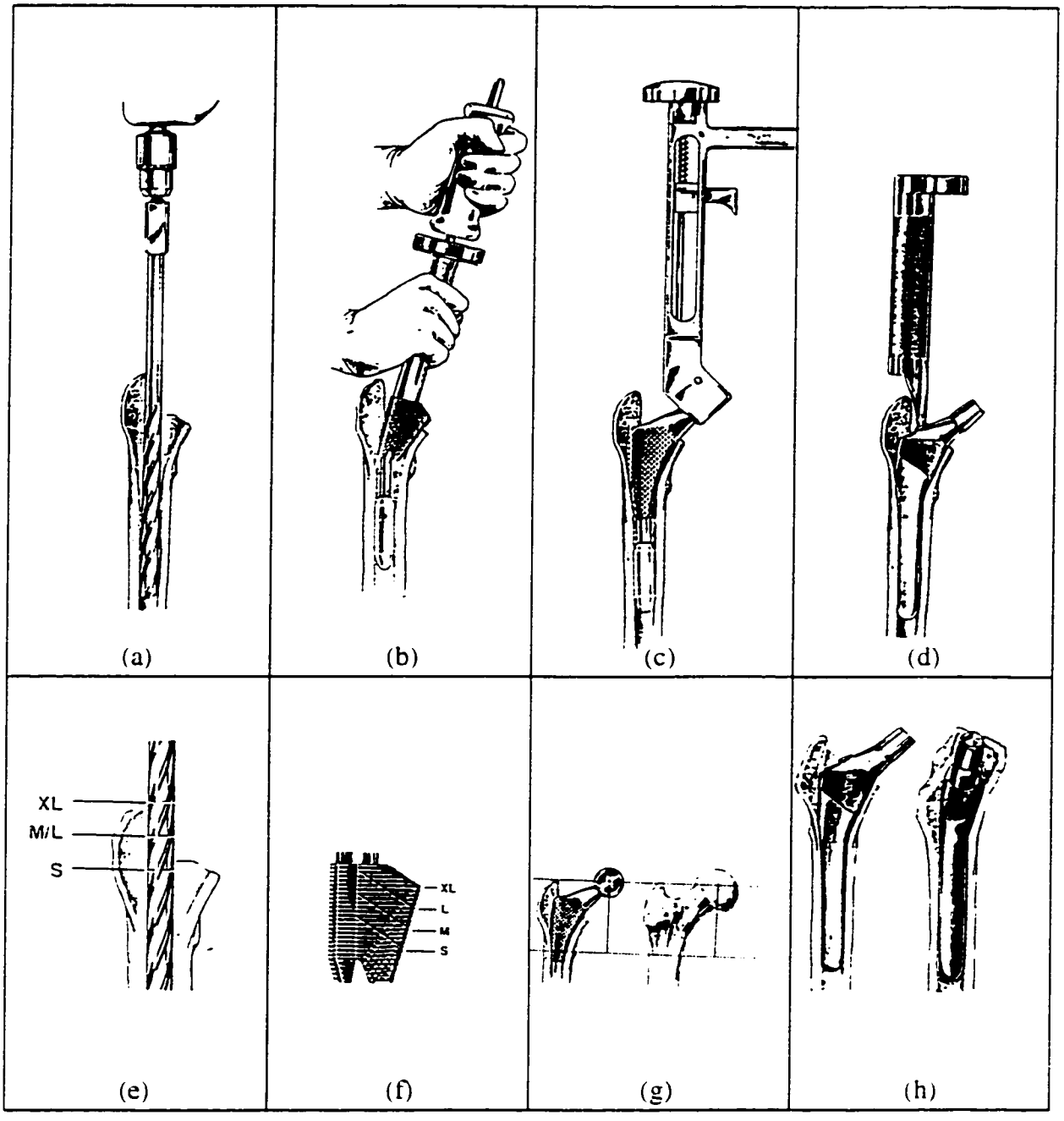

Figure 3. Schematic overview of implantation procedure for the Ranawat/Burstein femoral prosthesis. First the diaphysis is reamed (a), followed by broaching of the metaphysis (b) and complete seating of the rasp into the metaphysis (c), and finally impaction of the prosthesis (d). Marks on the reamers and broaches indicate proper insertion depth during surgery (e) and (f). The rasp is used as a final check of prosthesis position (g). A properly implanted prosthesis (h).

Source: Biomet manual Y-BMT 228/02592.

Each specimen was implanted with a single femoral prosthesis, using one of three different procedures designed to produce one of three types of fit. The first implantation procedure followed standard operating procedures to obtain an optimal fit, i.e. tight proximally and tight distally. The second implantation procedure produced a tight proximal and loose distal fit. This fit was achieved by reaming the canal 1 mm more than the optimal stem diameter indicated by the template sizing procedure, but implanting a prosthesis with a stem diameter equal to the optimal stem diameter. Ideally this would leave a 0.5 mm gap around the stem (however, during impaction the stems drifted until contacting the inner cortex). The third implantation procedure produced a loose proximal and tight distal fit. This was achieved modifying the broaching/rasping procedure. Broach size progression was stopped one size before that indicated from the template sizing. The rasp corresponding to the last broach size was then used. Subsequently, the implanted prosthesis, equal in size to the rasp, was one size smaller in height and width than indicated by the template sizing. This resulted in prosthesis apposition to cancellous bone in the metaphysis, rather than the normally achieved apposition to cortical bone.

Fit classification was documented for all specimens with AP and lateral post-implantation radiographs (Figure 4). Loose distal fit was indicated when two continuous gaps between the prosthesis stem and cortex could be identified from the radiographs (Figure 5). Loose proximal fit was indicated when the prosthesis did not abut cortical bone in the calcar region (Figure 6).

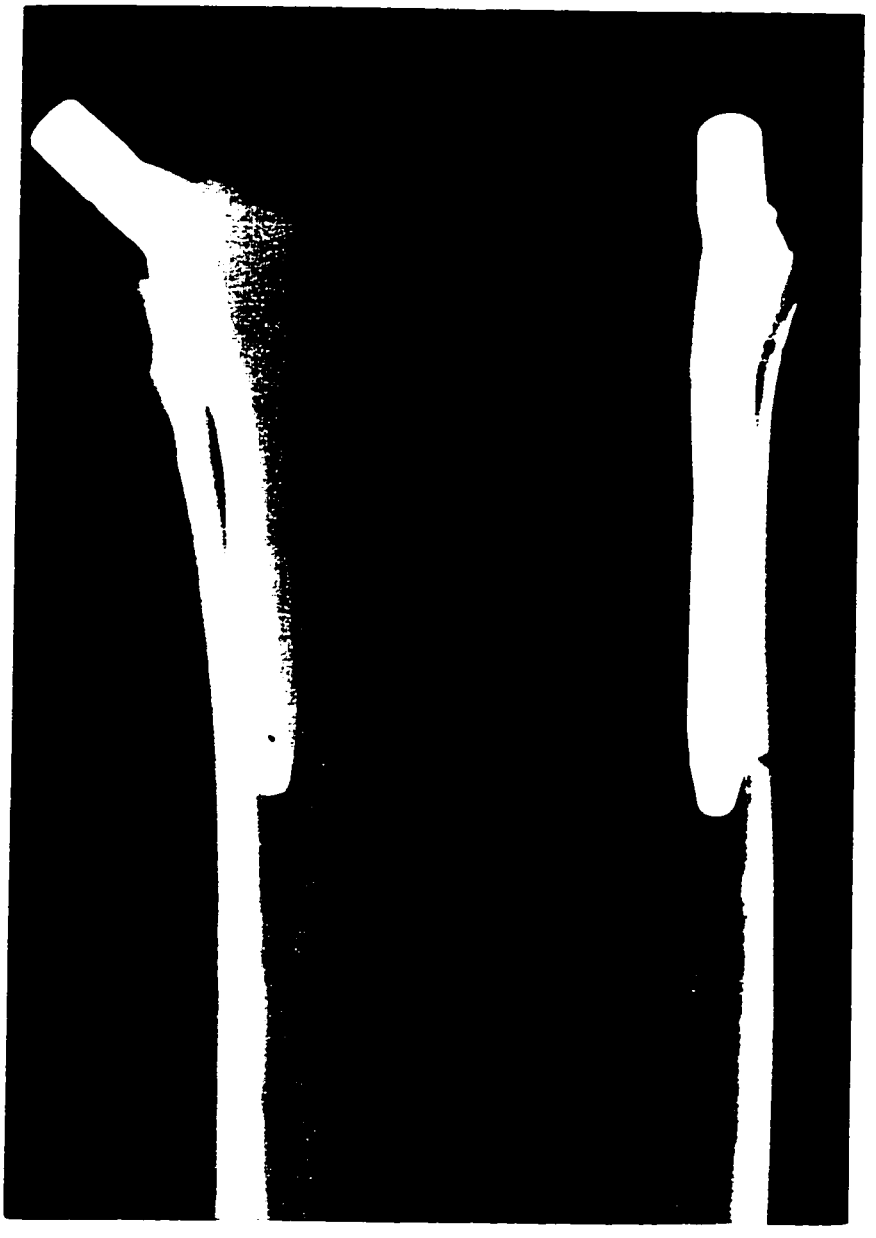

Figure 4. Example of AP (left) and lateral (right) views used to verify fit classification (example is from tight/tight specimen).

Figure 5. Example radiographs of a tight/loose specimen. Arrows indicate gaps between the prosthesis and the inner cortex.

Figure 6. Example radiographs of a loose/tight specimen. The arrow points to the area where the prosthesis normally abuts cortical bone, but the modified surgical procedure produces apposition to cancellous bone.

3.1.2 Determination of Quasi-Physiologic Loads

To predict clinical performance of femoral prostheses from results of *in vitro* tests, the applied loads and specimen support conditions should replicate the *in vivo* environment as closely as possible. To that end, a test apparatus and applied load regimen were developed to reproduce, *in vitro*, the temporally- and directionally- variant three-dimensional loads observed to be acting at the head of the prosthesis *in vivo*.

The test apparatus and load regimen attempted to match the *in vivo* forces acting on the head of the femoral prosthesis reported by Kotzar et al. (1991). Kotzar et al. reported three orthogonal force components, referenced to a femur-based coordinate system. Their data show that the line of action of the JRF varies with respect to the femur during gait. Knowledge of the position of the femur with respect to the standard anatomic reference frame (Figure 7) during gait allows conversion of the reported loads from a femur-based coordinate system into the standard anatomic reference frame. The test apparatus for the femur oriented the specimens with the transverse anatomic plane (defined by the anterior-posterior (AP) and medial-lateral (ML) axes) parallel to the base of the testing machine. The anatomic superior-inferior (SI) axis was parallel to the axis of one of the testing machine actuators. All specimens were tested in an MTS Bionix (MTS Systems Corp., Minneapolis, MN) material testing machine. The Bionix machine has two actuators, one axial for applying force, and one rotational for applying torque. Both load channels can be varied simultaneously and independently. The combination of specimen orientation and dual-load channel control enabled application of coronal plane forces with actuator axial loads and AP, or "out-of-plane", forces with actuator torsional loads. Analysis of the test apparatus determined the relationship between the applied actuator loads and the JRF.

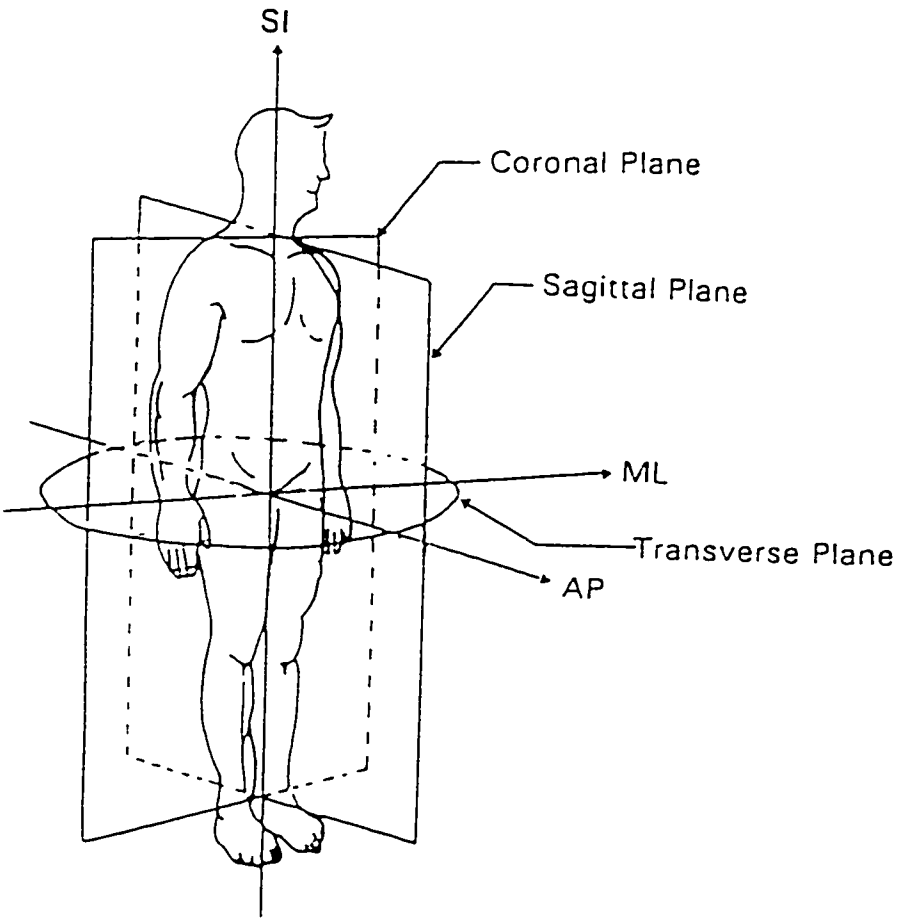

Figure 7. Schematic of the standard anatomic reference frame.
Source: Figure reprinted, with modifications, from Watkins and Glen, Scientific Bases for Human Movement, Baltimore, Williams and Williams, 1988.

3.1.2.1 Femur Test Apparatus

The femur test apparatus consisted of three components: a hemi-pelvis fixture, the specimen itself, and a support fixture (Figure 8). The hemi-pelvis fixture was comprised of an actuator-pelvis adapter, a prosthesis clamp, a strap to simulate the abductor muscle group, and a square bar. The adapter, clamp, and strap were connected

to the bar by brackets with square slots, which allowed them to be positioned at will along the length of the bar. The abductor bracket could also be adjusted vertically. Loads were transmitted to the hemi-pelvis fixture by the actuator-pelvis adaptor, a universal

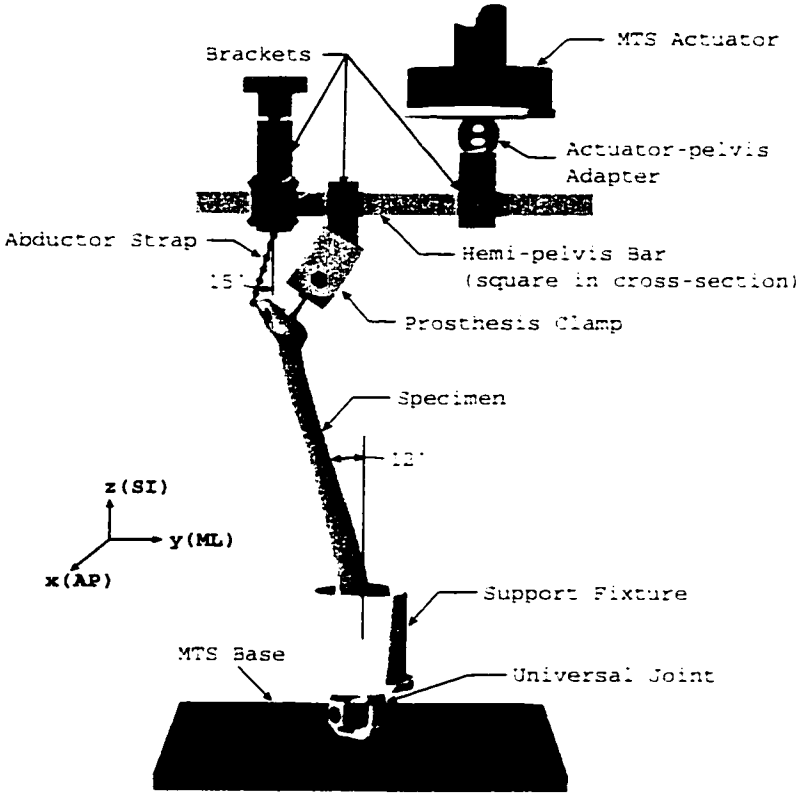

Figure 8. Schematic of the femur test apparatus showing the femur in standard anatomic position.

joint. The applied loads were transferred to the prosthesis and femur via the prosthesis clamp and the abductor strap, respectively. The clamp and strap were connected to their respective brackets with pins that allowed rotation about the AP axis. A combination of screws, bolts, and wires affixed the strap to the greater trochanter of the specimen. The shaft of the femur and the abductor strap were oriented 12° and 15° from vertical,

respectively, based on the anatomical findings of McLeish and Charnley (1970). The femoral condyles were potted with PMMA into a support fixture, consisting of a cup supported by a universal joint that was in turn clamped to the base of the MTS machine. Proper orientation of the specimen aligned the points of loading (head of the femoral prosthesis, universal joints, hemi-pelvis centerlines, and the abductor strap) in a plane parallel to the coronal plane.

The use of universal joints at the MTS base and actuator to constrain the test apparatus resulted from design and necessity. A universal joint was used at the base of the apparatus to simulate knee reaction forces. A universal joint at the MTS actuator was required so that the relationship between reaction forces and applied loads could be uniquely determined. If the universal joint were to have been replaced with a pinned joint, the resulting system of equations used to solve for the reaction forces would have been indeterminate. This determinancy requirement also affected application of the AP force. Both universal joints transmit moments only about the SI axis.

3.1.2.2 Analysis to Determine the Applied Load Regimen

Static equilibrium analysis of the femur test apparatus elucidated the relationship between the applied actuator loads and the forces acting on the head of the prosthesis. The analysis was performed in three steps. The first step was to determine the relationship between the applied MTS loads and the reaction forces acting on the test apparatus. The second step was to determine the relationship between the applied actuator axial load and the coronal plane components of the JRF. Knowledge of the reaction forces was a prerequisite to this step of the analysis. The third step of the analysis was to determine the relationship between the applied actuator torque and the out-of-coronal plane forces.

3.1.2.2.1 Reaction Force Calculation

A free-body diagram of the femur test apparatus (Figure 9) was used to generate a system of equations relating the applied loads **L** and **T** (which represent the applied actuator axial force and applied actuator torque, respectively) to the support reactions **R** and **M** (which designate reaction force and moment, respectively). The two subscripts define direction and point of reaction. In this and subsequent free-body diagrams, all forces and moments are depicted as positive to avoid confusion when deriving the equilibrium equations (note: bold font depicts vectors and normal font depicts scalar quantities or labels).

The following equilibrium equations were derived from the free-body diagram, where moments were summed about P_2:

$$\sum \mathbf{F}_x = \mathbf{R}_{x2} + \mathbf{R}_{x3} = 0 \tag{1}$$

$$\sum \mathbf{F}_y = \mathbf{R}_{y2} + \mathbf{R}_{y3} = 0 \tag{2}$$

$$\sum \mathbf{F}_z = \mathbf{L} + \mathbf{R}_{z2} = 0 \tag{3}$$

$$\sum \mathbf{M}_x = d_2\mathbf{L} - d_1\mathbf{R}_{y3} = 0 \tag{4}$$

$$\sum \mathbf{M}_y = -d_1\mathbf{R}_{x3} = 0 \tag{5}$$

$$\sum \mathbf{M}_z = \mathbf{T} + \mathbf{M}_z - d_2\mathbf{R}_{x3} = 0\,. \tag{6}$$

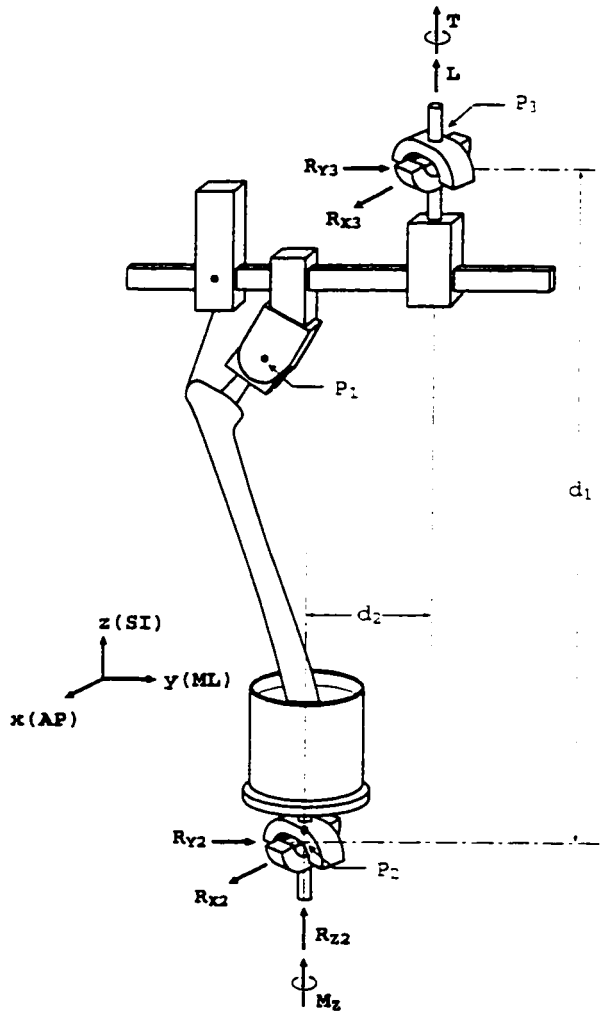

Figure 9. Diagram of femur test apparatus showing the applied loads, **L** and **T**, and force and moment constraints.

In developing this system of equations the weights of the specimen, prosthesis, and test fixture were omitted for two reasons. First, the specimen/prosthesis construct weight was small compared to the applied loads (approximately 20 N compared to 1000 N). Second, the weight of the test fixture was deducted from the system using the tare feature of the MTS testing machine. Static equilibrium analysis was deemed reasonable because of the small inertial forces estimated (two orders of magnitude less than the applied loads).

Solution of this system of equations, and subsequent analyses of the femur test apparatus, included the following assumptions: applied loads act through the center of the upper universal joint, point P_3, and reaction loads at the base act through the center of the lower universal joint, point P_2; points P_1, P_2, and P_3 remain in the coronal plane; and the hemi-pelvis bar remains horizontal during testing. These assumptions simplify the analysis by making the following true: all horizontal and vertical distances are constant during testing; the applied actuator axial load **L** generates only coronal plane forces at the head of the prosthesis; and the applied actuator torque **T** generates a moment about the MTS actuator axis which was parallel to the anatomic SI axis. Based on these assumptions, the solution for the system of Eqs. (1) - (6) is:

$$\mathbf{R}_{x2} = -\mathbf{R}_{x3} = 0 \tag{7}$$

$$\mathbf{R}_{y2} = -\mathbf{R}_{y3} \tag{8}$$

$$\mathbf{R}_{z2} = -\mathbf{L} \tag{9}$$

$$\mathbf{R}_{y3} = \frac{d_2}{d_1}\mathbf{L} \tag{10}$$

$$\mathbf{M}_z = -\mathbf{T}. \tag{11}$$

3.1.2.2.2 Coronal Plane Forces

With all external reaction forces thus determined, the relationship between applied axial load and the coronal plane components of the JRF can be established. Elucidating this relationship begins with construction of a coronal plane free-body diagram for the hemi-pelvis fixture (Figure 10). Here $\mathbf{F}_A$ is the abductor force, **J** is the resultant of the coronal plane components of the JRF, the angle β defines the line of action of **J**, and d_3

through d_6 are dimensions of the test apparatus measured after the specimen is "anatomically" positioned. All joints allow rotation about axes parallel to the AP axis.

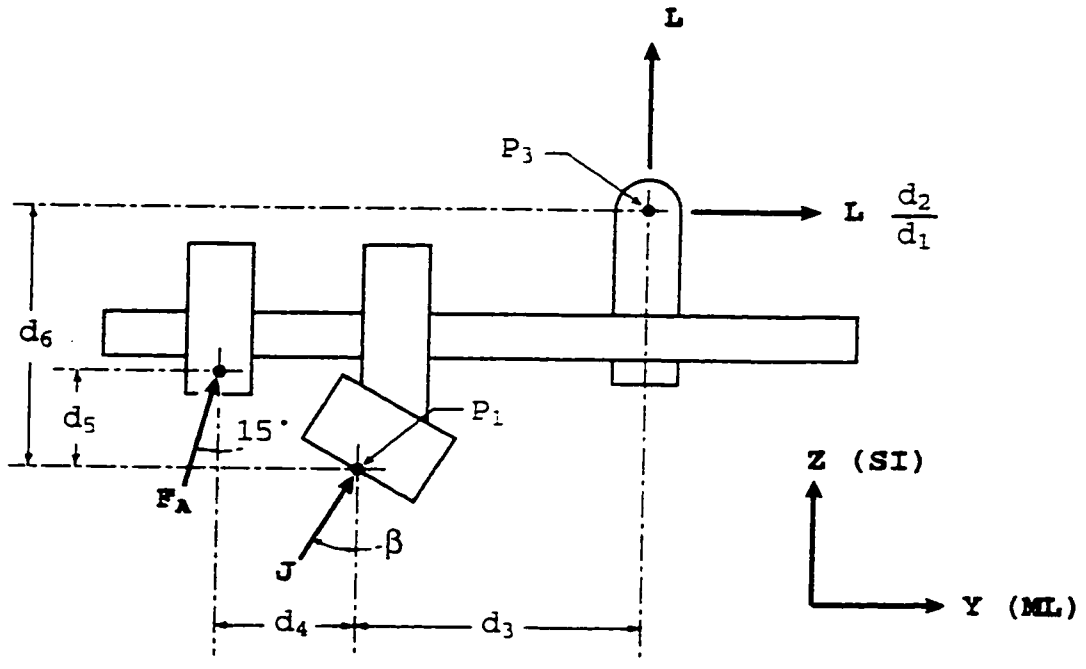

Figure 10. Coronal plane free-body diagram of the hemi-pelvis fixture.

The system of static equilibrium equations for the coronal plane forces acting on the hemi-pelvis fixture, with moments summed about point P_1, is:

$$\sum \mathbf{F}_y = \frac{d_2}{d_1}\mathbf{L} + \mathbf{F}_A \sin 15° + \mathbf{J}_y = 0 \tag{12}$$

$$\sum \mathbf{F}_z = \mathbf{L} + \mathbf{F}_A \cos 15° + \mathbf{J}_z = 0 \tag{13}$$

$$\sum \mathbf{M}_x = d_3\mathbf{L} - d_6\frac{d_2}{d_1}\mathbf{L} - d_4(\mathbf{F}_A \cos 15°) - d_5(\mathbf{F}_A \sin 15°) = 0. \tag{14}$$

where $\mathbf{J}_y$ and $\mathbf{J}_z$ are the ML and SI components of the JRF, respectively.

If $\mathbf{J}_y$ and $\mathbf{J}_z$ are considered as being predetermined from *in vivo* data, this system of equations is redundant because there are only two unknowns, $\mathbf{F}_A$ and $\mathbf{L}$. Solution of

the above system of equilibrium equations therefore requires the identification of another "unknown". If $\mathbf{J}_y$ and $\mathbf{J}_z$ were to be prescribed, one of the apparatus dimensions (d_1, d_2, d_3, d_4, d_5, or d_6) in fact would need to be considered as "variable", in order to achieve a solution. However, while **L** can be varied continuously to reproduce the continuously varying **J** that occurs *in vivo*, the solution of the above equation system would in turn require that this "unknown" apparatus dimension be varied continuously. While the MTS machine enables **L** to be varied continuously, it is physically impossible to continuously vary any of the apparatus dimensions (d_1, d_2, d_3, d_4, d_5, or d_6). For this reason, solution of the equation requires that either the magnitude or the direction of **J** be considered unknown. It was decided to let the magnitude of **J** remain a known quantity, but to treat its direction (i.e. the angle β) as an unknown. Thus, equation system (12) - (14) could be uniquely solved for $\mathbf{F}_A$, **L**, and β.

A solution was obtained in the following manner. First, β is introduced by substituting the definitions $\mathbf{J}_Y=\mathbf{J}\sin\beta$ and $\mathbf{J}_Z=\mathbf{J}\cos\beta$ into the equilibrium equations (Eqs. (12) and (13), $\Sigma\mathbf{F}_y$ and $\Sigma\mathbf{F}_Z$ respectively). Rearranging Eqs. (12) and (13), respectively, gives:

$$\mathbf{F}_A \sin 15° = -\frac{d_2}{d_1}\mathbf{L} - \mathbf{J}\sin\beta \qquad (15)$$

$$\mathbf{F}_A \cos 15° = -\mathbf{L} - \mathbf{J}\cos\beta.. \qquad (16)$$

After dividing the left and right sides of Eq. (15) by the left and right sides of Eq. (16), **L** can be solved for in terms of β and **J** (note that $\tan 15°=0.268$):

$$\tan 15° = \frac{\frac{d_2}{d_1}\mathbf{L} + \mathbf{J}\sin\beta}{\mathbf{L} + \mathbf{J}\cos\beta}$$

$$0.268(\mathbf{L} + \mathbf{J}\cos\beta) = \frac{d_2}{d_1}\mathbf{L} + \mathbf{J}\sin\beta$$

$$\boxed{\mathbf{L} = \frac{\mathbf{J}(0.268\cos\beta - \sin\beta)}{\frac{d_2}{d_1} - 0.268}}. \tag{17}$$

Next, F_A is solved for, again beginning with Eqs. (15) and (16). First, these two equations are rearranged to move **L** to the left hand side of each:

$$\frac{d_2}{d_1}\mathbf{L} = -\mathbf{J}\sin\beta - \mathbf{F}_A\sin 15° \tag{18}$$

$$\mathbf{L} = -\mathbf{J}\cos\beta - \mathbf{F}_A\cos 15°.. \tag{19}$$

Next divide the left and right sides of Eq. (18) by the left and right sides of Eq. (19), and solve for F_A:

$$\frac{d_2}{d_1} = \frac{\mathbf{J}\sin\beta + \mathbf{F}_A\sin 15°}{\mathbf{J}\cos\beta + \mathbf{F}_A\cos 15°}$$

$$\frac{d_2}{d_1}\mathbf{J}\cos\beta + \frac{d_2}{d_1}\mathbf{F}_A\cos 15° = \mathbf{J}\sin\beta + \mathbf{F}_A\sin 15°$$

$$\boxed{\mathbf{F}_A = \frac{\mathbf{J}\left(\sin\beta - \frac{d_2}{d_1}\cos\beta\right)}{\left(\frac{d_2}{d_1}\cos 15° - \sin 15°\right)}}. \tag{20}$$

Now solve for β by substituting the right hand side of Eq. (17) for **L**, and the right hand side of Eq. (20) for $\mathbf{F}_A$, into the original moment equation, Eq. (16):

$$\left(d_3 - \frac{d_2}{d_1}d_6\right)\frac{\mathbf{J}(0.268\cos\beta - \sin\beta)}{\left(\frac{d_2}{d_1} - 0.268\right)} - \frac{\mathbf{J}\left(\sin\beta - \frac{d_2}{d_1}\cos\beta\right)}{\left(\frac{d_2}{d_1}\cos 15° - \sin 15°\right)}\left(d_4\cos 15° + d_5\sin 15°\right) = 0.$$

Dividing by cosβ and factoring out **J** gives:

$$\left(d_3 - \frac{d_2}{d_1}d_6\right)\frac{(0.268 - \tan\beta)}{\left(\frac{d_2}{d_1} - 0.268\right)} - \frac{\left(\tan\beta - \frac{d_2}{d_1}\right)}{\left(\frac{d_2}{d_1}\cos 15° - \sin 15°\right)}(d_4 \cos 15° + d_5 \sin 15°) = 0.$$

Rearranging:

$$(0.268 - \tan\beta) = \frac{\left(\frac{d_2}{d_1} - 0.268\right)\left(\tan\beta - \frac{d_2}{d_1}\right)}{\left(\frac{d_2}{d_1}\cos 15° - \sin 15°\right)\left(d_3 - \frac{d_2}{d_1}d_6\right)}(d_4 \cos 15° + d_5 \sin 15°). \qquad (21)$$

Introducing the following abbreviation:

$$k_1 = \frac{\left(\frac{d_2}{d_1} - 0.268\right)(d_4 \cos 15° + d_5 \sin 15°)}{\left(\frac{d_2}{d_1}\cos 15° - \sin 15°\right)\left(d_3 - \frac{d_2}{d_1}d_6\right)}$$

Eq. (21) is then solved for β:

$$0.268 - \tan\beta = k_1\left(\tan\beta - \frac{d_2}{d_1}\right)$$

$$k_1 \tan\beta + \tan\beta = 0.268 + k_1 \frac{d_2}{d_1}$$

$$\boxed{\tan\beta = \frac{0.268 + k_1 \frac{d_2}{d_1}}{1 + k_1}}. \qquad (22)$$

For a given fixed geometry d_1 through d_6, Eq. (22) can be used to calculate β, and Eq. (17) can subsequently be used to calculate **L**. The fact that β is constant in the test setting implies a constant proportionality between the coronal plane force components J_y^* and

$\mathbf{J}_z^*$, generated *in vitro* by applying **L**. However, during the *in vivo* loading cycle, the proportionality between the force components $\mathbf{J}_y$ and $\mathbf{J}_z$ is variable. Hence, there is an intrinsic disparity between $\mathbf{J}_y^*$, $\mathbf{J}_z^*$ and $\mathbf{J}_y$, $\mathbf{J}_z$.

The solution to Eq. (17) allows calculation of **L** at any given instant of the gait cycle. For subsequent purposes of programming the Bionix machine to approximate **L** versus time in terms of a set of concatenated linear ramps. **L** was calculated at a series of specific instants during the gait cycle at which the data of Kotzar et al. showed distinct changes in one or more of the three hip contact force components (Figure 11). This allowed approximation of the force components, and consequently the *in vivo* JRF, in terms of piecewise linear continuous curves. This approximation divided the level walking waveform into eleven segments and the stair climbing waveform into nine segments.

It is noteworthy that in the experimental setup, the angle β of the hip contact resultant in the coronal plane depends only on the dimensions of the test apparatus (Eq. 22), and hence is an "investigator-controllable" constant during the loading cycle. Therefore, while at any general instant in the loading cycle there is a disparity between *in vitro* and *in vivo* hip contact force components, one can in principle choose a β that in some sense minimizes that disparity. It was determined that an analysis be performed to calculate an "optimum" β, termed $\hat{\beta}$, that minimized the disparity between the *in vitro* and *in vivo* hip contact resultants by minimizing the sum of the disparities from each segment of the loading cycle waveform. The specimen position corresponding to $\hat{\beta}$ was defined as the "optimum specimen position".

To determine $\hat{\beta}$, one must recall that the internal test apparatus dimensions, d_1 - d_6, are not fixed apriori. Rather, the only dimensional requirements are that standard anatomic orientations be maintained for the femur and the abductor strap. Consequently,

after proper orientation, the brackets of the test apparatus can be translated along the hemi-pelvis bar, i.e. in the ML direction, and the support fixture slid across the MTS base by the same amount, without compromising the integrity of the specimen orientation (Figure 8). Translation of the apparatus in the ML direction only affects the dimensions

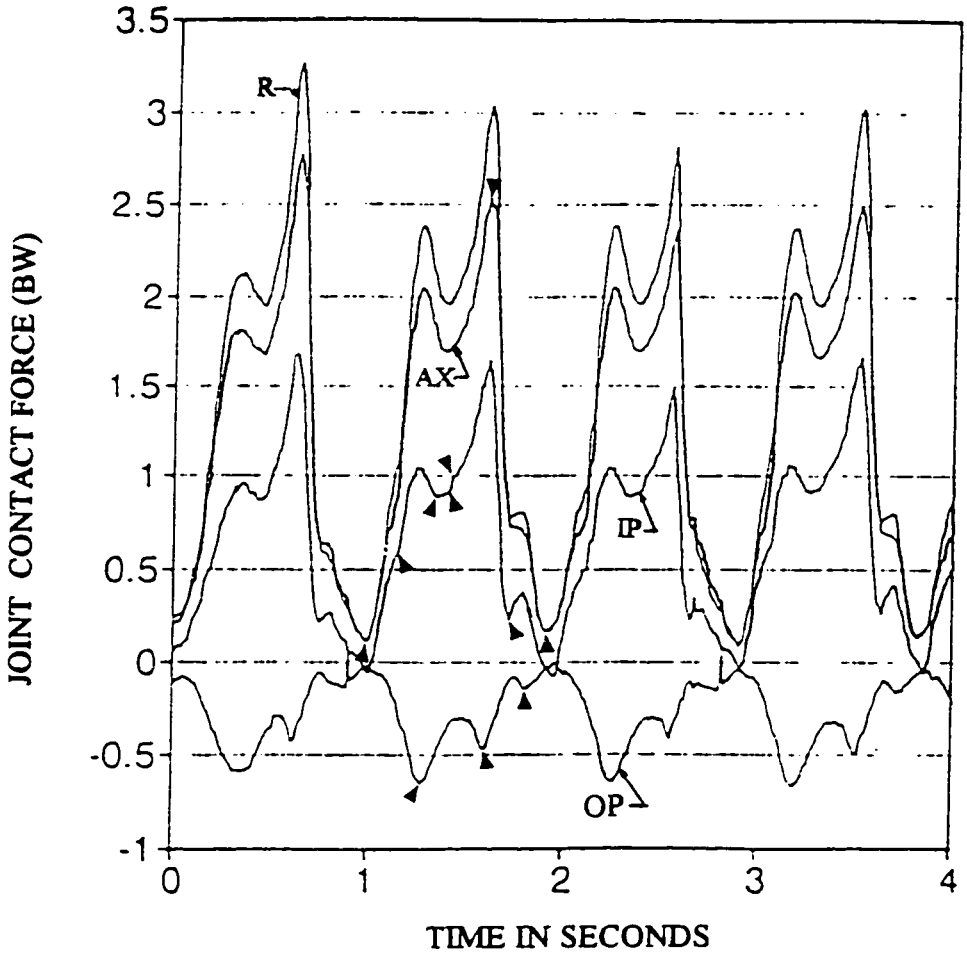

Figure 11. Level walking gait waveform. The arrowheads indicate the instants used to create a piecewise linear approximation of the waveforms. AX represents force along the neck of the prosthesis, IP represents force perpendicular to the neck in the plane of the prosthesis, OP represents force perpendicular to the neck normal to the plane of the prosthesis, and R is the resultant force magnitude.

Source: Reprinted from Kotzar et al. 1991.

d_2 and d_3 (Figures 9 and 10). (The other dimensions must remain constant to insure proper specimen orientation). Thus, from the relation derived in Eq. (22), β depends on d_2 and d_3, and since translation of the apparatus in the ML direction changes d_2 and d_3 by the same amount, β was considered to be only a function of d_3. The actual process of calculating the "optimum specimen position" was pursued algebraically by calculating the optimal value $\hat{d}_3$.

The process of determining $\hat{d}_3$ began by solving for d_3 as a function of the *in vivo* loads from the hemi-pelvis coronal plane system of equations (Eqs. (12), (13), and (14)). For this solution, both the magnitude and line of action of **J** were treated as known quantities. The solution was determined in the following manner:

By defining the term $q=d_2/d_1$, Eqs. (12) and (14) can be written in condensed form:

$$q\mathbf{L} + \mathbf{F}_A \sin 15° + \mathbf{J}_y = 0 \tag{23}$$

$$(d_3 - qd_6)\mathbf{L} - (d_4 \cos 15° + d_5 \sin 15°)\mathbf{F}_A = 0. \tag{24}$$

Eqs. (23) and (13) can each be solved for L:

$$\mathbf{L} = \frac{-\mathbf{F}_A \sin 15° - \mathbf{J}_y}{q}. \tag{25}$$

$$\mathbf{L} = -\mathbf{F}_A \cos 15° - \mathbf{J}_z. \tag{26}$$

Setting the corresponding expressions for **L** equal:

$$\mathbf{F}_A \cos 15° + \mathbf{J}_z = \frac{\mathbf{F}_A \sin 15° + \mathbf{J}_y}{q}. \tag{27}$$

Substituting the expression for **L** from Eq. (26) into the moment equilibrium equation, Eq. (24), gives:

$$(-\mathbf{F}_A \cos 15° - \mathbf{J}_z)(d_3 - qd_6) = \mathbf{F}_A (d_4 \cos 15° + d_5 \sin 15°). \tag{28}$$

Expanding:

$$-\mathbf{J}_z (d_3 - qd_6) = \mathbf{F}_A \left[\cos 15° (d_3 - qd_6) + d_4 \cos 15° + d_5 \sin 15°\right].$$

Solving for $\mathbf{F}_A$:

$$\mathbf{F}_A = \frac{-\mathbf{J}_Z (d_3 - qd_6)}{\left[\cos 15° (d_3 - qd_6) + d_4 \cos 15° + d_5 \sin 15°\right]} \tag{29}$$

Next, solve Eq. (27) for $\mathbf{F}_A$:

$$\mathbf{F}_A = \frac{\mathbf{J}_y - q\mathbf{J}_z}{(q \cos 15° - \sin 15°)}. \tag{30}$$

Then equate the right-hand sides of Eqs. (29) and (30), and multiply each denominator by $1/\cos 15°$ (note that $\tan 15° = 0.268$) to obtain:

$$\frac{\mathbf{J}_y - q\mathbf{J}_z}{(q - 0.268)} = \frac{-\mathbf{J}_z (d_3 - qd_6)}{\left[(d_3 - qd_6) + d_4 + 0.268 d_5\right]}. \tag{31}$$

Eq. (31) is then cross multiplied, like terms (i.e. $d_3 q$ and q^2) canceled, and terms containing d_3 and q collected on the left side of the equation and factored:

$$d_3 (\mathbf{J}_y - 0.268\mathbf{J}_z) + q(0.268 d_6 \mathbf{J}_z - d_6 \mathbf{J}_y - d_4 \mathbf{J}_z - 0.268 d_5 \mathbf{J}_z) = -d_4 \mathbf{J}_y - 0.268 d_5 \mathbf{J}_y \tag{32}$$

Eq. (32) can be written in the more compact form:

$$d_3 (\mathbf{J}_y - 0.268\mathbf{J}_z) + qk_2 = -d_4 \mathbf{J}_y - 0.268 d_5 \mathbf{J}_y. \tag{33}$$

where:

$$k_2 = 0.268 d_6 \mathbf{J}_z - d_6 \mathbf{J}_y - d_4 \mathbf{J}_z - 0.268 d_5 \mathbf{J}_z.$$

Substituting for q (= d_2/d_1) and multiplying both sides of Eq. (33) by d_1 allows solution for d_3:

$$d_3 d_1\left(\mathbf{J}_y - 0.268\mathbf{J}_z\right) + d_3 k_2 - d_7 k_2 = -d_1 \mathbf{J}_y\left(d_4 - 0.268 d_5\right)$$

$$d_3\left[d_1\left(\mathbf{J}_y - 0.268\mathbf{J}_z\right) + k_2\right] = d_7 k_2 - d_1 \mathbf{J}_y\left(d_4 - 0.268 d_5\right)$$

$$\boxed{d_3 = \frac{d_7 k_2 - d_1 \mathbf{J}_y\left(d_4 - 0.268 d_5\right)}{\left[d_1\left(\mathbf{J}_y - 0.268\mathbf{J}_z\right) + k_2\right]}}. \qquad (34)$$

Knowing d_3 as a function of the *in vivo* load at any given instant allowed calculation of $\hat{d}_3$ by trial and error. First, a specimen was properly oriented in the MTS machine and the appropriate test apparatus dimensions measured, including d_2 and d_3. Next, d_3 was calculated from the *in vivo* data using Eq. (34), for four instants during normal gait. Specifically, the instants were those at which the maximum magnitudes of $\mathbf{J}_y$, $\mathbf{J}_z$, $\mathbf{J}$, and JRF occur. In turn, β, $\mathbf{L}$, $\mathbf{J}_y^*$, and $\mathbf{J}_z^*$ were calculated for each of these four d_3 values. The criterion for choosing $\hat{d}_3$ was based on minimizing the error between the *in vitro* and *in vivo* force components acting in the z-direction. The specific error function minimized was the average of the individual errors occurring at the four discrete instants at which d_3 was evaluated. Minimization of the z-component error was used because its magnitude is two to six times the magnitude of the y-component during normal gait. The minimum error for both level walking and stair climbing gaits occurred when $\hat{d}_3$ was calculated using the maximum coronal plane resultant force, $\mathbf{J}_{max}$.

In summary, three specimen positions were analyzed. The initial position was used to orient the specimen in anatomical position and to measure the apparatus dimensions d_1, d_4, d_5, and d_6. Next, $\hat{d}_3$ was calculated for both level walking and stair climbing gait cycles. The specimen was then translated to (and analyzed for), one of the optimum positions, depending on which loading cycle was to be applied.

3.1.2.2.3 Out-of-Plane Forces

Ideally, the test apparatus would allow application of a force to the prosthesis head, directed in the AP direction, to simulate the *in vivo* data. Determination of the relationship between the out-of-coronal-plane forces and the applied torque, derived from the solution for the reaction forces:

$$\mathbf{R}_{x2} = \mathbf{R}_{x3} = 0 \tag{7}$$

$$\mathbf{T} = -\mathbf{M}_z \tag{11}$$

revealed that the test apparatus resists applied torque with a moment (force couple) at P_2 and no AP reaction force is generated in the setup (recall that the x-direction was defined parallel to the AP axis). With no AP reaction force there can be no AP force generated at the head of the prosthesis. Changing either of the two universal joints to pinned joints would generate an AP reaction force and possibly enable generation of an AP force at the head of the prosthesis. However, this structural change would cause the corresponding system of equations for static equilibrium of the test apparatus (Eqs. (1) - (6)) to be indeterminate, having seven unknowns and only six equations. Consequently, the applied torque, T, was set equal to the torque the *in vivo* AP force generates about the prosthesis stem. The *in vivo* torque was calculated by multiplying the AP force, J_x, by the distance from the head of the prosthesis to the centerline of the stem, termed r. (this distance was measured from the vendor supplied templates). Hence, the value of T was calculated from the following equation:

$$\mathbf{T} = r\mathbf{J}_x. \tag{35}$$

Applied as a pure couple, which is a free vector, T can be considered to act equivalently about any parallel axis. If perfectly aligned with the femur the prosthesis stem is oriented 15° from vertical, reducing the applied stem torque by 3%. However,

because the actual stem angle depended on the surgical technique and could change during loading (which was qualitativley observed to occur for the loose/tight specimens and tight/loose specimens) no adjustment was made for the prosthesis stem not being parallel to the Bionix rotation axis.

3.1.2.2.4 Experimental Validation of the Applied Load Analysis for the Femur

The Bionix was digitally controlled via a personal computer. Programs to apply loads and collect data (one program for level walking gait and one for stair climbing gait) were created using vendor-supplied software (TestWare-SX) running on a desktop computer (Compaq Deskpro 486s/20). A subroutine within the programs concatenated a series of axial and torsional ramp loads so as to simulate the dynamic loading patterns observed *in vivo*. The concatenated series of axial and torsional ramps were used to create a load cycle for each gait type, i.e. level walking or stair climbing load cycle.

Results from the coronal plane analysis indicate instantaneous errors between *in vivo* and *in vitro* coronal plane force components to be less than 8% of the maximum *in vivo* JRF. The maximum *in vivo* JRF reported by Kotzar et al. was 2.84 times body weight (BW) for level walking and 2.04 times body weight for stair climbing. The maximum instantaneous error calculated for $\mathbf{J}_y$* was 0.21 BW for level walking and 0.16 BW for stair climbing. The corresponding errors for $\mathbf{J}_z$* were 0.08 BW and 0.06 BW respectively. For both gait cycles $\mathbf{J}_z$* was within three percent of $\mathbf{J}_z$, except at one instant during the stair climbing load cycle.

The load analysis showed that the applied actuator torque would not generate an AP force component acting on the head of the prosthesis. Instead, the applied torque was calculated to exactly match the stem torque corresponding to the observed *in vivo* AP

force component. Due to the orientation of the femur in the test apparatus, an error of 3% exists between the *in vivo* stem torque and calculated *in vitro* stem torque.

The difference between measured *in vitro* force components and calculated *in vitro* force components depends solely on the Bionix system and in principle should be small. The load waveform of *in vitro* and *in vivo* force components for both level walking (Figures 12, 13, and 14) and stair climbing was charted. The comparison was indirect because the *in vitro* force components were not measured directly, but rather were calculated from measured values of **L** and **T**. The time histories of the *in vitro* component forces indicated that the test apparatus/MTS machine system accurately reproduced the calculated waveforms for **L** and **T**. The error between the resultant JRF calculated from measured values of **L** and **T** and the *in vivo* resultant JRF was less than 8% of the maximum *in vivo* JRF during the level walking and stair climbing load cycles.

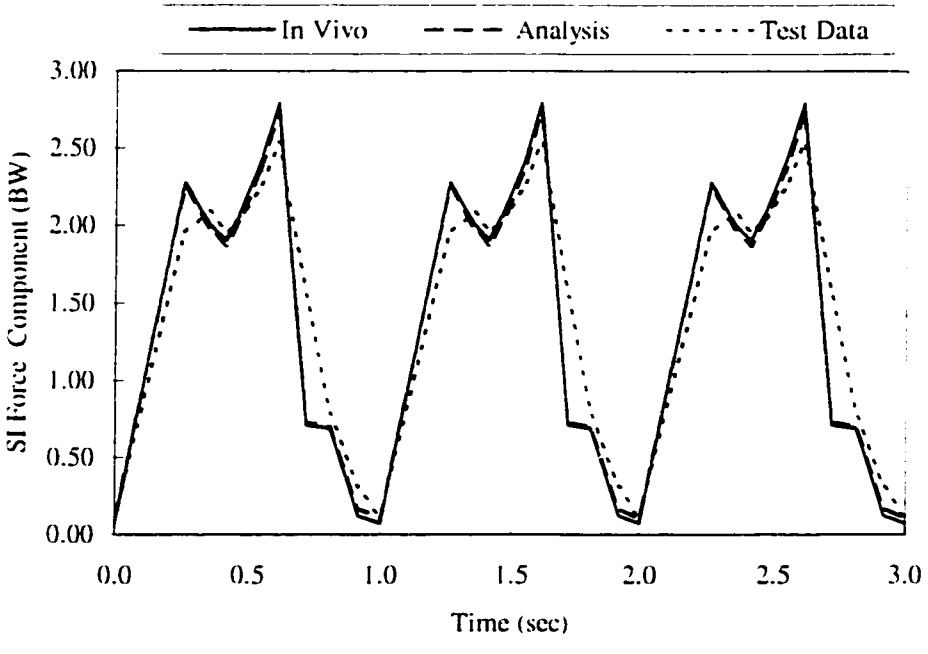

Figure 12. Comparison of the SI force component of the JRF observed *in vivo*, calculated from the load analysis, and calculated from test data.

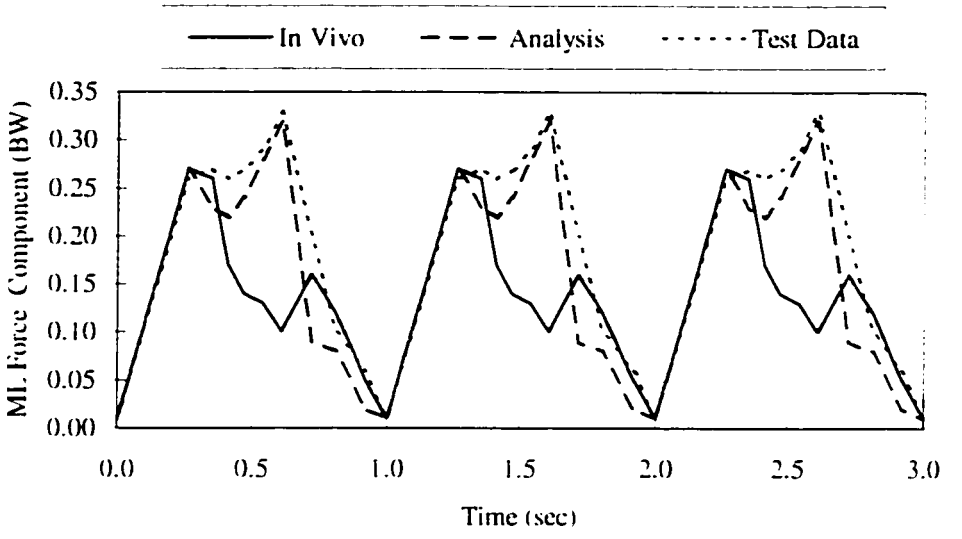

Figure 13. Comparison of the ML force component of the JRF observed *in vivo*, calculated from the load analysis, and calculated from test data.

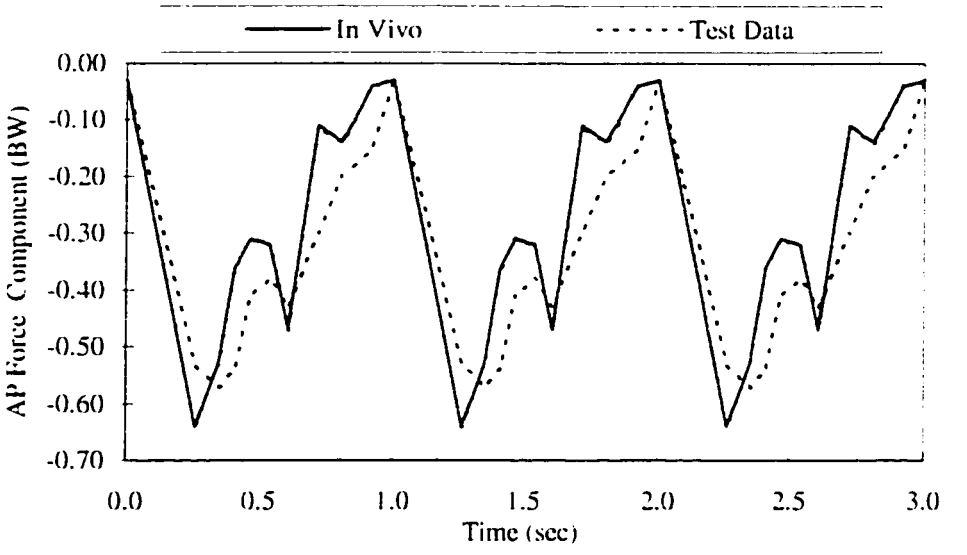

Figure 14. Comparison of the AP force component of the JRF observed *in vivo*. In this instance, since the applied actuator torque **T** could be modulated to produce the desired *in vivo* AP force waveform, there was no "error" between the *in vivo* and theoretically applied waveform.

During the pilot runs conducted to verify the applied actuator loads **L** and **T**, the specimen was observed to rotate out of the coronal plane up to five degrees, and the bar of the hemi-pelvis fixture pivoted about the head of the prosthesis typically ten to fifteen degrees. This behavior called into question the assumption of coronal plane containment of the abductor muscle strap, and made it seem prudent to validate the accuracy of the free-body equilibrium analysis. One potential method to verify the forces acting on the head of the prosthesis would be by attaching strain gages at the neck, as has been done for instrumented prostheses by Kotzar et al. (1991) and Bergmann et al. (1993). However, this is a difficult and complicated task to undertake simply for the purpose of validating a mathematical analysis. As an alternative, validation of the coronal loads was achieved by measuring the force in the abductor chain and comparing it to the calculated abductor force. This was accomplished by installing a proving ring in the abductor chain, and applying static and dynamic loading to the specimen. The measured abductor loads were within five per cent of the calculated loads over the entire gait cycle (Figure 15), an outcome which verified that there were no conceptual or algebraic errors in the (rather complex) free-body analysis. Also this indicated that the observed motion of the hemi-pelvis fixture did not appreciably affect coronal plane loads.

An additional series of tests using a modified test apparatus further verified the free-body assumptions regarding out-of-plane loading. First, the z-axis moment constraint of the support fixture was removed, to see if any AP force developed under static torsional loading. As predicted, the specimen rotated freely. Next, to determine if an "out-of-plane" abductor strap could resist torque, a specimen was tested with the strap left slack. The specimen was then loaded with the applied torque portion of the level walking load cycle, but with the axial load set to zero. The apparatus rotated the same amount, approximately 5°, as during normal tests, indicating that the abductor strap does

not contribute to resisting the applied torque. Lastly, the torque data from the test with a slack abductor strap were compared to torque data under normal setup conditions. The torque data were the same, thus supporting the assumption that coronal plane forces and AP directed forces are indeed independent of each other for the defined test setup and that twist of the test setup does not significantly affect the applied loads.

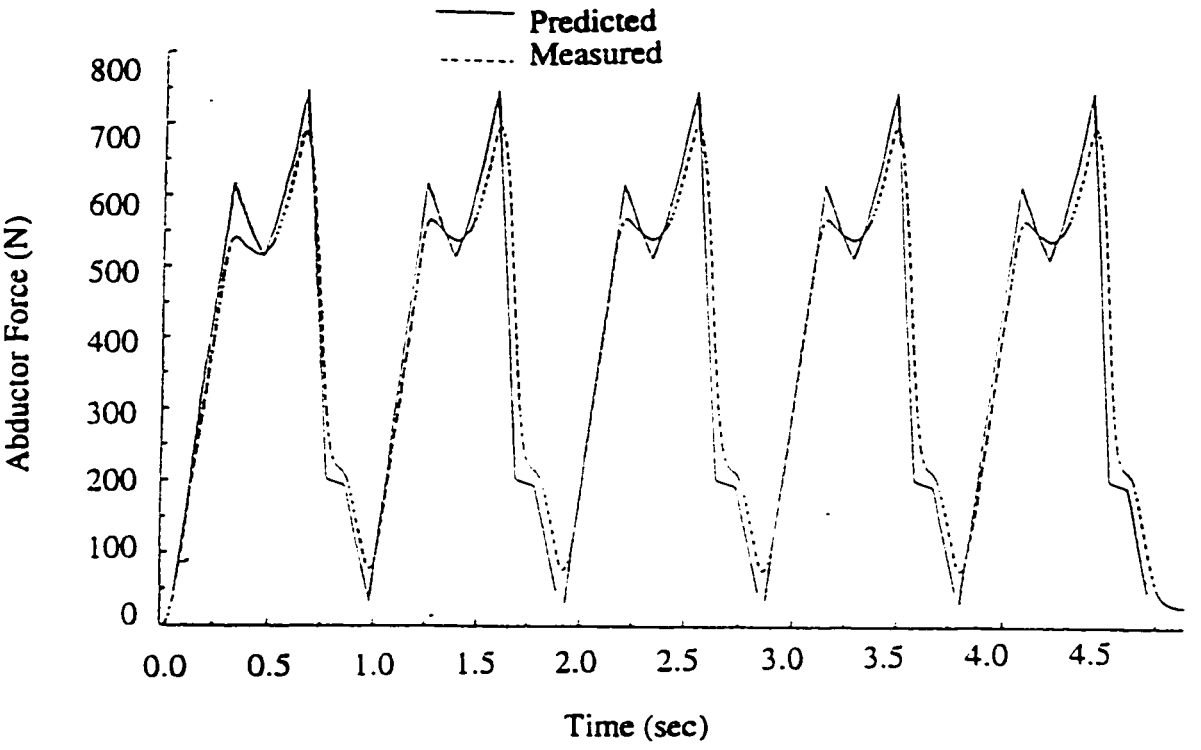

Figure 15. Comparison of calculated abductor chain force to that measured during testing.

3.1.2.3 Loading Protocol

The femur loading protocol consisted of 1000 loading cycles, divided into 980 level walking (LW) load cycles and 20 stair climbing (SC) load cycles. The load cycles were further sub-divided into ten load series (Table 1). Data were recorded over the last

five load cycles of each load series (i.e. load cycles 1-5, 6-10, 51-55, 56-60, 101-105, 106-110, 151-155, 251-255, 256-260, and 996-1000) except in the last load series, where data were also recorded during cycles 501-505. Stair climbing data capture load cycles immediately followed level walking data capture load cycles to allow for the most direct comparison of results for these alternative loading conditions. The large number of cycles was considered necessary to ensure data were recorded under conditions where subsidence had ceased. The sampling rate was 100 Hz.

Table 1. Femoral component load regimen.

Load Series	Cycle Number	Gait Type	Load Series	Cycle Number	Gait Type
1	1-5	LW	6	105-110	SC
2	6-10	SC	7	111-155	LW
3	11-55	LW	8	156-255	LW
4	56-60	SC	9	256-260	SC
5	61-105	LW	10	261-1000	LW

3.1.3 Calculation of Micromotion

Calculation of relative interfacial motion between the prosthesis and the bone, i.e. micromotion, was accomplished in two steps. First, relative displacements between the prosthesis and femur were measured at three points. A rigid-body motion analysis was then performed, using the measured displacements to calculate the micromotion at any point on the surface of the prosthesis.

3.1.3.1 Measurement of the Relative Displacement of the Prosthesis

Relative displacements between the bone and prosthesis were measured using liquid metal strain gages (LMSGs). A gage fixture was designed to allow measurements

in three orthogonal directions (Figure 16). The fixture consisted of an outrigger attached to the prosthesis, an outrigger attached to the specimen, a block, and a frame. The

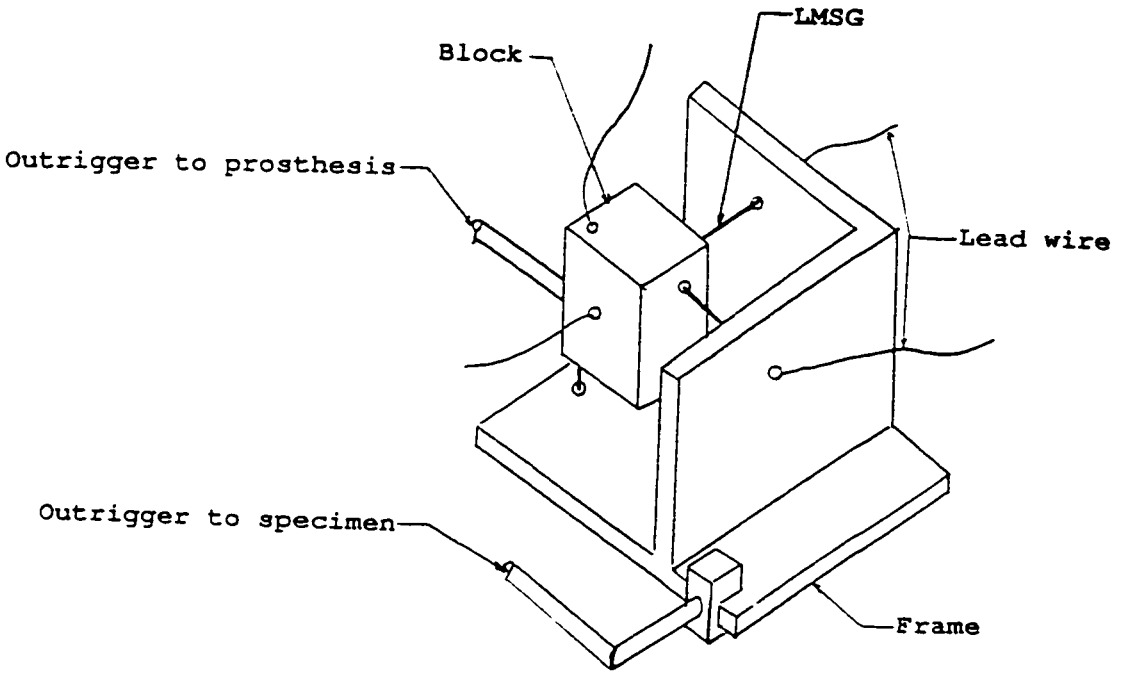

Figure 16. Schematic of femoral gage fixture.

prosthesis outrigger was screwed into the prosthesis through a hole pre-drilled through the specimen cortex. The specimen outrigger was attached to the femur via a circular clamp at the same level as the prosthesis outrigger. The block and frame were connected to the prosthesis and specimen outriggers, respectively. Consequently, relative displacements between the prosthesis and bone created relative displacements between the block and frame. LMSGs stretched between the block and frame measured the relative displacements in three orthogonal directions. The rigid-body motion analysis required the displacement of a specific point to be measured. This could be accomplished with LMSGs only if three orthogonal gages intersected at one point. This would require a

much more complicated fixture. The point of measurement was defined as the end of the outrigger, whose location was at the center of a fictitious cube defined by using the three orthogonal gage axes as three non-intersecting edges of the cube.

3.1.3.1.1 Liquid Metal Strain Gages

The liquid metal strain gage measures the change in resistance of a mercury column encased in a silastic tube. Electrical resistance of the gage is related to the length and cross-sectional area of the mercury column. Changes in the length and cross-sectional area of the column result from straining the gage.

The resistance of a slack LMSG is approximately 1 ohm (Ω). The gages were placed in series with a 120 Ω resistor to comprise the active arm of a nominal 120 Ω Wheatstone bridge circuit. Sensitivity varies from gage to gage, but was observed to be relatively consistent for a specific gage from test to test. The average sensitivity for the gages was 10 μm/mV, ranging from 7 - 12 μm/mV. The gage analog signal was amplified and digitized by a DC signal conditioner internal to the MTS hardware. Settings for the amplifier (bridge excitation voltage = 5 V, gain = 10,000) produced a resolution of approximately 1 mV, corresponding to an overall positional resolution of approximately 10 μm.

The LMSG relationship between gage response and engineering strain is minimally nonlinear below 10% strain (Brown et al. 1986). The pre-test calibration eliminated the effects of non-linearity by determining the voltage range where the output was linear. Then, when placed in the gage fixtures, the gages were pre-stretched until their output was within the linear range. The gages were also calibrated after testing, with the average of the two calibrations being used in subsequent calculations to minimize the effects of drift. The relative change in calibration factors ranged from 1% to 8%.

3.1.3.2 Rigid-body Analysis

Assuming both the femur and prosthesis to be rigid bodies, a technique was developed to determine micromotion at any point on the surface of the prosthesis. The technique treated the femur as fixed. Consequently, relative motion measured between the prosthesis and specimen defines rigid-body displacement of the prosthesis. In turn, displacement of a point on the surface of the prosthesis describes the micromotion of the prosthesis relative to the femur at that point. By definition the displacement of an arbitrary point, D, on the surface of the prosthesis is the difference between its final (primed) position and its initial position:

$$\delta_D = \mathbf{D}' - \mathbf{D} = \text{micromotion at point D.} \tag{36}$$

D and **D'** can be determined for any global coordinate system in the following manner. First, define point Q, a point on the rigid body containing point D, as the origin of a body-fixed coordinate system. The initial position of point D in the global coordinate system is defined by the following equation:

$$\mathbf{D} = \mathbf{Q} + [R]\rho \tag{37}$$

where **Q** is the coordinate vector of point Q defined in the global coordinate system, ρ is the vector from point Q to point D defined in the body-fixed coordinate system, and [R] is the rotation matrix which transforms vectors from the body-fixed coordinate system into the global coordinate system. After general three-dimensional rigid-body motion the final position of point D in the global coordinate system is defined by the following equation:

$$\mathbf{D}' = \mathbf{Q}' + [R']\rho \tag{38}$$

where **Q'** is the coordinate vector of the final position of point Q defined in the global coordinate system, ρ is unchanged, and [R'] is the rotation matrix which transforms

vectors from the final orientation of the body-fixed coordinate system into the global coordinate system.

The minimum number of linear displacements to completely define rigid-body motion is seven. The technique described herein measured the required displacements of the prosthesis at three non-collinear points (three displacements at each of two points, and the seventh displacement at the third point). The remainder of the technique development describes the way in which initial test configuration dimensions and the seven measured displacements were used to determine the values on the right-hand side of Eqs. (37) and (38), and consequently the micromotion of any point on the surface of the prosthesis.

3.1.3.2.1 Definition of Coordinate Systems

A body-fixed, or outrigger, coordinate system was defined based on the locations of the three non-collinear points where the required displacement measurements were recorded, i.e. at the end of the prosthesis outriggers. Two outriggers were positioned anteriorly, one located proximally in the porous-coated region, and the other located 1.25 cm proximal to the distal tip of the prosthesis. The free ends of these outriggers were defined as points A and B respectively. The third outrigger was positioned posteriorly in the porous-coated region. Point C was defined at the free end of the third outrigger. Axes of the outrigger coordinate system were defined as follows: the i-axis lies along the proximal outriggers directed from point C to point A (alignment was ensured by threading these two outriggers into a common threaded hole); the k-axis lies along the vector from point B to point A; and the j-axis is determined from the cross product of $\mathbf{k}$ and $\mathbf{i}$. This formulation implies the vectors **CA** and **BA** are perpendicular. This was not strictly the case. Positions of the outriggers minimized the deviation from perpendicular to 3° or less. This magnitude of deviation had no effect on the calculated micromotion. The origin of the local coordinate system was located at point A (Figure 17). The initial

positions of points A, B, and C in the outrigger coordinate system were measured with a vernier caliper. Coordinate accuracy equaled ±0.5 mm.

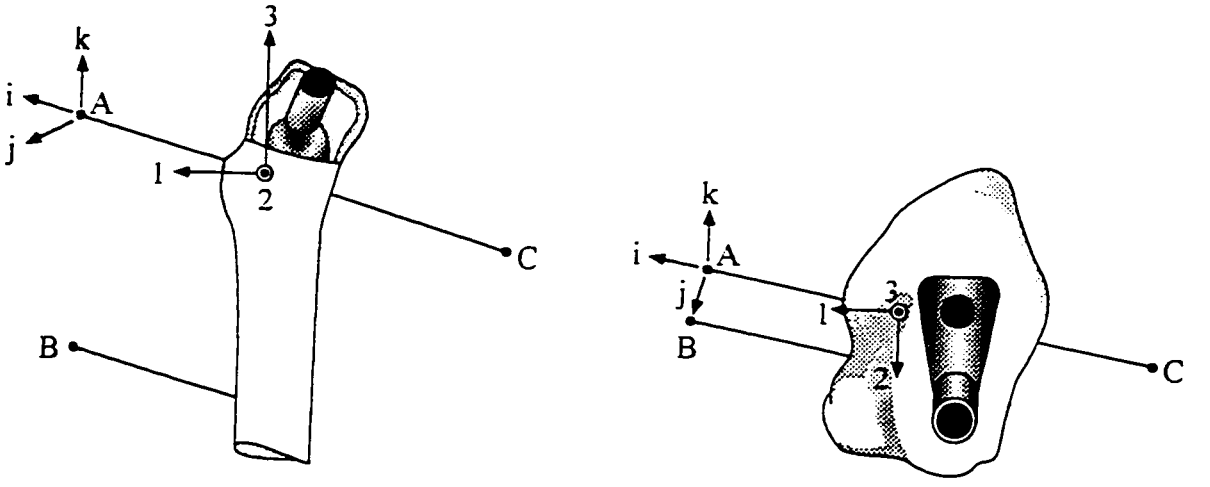

Figure 17. Schematic of medial (left) and top (right) views of the femur showing the outrigger and femur coordinate systems.

For ease in interpretation of the data, micromotion was calculated in the directions of the standard anatomic reference frame. To this end, a femur coordinate system was defined as being parallel to the standard anatomic reference frame and fixed with respect to the femur. Femur coordinate system axes were defined as the 1, 2, and 3 directions (Figure 17). Coordinate system orientation aligned the 1, 2, and 3 axes parallel to the AP, ML, and SI axes, respectively. The origin of the femur coordinate system was defined as the location where the outrigger to point A entered the prosthesis.

3.1.3.2.2 Calculation of the rotation matrix [R]

The expression for the rotation matrix [R] to convert vectors from the outrigger coordinate system into the femur coordinate system was developed using the same

method as that used to determine Euler angles for airplanes (Greenwood, 1965). This method generates a rotation matrix to transform from the fixed reference frame into the body reference frame, i.e., from the femur coordinate system into the outrigger coordinate system. To transform in the opposite (desired) direction, the inverse of the rotation matrix must be used (where $c\theta_1 = \cos\theta_1$, $s\theta_1 = \sin\theta_1$, etc.):

$$[R] = \begin{bmatrix} c\theta_2 c\theta_3 & s\theta_1 s\theta_2 c\theta_3 - c\theta_1 s\theta_3 & s\theta_1 s\theta_3 + c\theta_1 s\theta_2 c\theta_3 \\ c\theta_2 s\theta_3 & c\theta_1 c\theta_3 + s\theta_1 s\theta_2 s\theta_3 & -s\theta_1 c\theta_3 + c\theta_1 s\theta_2 s\theta_3 \\ -s\theta_2 & s\theta_1 c\theta_2 & c\theta_1 c\theta_2 \end{bmatrix}. \quad (39)$$

The three rotations, namely θ_1, θ_2, and θ_3, were defined in the following manner. The outrigger and femur coordinate systems were initially coincident. The first rotation θ_1 was about the i-axis (since the i-axis began coincident to the 1-axis this angle was 12° for each specimen based on the orientation of the femur in the test apparatus), resulting in the first intermediate coordinate system. The second rotation θ_2 was about the first intermediate j-axis, resulting in a second intermediate coordinate system. The third rotation θ_3 was about the second intermediate k-axis, resulting in the final outrigger coordinate system. Angles were measured using an angle finder with an accuracy of 1°.

3.1.3.2.3 Calculation of the final rotation matrix [R']

The rotation matrix [R'] was calculated from the final position vectors of points A, B, and C in the femur coordinate system, namely $\mathbf{A'}$, $\mathbf{B'}$, and $\mathbf{C'}$. The final positions of points A, B, and C in the femur coordinate system are:

$$\mathbf{A'} = [R](\mathbf{A} + \delta_A) \quad (40)$$

$$\mathbf{B'} = [R](\mathbf{B} + \delta_B) \quad (41)$$

$$\mathbf{C'} = [R](\mathbf{C} + \delta_C) \quad (42)$$

where **A**, **B**, and **C** are the initial coordinates of points A, B, and C in the outrigger coordinate system, and δ_A, δ_B, and δ_C are the displacements in the outrigger coordinate system of the same points. With the final positions of points A, B, and C in the femur coordinate system determined, the unit vectors of the final outrigger coordinate system can be calculated from the following equations:

$$\mathbf{i}' = \frac{(\mathbf{A}'-\mathbf{C}')}{|\mathbf{AC}|}, \quad \mathbf{k}' = \frac{(\mathbf{A}'-\mathbf{B}')}{|\mathbf{AB}|}, \quad \mathbf{j}' = \mathbf{k}' \times \mathbf{i}'. \tag{43}$$

Finally, [R′] is constructed from the components of the primed unit vectors:

$$[R'] = \begin{bmatrix} i_1' & j_1' & k_1' \\ i_2' & j_2' & k_2' \\ i_3' & j_3' & k_3' \end{bmatrix}. \tag{44}$$

It was necessary to measure only seven of the nine displacements required to solve Eqs. (40)-(42). Two orthogonal gage triads measured displacements at points A and B. A seventh gage located at point C measured displacement in the j-direction, i.e. δ_{Cj}. Gage fixture orientation aligned the LMSGs parallel to the axes of the outrigger coordinate system (Figure 18).

The two displacements not measured were calculated in the following manner. The assumption that the prosthesis is a rigid body implies that the distances between points A, B, and C (the ends of the specimen outriggers) remain unchanged. Thus,

$$L_{AC}^2 = \left(C_i' - A_i'\right)^2 + \left(C_j' - A_j'\right)^2 + \left(C_k' - A_k'\right)^2 \tag{45}$$

$$L_{BC}^2 = \left(C_i' - B_i'\right)^2 + \left(C_j' - B_j'\right)^2 + \left(C_k' - B_k'\right)^2 \tag{46}$$

where L_{AC} and L_{BC} are the distances between points A and C and B and C, respectively.

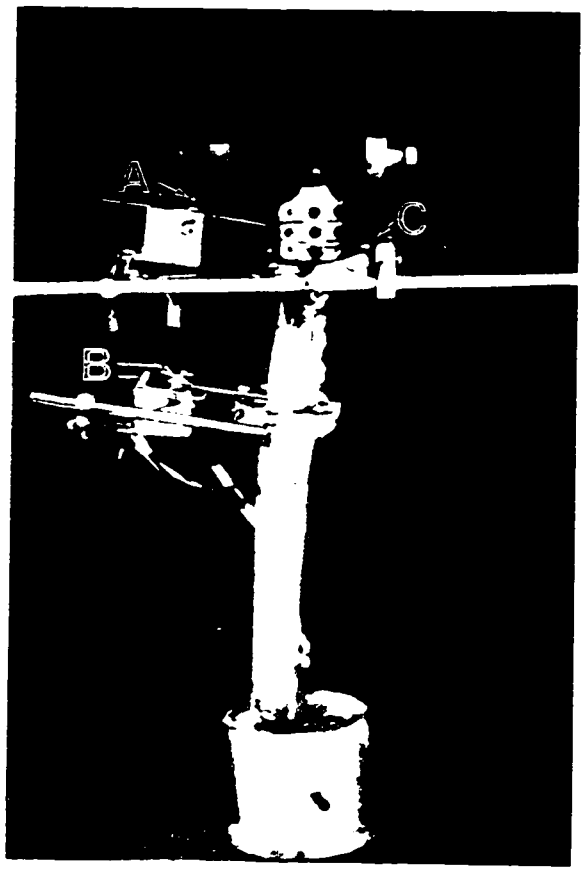

Figure 18. Picture of gage fixtures attached to the femur.

Solving Eqs. (45) and (46) simultaneously, the following expressions for C_i' and C_k' are obtained:

$$C_i' = -H_2 \pm \sqrt{H_2^2 - 4H_1H_3} \tag{47}$$

$$C_k = G_1 - C_i'G_2 \tag{48}$$

where

$$G_1 = \left[\frac{L_{BC}^2 - L_{AC}^2 + (A_j - C_j)^2 - (B_j - C_j)^2 + A_i^2 - B_i^2 + A_k^2 - B_k^2}{2(A_k - B_k)} \right]$$

$$G_2 = \frac{A_i - B_i}{A_k - B_k}$$

$$H_1 = G_2^2 + 1$$

$$H_2 = 2\left[G_2\left(A_k - G_1\right) - A_j\right]$$

$$H_3 = -\left[L_{AC}^2 - \left(A_j - C_j\right) - A_1^2 - A_k^2 + 2A_k G_1 - G_1^2\right].$$

The non-unique solution for C_i' from Eq. (47) was resolved by computing both solutions, and because the displacements were small compared to the magnitude of the position vectors, the solution closest to the previous location was used.

3.1.3.2.4 Calculation of ρ

The only remaining term from Eqs. (37) and (38) not yet determined is ρ. To determine this vector, coordinates of points on the prosthesis must be known in the outrigger coordinate system. To obtain the desired coordinates a plaster cast of each femoral prosthesis was made. The casts were made from dental alginate molds. Indentations of the screw holes (the mold and hence the cast included indentations at the screw holes where the outriggers attached) were used to define a cast-based coordinate system with axes parallel to the outrigger coordinate system axes. The positions of 122 points on the cast were recorded in the cast-based coordinate system using a three-dimensional digitizer (3-Space Digitizer, Polhemus, Colchester, VT), and subsequently were transformed into the outrigger coordinate system. Qualitative fidelity of the casts was excellent, in that even the texture of the porous-coated region was captured. Quantitative accuracy of the casts was determined by comparing various dimensions of the cast with those of the prosthesis, using a vernier caliper. The maximum observed error in prosthesis dimensions was 0.2 mm.

3.1.3.2.5 Validation of the Rigid-body Analysis

A computer program (FORTRAN programming language) was written, implementing the rigid-body motion technique developed above, to calculate micromotion at the 122 points on the prosthesis. A wire-frame computer model using nominal positions for points A, B, C, and two "points", D_1 and D_2, on the prosthesis was created in PATRAN, a finite element software package (MSC, Los Angeles, CA). Application of a three-dimensional rotation to the computer model generated an ideal set of "measured" displacement data for verification of the rigid-body motion technique. Displacements calculated for points D_1 and D_2 using the rigid-body motion program matched exactly the displacements calculated directly in PATRAN. Next, the ideal data from the PATRAN model was perturbed 10 - 30 μm. "Measured" gage displacements were perturbed individually and in random combinations. The perturbations caused less than 5% change in computed micromotion for points D_1 and D_2.

Bench top tests were used to additionally validate the rigid-body analysis, using real LMSG data. A special test fixture input known displacements into a mock gage fixture/prosthesis setup. The mock setup attached the gage fixture frames to a rigid fixed base and the gage fixture blocks to a rigid movable platform. A modified micrometer was used to input known one-dimensional displacements to the platform. Results showed the algorithm worked with real gage data. Lastly, the effect of inaccurate measurements of the initial test configuration was investigated by varying the coordinates of points A, B, and C by ±5.0 mm, the coordinates for all points on the prosthesis by ±2.0 mm, and the three angles measured to calculate [R] by ±5°. These perturbations produced less than 5% change in resultant micromotion calculations.

3.1.3.2.6 Validation of the Assumption of Rigid-Body Motion

To validate the rigid-body motion assumption, displacement data at a site independent (the outrigger for point B was moved from the anterior side to the posterior side of the prosthesis) of the normal gage locations were recorded. The measured data from the independent location were compared to the motion predicted by the rigid-body motion program at that location. Peak-to-peak micromotion differed by approximately 10 μm in the AP and ML directions, and by approximately 25 μm in the SI direction (Figures 19, 20, and 21). Resultant micromotion differed less than 5% (110 μm vs. 106 μm).

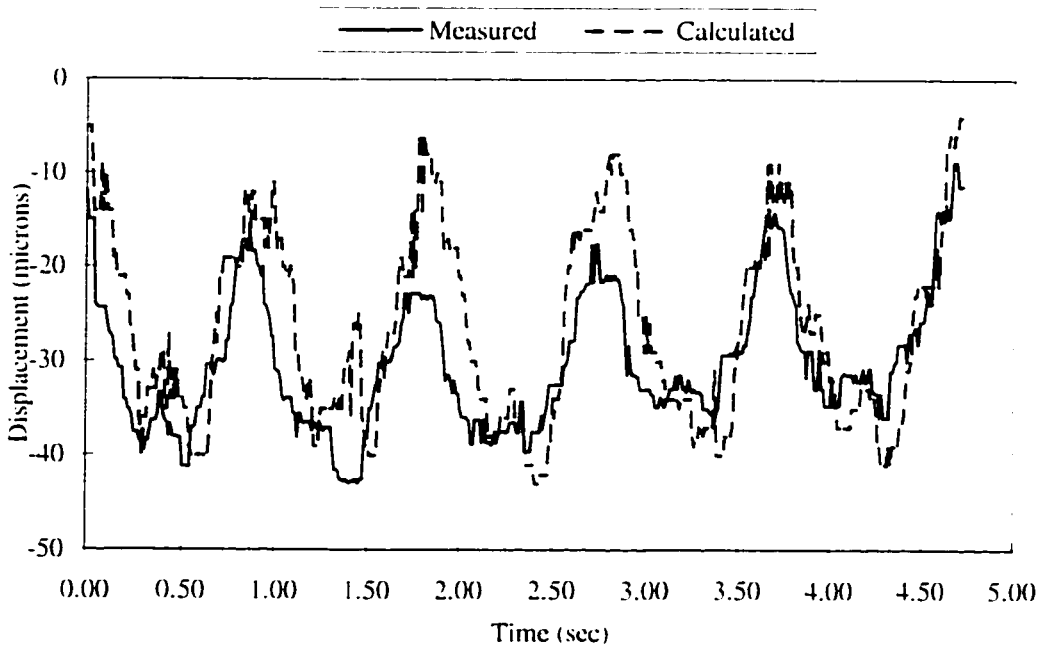

Figure 19. Plot of calculated vs. measured displacement in the AP direction at an arbitrary point.

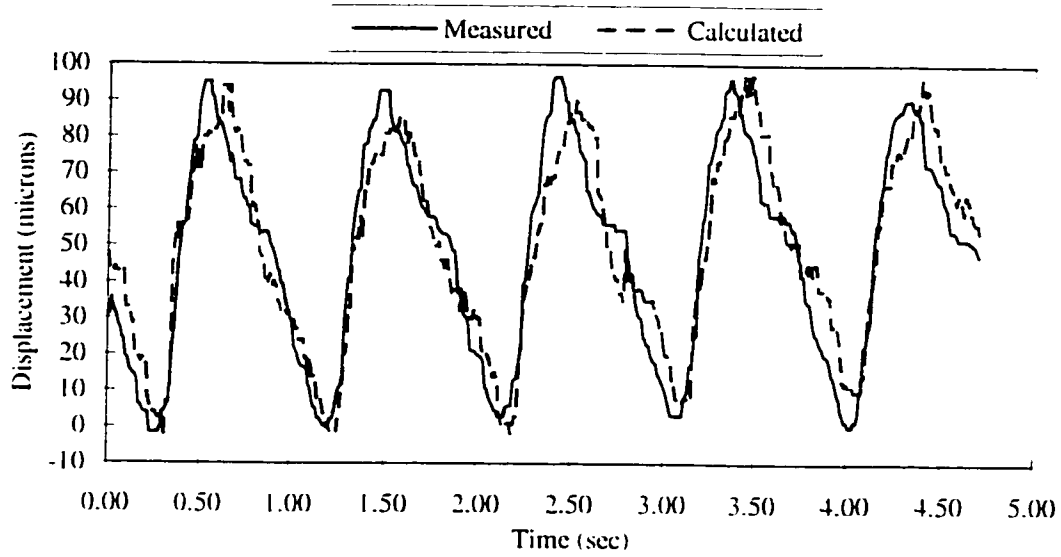

Figure 20. Plot of calculated vs. measured displacement in the ML direction at an arbitrary point.

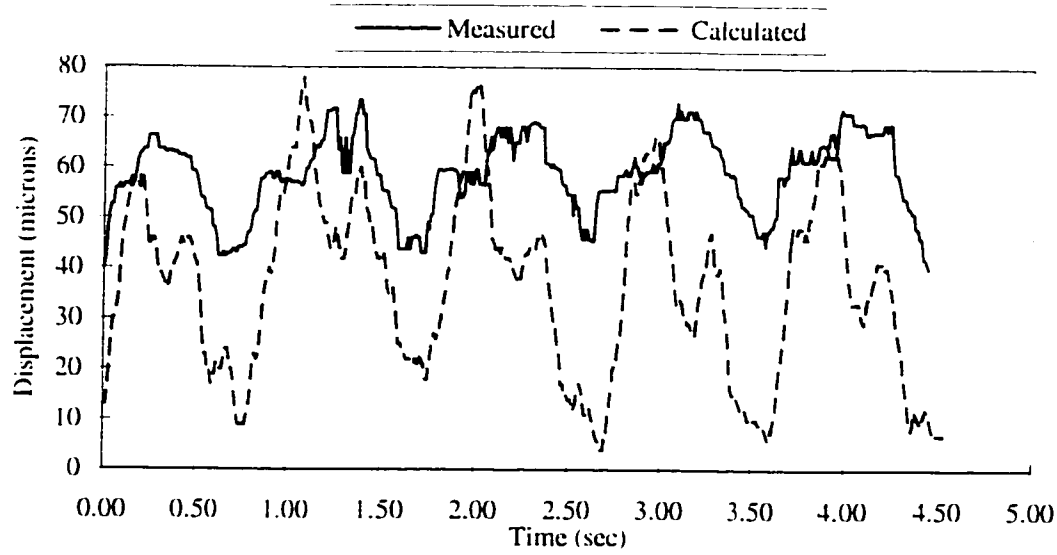

Figure 21. Plot of calculated vs. measured displacement in the SI direction at an arbitrary point.

3.1.4 Data Analysis

Prior to any calculations the data were filtered to remove noise from the recorded waveforms. The filtering process was performed using filtering algorithms that are part of the PV-WAVE image analysis software package (Precision Visuals, Boulder, CO). First, a median filter with a neighborhood of nine was applied. Second, a smoothing filter with a neighborhood of three was applied to the median-filtered data (Figure 22). A series of neighborhood sizes were examined for each filter to determine which combination maximized noise reduction without losing data information.

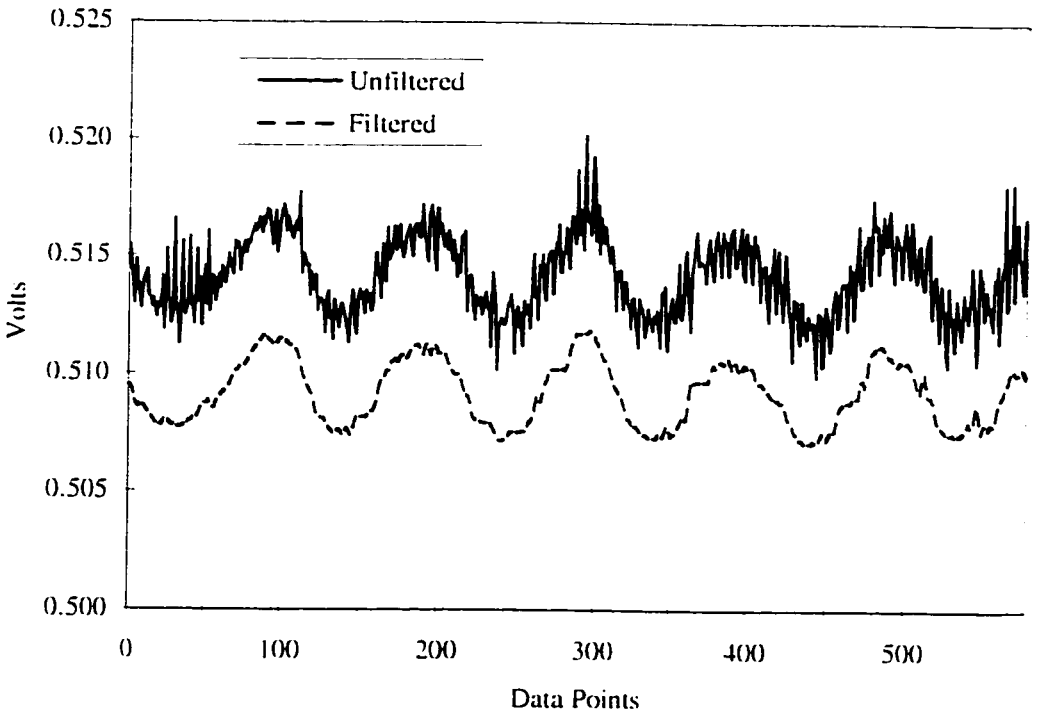

Figure 22. Example of the effect of applying median and smoothing filters to individual gage data, with curves offset for clarity.

3.1.4.1 Micromotion

The filtered data were input into the rigid-body motion program to calculate the maximum and minimum femur coordinates of the 122 digitized points on the prosthesis for each of five consecutive gait cycles, i.e. five maxima and five minima for each coordinate. Micromotion in each direction was defined as the difference between the average of the maxima and the average of the minima of the respective coordinates. Micromotion was defined by the maximum and minimum coordinate values because displacement from an initial position may underestimate the interfacial motion. For example, the extreme delta values for a point may be -10 μm and +15 μm, but the total relative interfacial micromotion is 25 μm (Figure 23, where P_0 is the initial position, and P_1 and P_2 are the extreme positions during the loading cycle). The total micromotion of each point is defined as the Pythagorean resultant of the three components of micromotion.

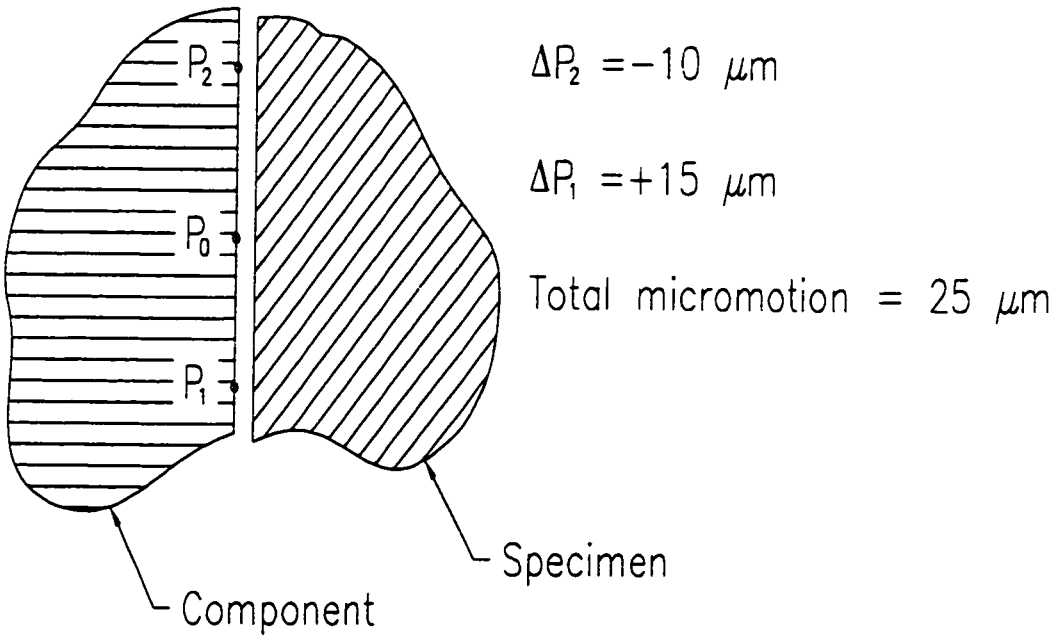

Figure 23. Schematic representation of micromotion in one direction.

Comparison of micromotion between different fit categories could not be made in a point-to-point manner because the locations of the 122 points used to compute motion were not consistent from one prosthesis to another (due to component size differences). Instead, comparisons were made using the percentage of the porous-coated region experiencing specific ranges of micromotion. The ranges of interest are: less than 50 μm, where bone ingrowth is likely to occur; 50 - 150 μm, where fibrous ingrowth is predicted; and greater than 150 μm, where no ingrowth is predicted to occur. The digitized points on the porous-coated region were used to divide it into trapezoidal areas. The micromotion attributed to each area was determined by averaging the micromotion of the four corner points. Comparisons between "distal" and "proximal" motion were made between values observed at the distal tip and the average of the motion observed for the center trapezoid of the anterior and posterior faces of the porous-coated region.

Models of each prosthesis were created in PATRAN using the digitized points. Displacement data from each point were supplied to the model and a contouring routine within PATRAN was run to assemble continuous mappings over the entire surface of the component.

3.1.4.2 Subsidence

Data profiles required manual calculation of subsidence. The process was very time consuming, so subsidence was only calculated at the distal tip and for the trapezoidal area at the center of the porous-coated region on the anterior surface of the prosthesis.

3.2 Experimental Procedure for the Acetabulum

3.2.1 Prosthesis Implantation

Sixteen acetabulae from eight fresh-frozen whole pelvis cadaver specimens, average age 74 years, were implanted with a noncemented cup from the Duraloc Acetabular Cup System (1200 Series, DePuy Inc., Warsaw, IN). The cup consists of a titanium hemi-spherical shell and a polyethylene liner. The shell has two concentric circles of holes for screw fixation. A porous coating made from titanium beads sintered to the shell covers the remaining outer surface (Figure 24).

Figure 24. DePuy 1200 series acetabular cup.

Standard operating procedure for the Duraloc cup calls for preparation of the acetabulum with a spherical reamer. Reaming begins with the largest reamer that easily

fits within the acetabulum. Reaming continues, using progressively larger reamers (incremented by 2 mm in diameter), until the appropriate depth is obtained. The appropriate depth depends on the surgeon's opinion of the bone stock. In this study reaming continued until the surface of the subchondral plate was removed. After completion of reaming a cup with the same diameter of the last reamer used was impacted into the acetabulum. This achieves what is termed an "on-line" fit even though the hemispheres of the cup and acetabulum are not exact matches due to the elasticity of the acetabulum.

3.2.2 Determination of Quasi-Physiologic Loads

The procedure for determining the *in vitro* loads to be applied to the acetabulum paralleled that of the femur. The test apparatus and load regimen attempted to match *in vivo* data from the same patient as for the femur. However, level walking and stair climbing load cycles resulted from analysis of different data bases. Unpublished data (Pedersen et al.) of forces acting on the pelvis were used to calculate the level walking load cycle. The pelvis data included muscle forces, and so were considered to more accurately represent forces acting on the acetabulum than simply the vectorial reaction of the prosthesis head force data. Unfortunately, no such muscle force data existed for stair climbing gait, so the femur data from Kotzar et al. (1991) were inverted using Newton's third law. As for the femur, both load histories were converted into the standard anatomic reference frame.

Also as for the femur, coronal plane forces were applied via the axial load channel, and AP forces via the torsional load channel. This was achieved by orienting the coronal plane (defined by the two anterior-superior iliac spines and the pubis symphysis) of the specimen parallel to the MTS actuator. Static equilibrium analysis of the test apparatus determined the relationship between the applied loads and the JRF.

3.2.2.1 Acetabulum Test Apparatus

The acetabulum test apparatus consisted of a femoral prosthesis, pinned so as to allow rotation in the coronal plane, and a support fixture (Figure 25). The pelves were positioned upside down in the support fixture, and oriented so that the AP-ML plane of the specimen was parallel to the MTS machine base. Consequently, the axis of the MTS actuator was parallel to the SI axis. Design of the specimen support simulated *in vivo* load transfer from the torso to the pelvis, by only potting the sacrum in a block of PMMA. This left the iliac wings unconstrained and free to move during testing. Screws fixed the PMMA block in the support fixture, which in turn was clamped to the base of the MTS machine.

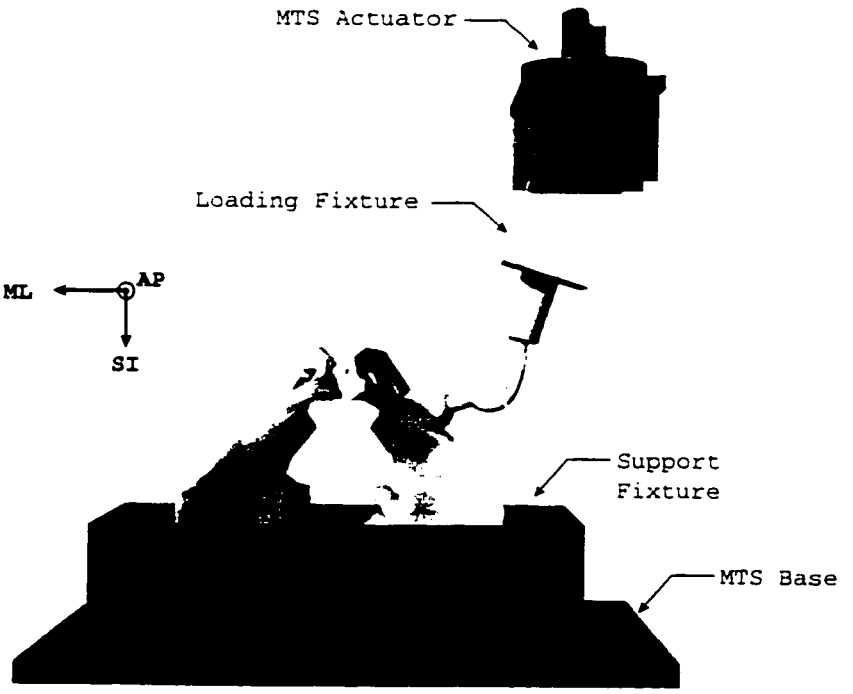

Figure 25. Drawing of acetabulum test setup.

3.2.2.2 Analysis to Determine the Applied Load Regimen

Static equilibrium analysis of a free-body diagram of the acetabulum loading fixture allowed determination of the relationship between applied actuator loads and the components of the JRF (Figure 26). As for the femur, the applied actuator axial load and applied actuator torsional load were designated as **L** and **T**, respectively. Again, **R** and **M** represent reaction force and moment, g is the horizontal distance from the center of the head of the femoral prosthesis (i.e. the center of the cup) to the center of the apparatus pin, and h is the corresponding vertical distance. The angle α is defined as the angle between the SI axis and the vector from the center of the apparatus pin to the head of the femoral prosthesis. J_{AP}, J_{ML}, and J_{SI} are the components of the JRF. It was assumed that no moment transfer occurred across the articular surface of the prosthesis.

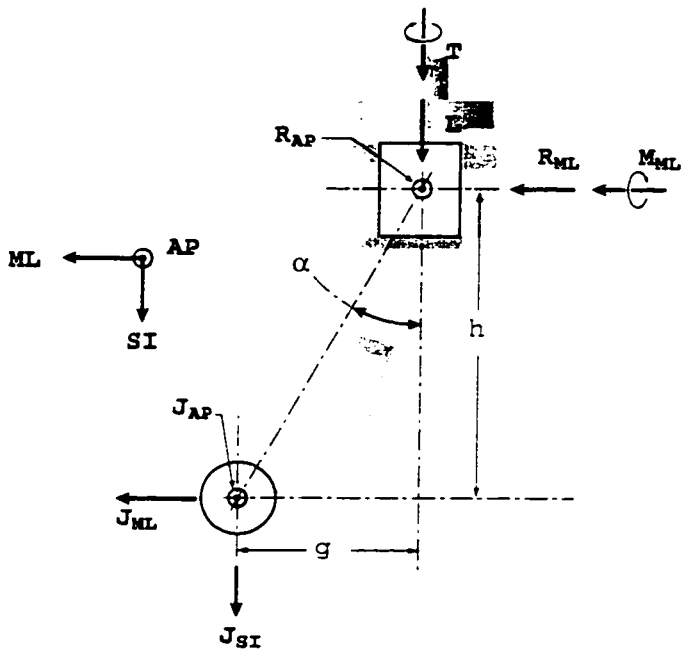

Figure 26. Free-body diagram of acetabulum loading fixture.

Derivation of the equilibrium equations included summing moments about the center of the head of the femoral prosthesis:

$$\sum \mathbf{F}_{AP} = \mathbf{R}_{AP} + \mathbf{J}_{AP} = 0 \tag{49}$$

$$\sum \mathbf{F}_{ML} = \mathbf{R}_{ML} + \mathbf{J}_{ML} = 0 \tag{50}$$

$$\sum \mathbf{F}_{SI} = \mathbf{L} + \mathbf{J}_{SI} = 0 \tag{51}$$

$$\sum \mathbf{M}_{AP} = -g\mathbf{L} + h\mathbf{R}_{ML} = 0 \tag{52}$$

$$\sum \mathbf{M}_{ML} = \mathbf{M}_{ML} - h\mathbf{R}_{AP} = 0 \tag{53}$$

$$\sum \mathbf{M}_{SI} = \mathbf{T} + g\mathbf{R}_{AP} = 0. \tag{54}$$

Noting that $\tan\alpha = g/h$, the solution for the applied loads in terms of the components of the joint reaction forces observed *in vivo* is:

$$\mathbf{T} = g\mathbf{J}_{AP} \tag{55}$$

$$\mathbf{L} = \frac{\mathbf{J}_{ML}}{\tan\alpha} \tag{56}$$

$$\mathbf{L} = -\mathbf{J}_{SI}. \tag{57}$$

As with the femur, the system of equations generated for the acetabulum test setup based on static equilibrium resulted in only five unknowns for the six equations. Resolution of this redundant set of equations for the femur was achieved by treating one of the geometric dimensions as a variable. Solution of the system of equations generated relationships for the applied loads which would require continuous repositioning of the specimen to be able to exactly match the *in vivo* loads at all instants of the gait cycle. Because this is not physically practical an optimum value for the geometric variable was computed. The same logic was applied to the acetabulum load analysis. Due to the direct

relationship between **L** and $\mathbf{J}_{SI}$ it was decided to match $\mathbf{J}_{SI}$ exactly, and choose α so as to minimize the error between the JRF generated by the applied loads (**L** and **T**) and the JRF observed *in vivo*. Eq. (56) was used to iteratively determine the "optimum" α. The optimization criterion for α was to minimize the average error of the JRF over both the level walking and stair climbing gait cycles simultaneously, to avoid having to reposition the specimen during testing. The result of the iteration revealed that the "optimum" $\alpha = 20°$. As for the femur, a combined series of concatenated axial and torsional ramps was used to create a load cycle for each gait type, i.e. the level walking or stair climbing load cycle. The maximum JRF observed *in vivo* was 3.14 BW for level walking and 2.04 BW for stair climbing. Maximum calculated error of the JRF was 0.08 BW for level walking and 0.04 BW for stair climbing. Test data showed *in vitro* forces to be in good agreement with *in vivo* forces for both level walking and stair climbing load cycles (Figures 27-30).

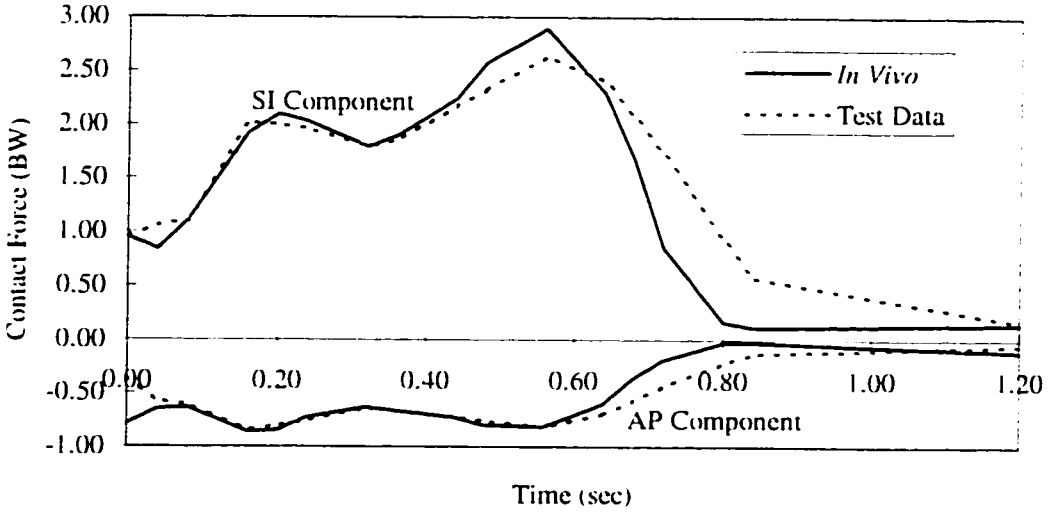

Figure 27. Comparison of the AP and SI components of the JRF observed *in vivo* and calculated from test data for level walking. The force components calculated from the load analysis match the *in vivo* waveform exactly and therefore are not plotted.

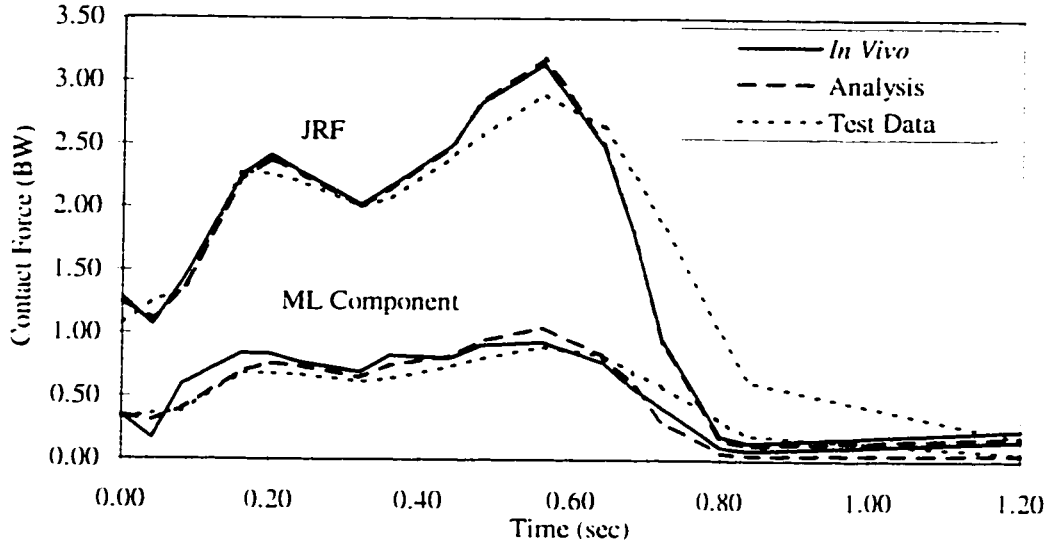

Figure 28. Comparison of the ML component and the JRF observed *in vivo*, calculated from the load analysis, and calculated from test data for level walking.

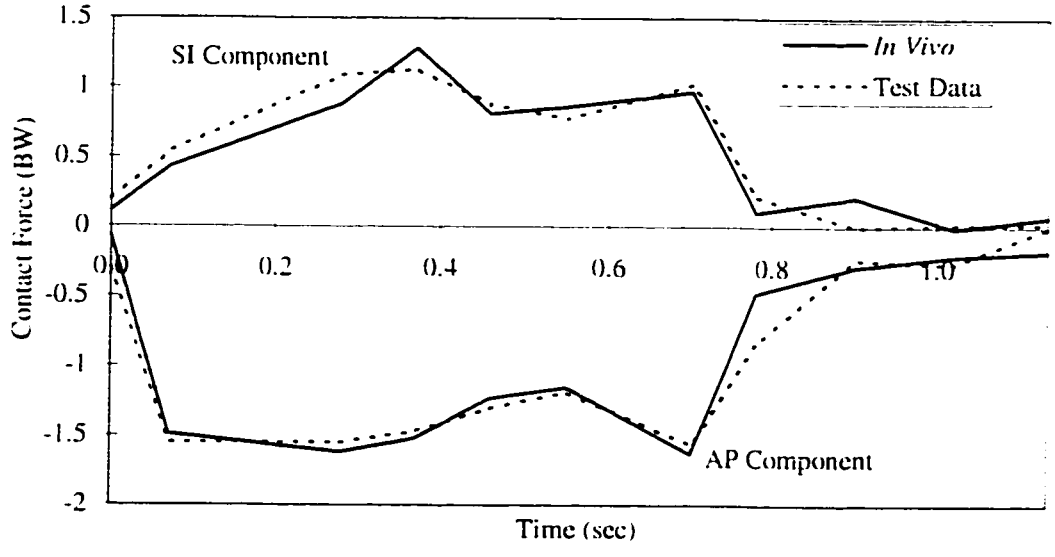

Figure 29. Comparison of the AP and SI components of the JRF observed *in vivo* and calculated from test data for stair climbing. The force components calculated from the load analysis match the *in vivo* waveform exactly and therefore are not plotted.

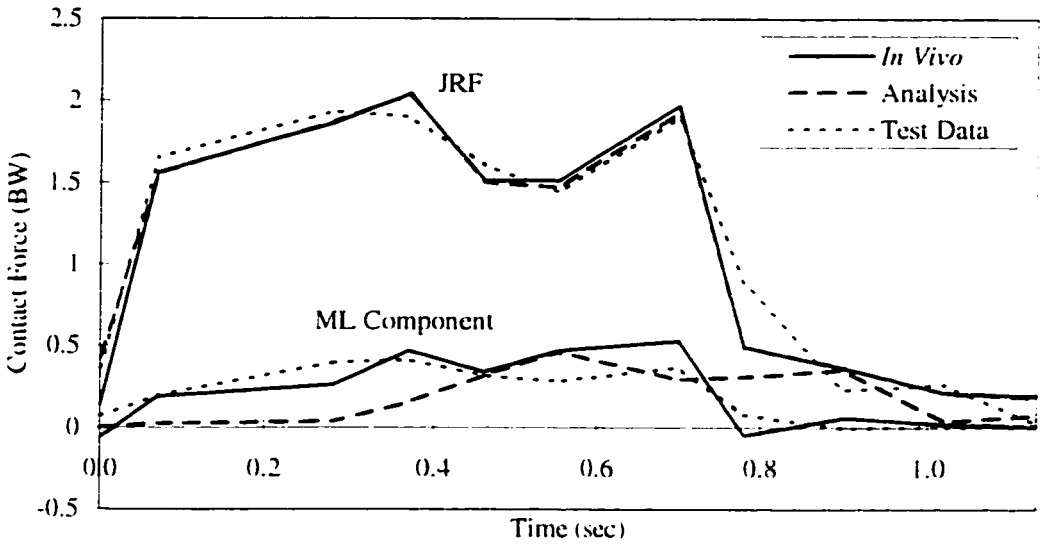

Figure 30. Comparison of the ML component and the JRF observed *in vivo*, calculated from the load analysis, and calculated from test data for stair climbing.

3.2.2.3 Loading Protocols

The acetabulum experiment included three loading protocols. Each loading protocol was defined by a unique combination of level walking and/or stair climbing load cycles. The first loading protocol was used to investigate the effect of screw configuration on the magnitude of micromotion, and also to examine the difference between applying a directionally variant JRF and a uni-directional JRF. The second protocol was used to compare micromotion during level walking versus micromotion during stair climbing. The third protocol was used to determine the effect of level walking on cup-to-bone gaps.

3.2.2.3.1 Loading Protocol 1

Nine acetabulae from five pelves were tested using loading protocol 1, which consisted of 70 loading cycles divided into seven identical load series. Each of these load series alternatively applied five level walking load cycles followed by five "uni-

directional" load cycles. The applied JRF vector was directionally variant for the level walking load cycle but for the uni-directional load cycle the JRF vector was always directed along the vector defined by the peak JRF . This single direction was chosen because many previous studies loaded specimens in this manner (Kamaric et al. 1996b, Perona et al. 1992, Won et al. 1995). The peak JRF and cycle duration were the same for each load cycle (Figure 31). Data were recorded at 100 Hz for all ten cycles in each load series.

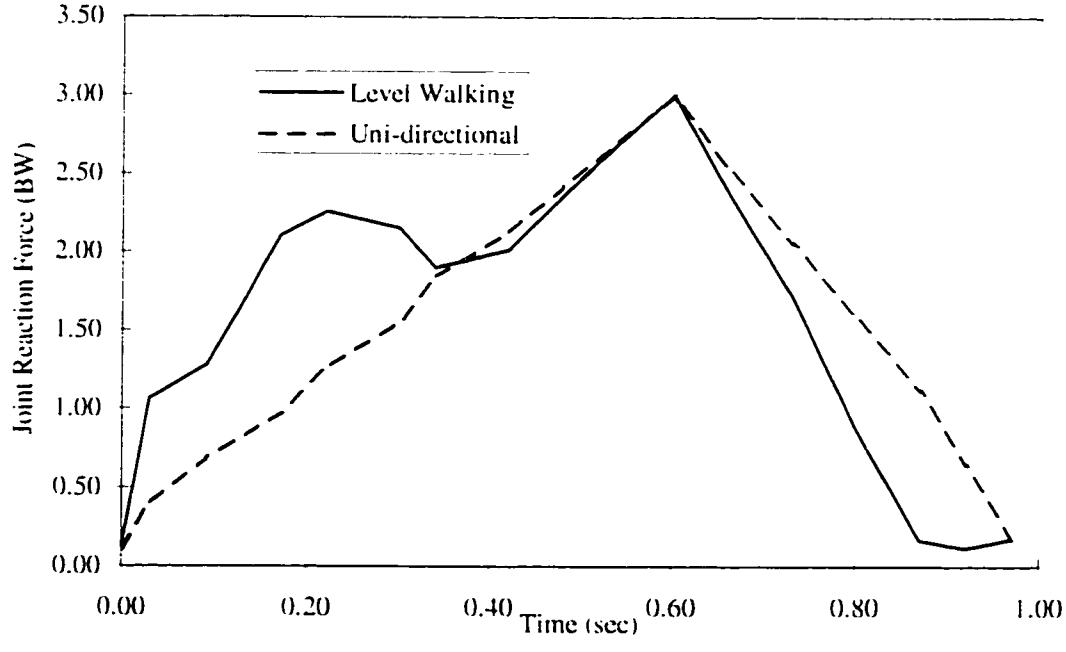

Figure 31. Normal level walking load cycle vs. Uni-directional load cycle.

A series of seven screw configurations were tested in each of nine acetabulae using loading protocol 1. The screw configurations consisted of combinations of one, two, or three screws in three holes (Table 2 and Figure 32). Two centrally located holes (A and B) directed screws into the posterior column and superior wall, respectively. The

third hole was directed toward the posterior wall, hole C. An experienced orthopaedic surgeon positioned the cup, giving priority to properly aligning screw hole A, then screw hole B. Screw hole A was given first priority because general clinical opinion is that a posterior column screw provides the best fixation due to the robustness of bone stock, and the length of screw that can be inserted. Bi-cortical purchase was attempted for all screws. After application of the first load series, the cup liner was removed and the screw configuration changed. The liner was then reinserted in the shell and the load series repeated. This process was continued until all seven screw configurations were tested.

Table 2. Order of screw configurations

Configuration	1	2	3	4	5	6	7
Hole Pattern	A	AB	ABC	AC	C	BC	B

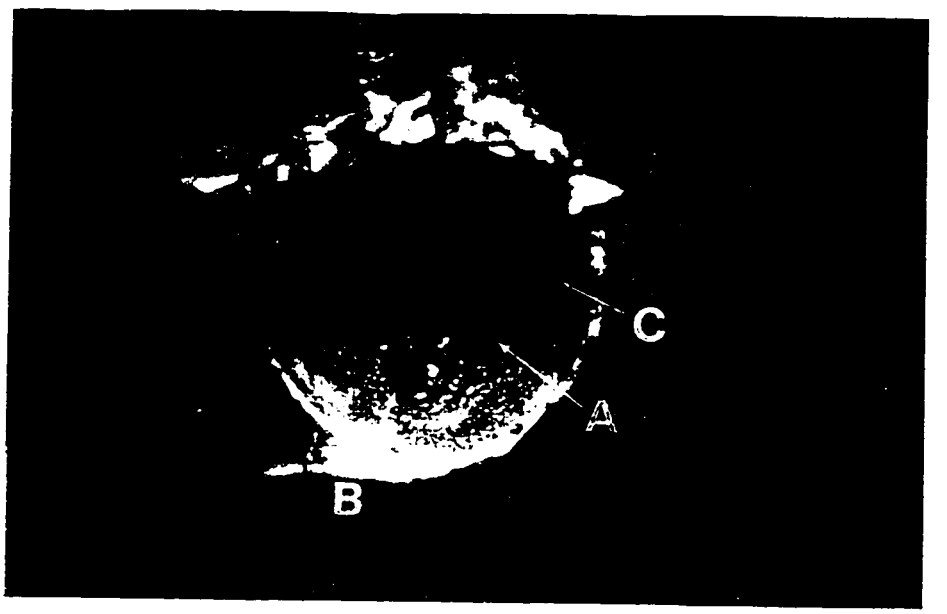

Figure 32. Picture of acetabulum showing location and definition of screw holes.

The screw configuration order minimized the number of screw insertions and removals. Only screw B was removed then reinserted during the test. Screw purchase

(uni- or bi-cortical) and insertion torque (measured with a torque-instrumented screwdriver) were recorded for each configuration.

Three of the nine acetabulae were tested twice with loading protocol 1, to see if the micromotion results were independent of screw configuration order. These three specimens tested three different sets of screw configuration orders (Table 3). The comparable trends indicated screw configuration order did not appreciably effect test results (Figure 33).

Table 3. Screw configuration orders used for independence of order test.

Screw Configuration Order		
Specimen 1	Specimen 2	Specimen 3
1-7	1, 7-2	7-1

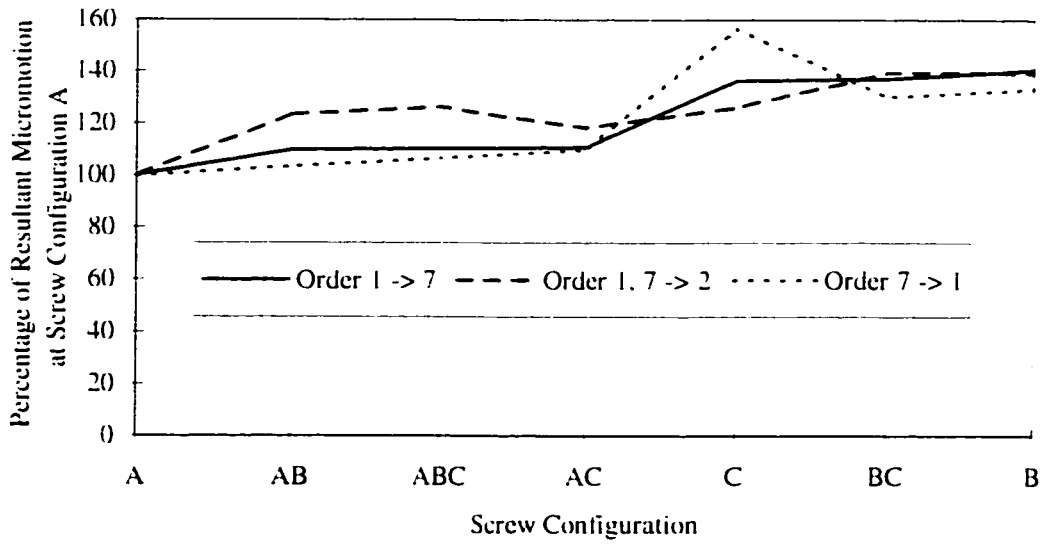

Figure 33. Relative measured displacement for each screw configuration with respect to the micromotion observed with screw configuration A. Data is from the measurement site at the pubis but is representative of the results at the ischium and ilium. The curves represent the average for two consecutive tests. The comparable trends, regardless of the first configuration or order, show that measured displacements do not depend on the order of screw configurations.

The age of the specimens initially caused concern about the possibility of stripping screw holes. However, stripping did not occur for screws having bi-cortical purchase. Screws with uni-cortical purchase did not strip during the initial insertion, but were prone to strip if the screw was removed and then reinserted. Preliminary testing indicated that between 300 and 400 cycles, screw fixation could degrade (uni-cortical more likely to than bi-cortical). For subsequent micromotion parametric testing, therefore, the number of cycles were limited to 210, to reduce fixation degradation.

3.2.2.3.2 Loading Protocol 2

Five of the nine acetabulae tested with loading protocol 1 were also tested using the second loading protocol, which combined level walking load cycles and stair climbing load cycles. The other four acetabulae from loading protocol 1 were lost due to specimen failure during loading protocol 2. The first two pelves (containing four intact acetabulae) subjected to the stair climbing load cycle fractured at the sacro-iliac joint. Originally, pelves were only supported at the sacra, which was adequate during the first loading protocol. To permit collection of data with stair climbing loads, three pelves (containing five intact acetabulae) were reinforced with additional PMMA covering most of the sacrum and approximately 30% of the iliac wing, and with screws inserted through the sacro-iliac joint.

Ideally, loading protocol 2 consisted of 70 load cycles, divided into seven identical load series, one for each screw configuration. Each load series applied five level walking load cycles followed by five stair climbing load cycles. However, because of difficulties in maintaining screw purchase, only one specimen completed the entire loading protocol. The other four acetabulae were tested using only configurations 1, 2, and 3, because the screw insertion torques for configurations 4 - 7 were significantly reduced. The reduction in screw torque was most substantial for screws with uni-cortical

purchase, i.e. screw A or screw B. Data were recorded at a frequency of 100 Hz for the ten loading cycles.

3.2.2.3.3 Loading Protocol 3 and the Cup-to-Bone Gap Study

As part of the cup-to-bone gap study, four acetabulae used in loading protocols 1 and 2 were additionally loaded with 790 to 860 level walking load cycles, until each accumulated a total of 1000 load cycles (the different number of cycles depended on the testing history of the individual acetabulum). The aim of this third loading protocol was to determine the effect of nominal gait loads on cup-to-bone gaps. The loads were applied without screw fixation, because after loading protocol 2, the specimens had only one screw with good purchase (not the same screw for each specimen).

Gaps were measured at six stages during the acetabulum experimental procedure: after cup implantation; after insertion of the first screw into hole A (hole A always received the first screw because of its optimum position as described above); after the first loading protocol (70 load cycles for the standard procedure or 140 load cycles for specimens used to test screw configuration order effects); and then three times during loading protocol 3 (after 250, 500, and 1000 total cycles). The number of total cycles included 30 to 70 loading cycles (depending on the number of screw configurations tested) from the second loading protocol. Due to the small number of cycles, gaps were not measured after loading protocol 2. As a result of preliminary loading tests and specimen failures the number of specimens available at each measurement stage varied (Table 4). Gap measurements were made with a custom designed depth gage, with a resolution of 0.025 mm, that fit into the holes in the cup without screws. A repeatability study showed the accuracy of the gap measurements to be 0.05 mm.

Table 4. Number of specimens for which cup-to-bone gaps were measured for each stage of the acetabulum experiment.

	Pre-screw A	Screw A	Protocol 1	250	500	1000
# Specimens	16	16	9	4	4	4

3.2.3 Calculation of Micromotion

Rigid-body motion proved an invalid assumption for the acetabulum test. Initially, the objective was to calculate micromotion of the cup in the same manner as for the femur, i.e. by measurement of seven relative displacements at three locations, followed by rigid-body motion analysis to estimate the micromotion at any point on the surface of the cup. Results from a preliminary test series of six acetabulae indicated that errors existed in the micromotion calculations. Specifically, displacements calculated on the cup surface were two to six times larger than the displacements measured at the three gage fixture sites (hereafter referred to as points A, B, and C, as for the femur), and increased toward the attachment screw locations (Table 5). This result did not make physical sense, because if two bodies are rigidly attached to each other, the minimum relative motion between the two bodies should occur at the attachment site.

Table 5. Example of resultant micromotion measured at two locations and calculated resultant micromotion at three locations on the cup surface.

Location	Point A	Point B	Rim	Midway from rim to pole	Pole
Micromotion (μm)	320	457	437	636	743

Several combinations of gage fixture configurations (locations and gage orientations) and rigid-body motion techniques were employed. All combinations worked with analytical models and some successfully completed mockup tests using known displacements. However, all failed to reliably calculate cup micromotion using LMSG data.

The geometry of the pelvis and test apparatus made the orientation of the gage fixtures, with respect to each other, different from specimen to specimen. To enable attachment of the gage fixture to the pelvis a new design was required (Figure 34). A screw attached the frame directly to the pelvis. The gage fixture blocks were located 0.5 cm to 1.5 cm above the cup rim and were attached to outriggers screwed into one of eight threaded holes in the cup rim. Because the threaded holes could not always be located in the same relative position to bony landmarks and because of the variations in block height above the cup rim (required to maintain gage triad orthogonality) there was no consistent relationship between the measurement axes at one point and any other point. In addition, gage triad orientations had no consistent relationship with respect to the plane containing points A, B, and C (hereafter referred to as the measurement plane). By contrast, for the

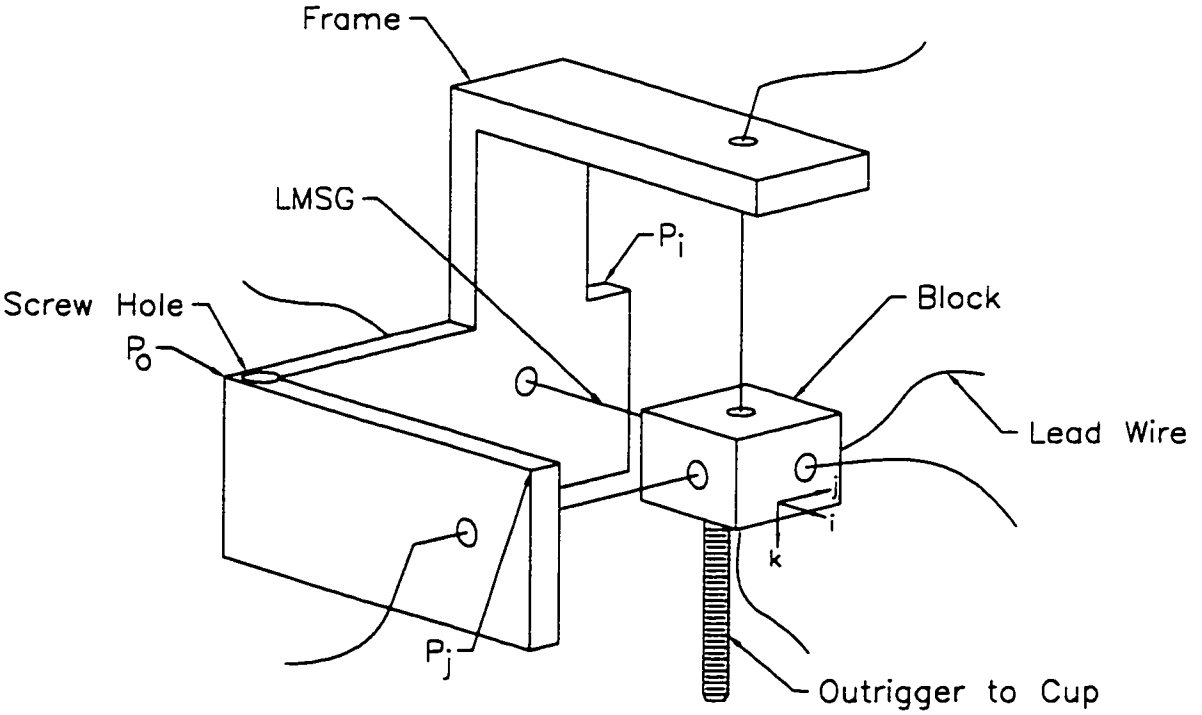

Figure 34. Schematic of acetabulum gage fixture.

femur test the displacements at the three measurement sites were measured along parallel axes. This allowed the calculation of the non-measured displacements to be made without any coordinate transformations. In addition, the vectors **AB** and **AC** were parallel to two of the measurement axes and the displacement measured at point C was perpendicular to the measurement plane.

To account for the differing gage axis orientations in the acetabulum tests, the algorithm from the rigid-body motion technique for the femur was modified. The modified algorithm defined a local coordinate system at each measurement site, i.e. A_{ijk}, B_{ijk}, C_{ijk}, based on the orientation of the LMSG's at each site (these local coordinate systems were parallel for the femur and defined as the outrigger coordinate system) and used eight measured displacements rather than seven (i.e. three at points A and B, and two at point C). The orientation of the local coordinate systems with respect to the acetabulum coordinate system (defined as a coordinate system with axes parallel to the anatomic reference frame with the origin located at the center of the cup) was calculated from measurements of three points on the gage fixture frame (P_o, P_i, and P_j, Figure 34) prior to testing. The origins of the local coordinate systems, points A, B, and C respectively, were defined as the centroid of the fictitious cube delineated by the lines of action of the gage triad. The acetabulum algorithm incorporated the measured displacements, transformed them into the acetabulum coordinate system, then calculated the non-measured displacement assuming (as the femur algorithm did) the interpoint distances between points A, B, and C remained constant.

The modified acetabulum algorithm was validated by hand calculations for translations along and rotations about the axes of the acetabulum coordinate system, but the questionable results from the six preliminary specimens necessitated a rigorous validation of the entire acetabulum technique. A review of the data indicated the error in

the estimation of micromotion occurred in the calculation of the non-measured displacement component at point C. Potential sources of error included the algorithm, the test setup, and bony deformations.

The first step was to validate the algorithm using LMSG data. To do this a special test setup was created where known displacements could be input via the MTS machine. For this test (and subsequent known displacement tests) the gage fixture frames were attached to the MTS base plate and the gage fixture blocks (i.e. points A, B, and C) were attached to the MTS ram. This gage configuration oriented the local coordinate systems such that the i-j plane of each local coordinate system was coplanar with the MTS base, and the k axes were parallel to the ram axis. While this configuration did not completely mimic a specimen test gage configuration, the i and j axes were not parallel between any two measurement sites. This configuration also simplified validation of displacement measurements with hand calculations. The test consisted of an axial ram displacement of ±100 μm. C_k was the non-measured displacement. Data from the gages showed peak-to-peak values representative of the input displacement (Table 6), but analysis of the gage data led to a computational error (the algorithm attempted to take the square root of a negative number). To investigate this phenomenon an artificial data file with a displacement vector of exactly [0, 0, ±100 μm] for each measurement site was created (i.e. one-dimensional rigid-body motion). Analysis of the artificial data led to the same

Table 6. LMSG peak-to-peak displacement, μm, for a known MTS ram displacement of 200 μm (actual ram motion).

	i-axis	j-axis	k-axis
Point A	13 (0)	12 (0)	211 (204)
Point B	6 (0)	26 (0)	194 (204)
Point C	9 (0)	17 (0)	n.a.

error in the algorithm. Review of rigid-body motion theory (Beggs 1983), and the femur test setup (including the study it was based on, Gilbert et al. 1993), indicated the displacement at point C perpendicular to the measurement plane may be required for solution of the non-measured displacement. The artificial data were analyzed again with C_j treated as the non-measured displacement and C_k as a measured displacement. This analysis did accurately calculate the displacement in the C_j direction and for points on a fictitious cup, D_n. The one-dimensional known displacement test was rerun with the gage initially measuring C_j displacement repositioned to measure C_k displacement (peak-to-peak 190 μm). Analysis of this LMSG data calculated the displacement to within 10 μm for C_j and D_n.

These results indicate that the algorithm produced accurate results using LMSG data if the displacement at point C perpendicular to the measurement plane is measured. However, the diverse gage orientations for the acetabulum specimens did not directly measure the displacement perpendicular to the measurement plane, suggesting the possibility that gage configuration might have been the cause of the inaccurate results. To address this possibility a computer point model was created (PATRAN software) using data from a test specimen. The model consisted of fifteen points: points P_o, P_i, and P_j defining the local coordinate system for each measurement site; the initial locations of points A, B, and C; and three points corresponding to points on the cup surface. All fifteen points could be moved as a unit to simulate rigid-body motion. To determine the relationship between the local coordinate system at point C and the measurement plane a coordinate system was defined based on the locations of the points A, B, and C, namely the acetabulum outrigger coordinate system. Axis direction was calculated by the following equations:

$$\hat{x} = \frac{\mathbf{AB}}{|\mathbf{AB}|}; \quad \hat{y} = \hat{z} \times \hat{x}; \quad \hat{z} = \frac{\mathbf{AB} \times \mathbf{AC}}{|\mathbf{AB} \times \mathbf{AC}|}$$

The rotation matrix relating the local coordinate system at point C to the xyz coordinate system:

$$R_{ijk-xyz} = \begin{bmatrix} 0.992 & -0.114 & -0.044 \\ 0.063 & 0.782 & -0.620 \\ 0.105 & 0.613 & 0.783 \end{bmatrix}$$

revealed that no axis of the local coordinate system was perpendicular to the measurement plane (if so one would expect: $R_{ik} = R_{kj} = 0$ for $i \neq j$ and $R_{ik} = R_{kj} = 1$ for $i = j$, for one row/column combination). The point model underwent general rigid-body motion by imparting a rotation of 10° about an axis from the acetabulum coordinates (0,0,0) to (1,2,3). Model displacements at points A, B, and C in their respective local coordinate system were input into the algorithm. The displacements calculated by the algorithm matched exactly the displacements from the point model for the non-measured displacement at point C and for points on a fictitious cup D_n (both C_j and C_k were treated as the non-measured displacement). Subsequently, a perturbation analysis was performed where the "measured" model displacements were randomly varied ±10 μm to simulate LMSG inaccuracies. The calculated displacements at all D_n changed by only 5 μm to 20 μm. This indicated that the algorithm works for rigid-body motion as long as a component of the displacement perpendicular to the measurement plane is measured at point C.

To validate the acetabulum test setup a general three-dimensional known displacement test was performed. The gage configuration was the same as for the one-dimensional known displacement test. Ram motion consisted of ±100 μm in the k-direction and ±0.05° rotation in the i-j plane. Gage data were compared with data from a second computer point model. Comparisons included micromotion in the local

coordinate systems (i.e. directly between LMSG data and the model, ijk) and micromotion in the acetabulum coordinate system (i.e. after calculation by the algorithm). The cup locations were only compared in the acetabulum coordinate system because no gage data were available at these points. The gage data generally agreed with the rigid-body motion data from the computer model (Table 7). The 23 μm difference in the B_j direction led to a retest using an LVDT to measure displacement. LVDT data were collected in four directions, B_i, B_j, C_i, and C_j. In all four cases the LVDT measured

Table 7. Comparison between micromotion measured with LMSG's and rigid-body motion predicted by the computer model (μm).

Site	LMSG Data			Computer Model			LMSG Data			Computer Model		
	i	j	k	i	j	k	AP	ML	SI	AP	ML	SI
A	72	196	197	86	194	200	93	196	197	100	186	200
B	97	111	210	101	134	200	145	18	207	170	14	200
C	51	190	190	48	211	200	199	83	186	202	83	200
D1							22	32	197	2	43	200
D2							49	11	195	37	21	200
D3							15	14	198	4	6	200

Note: Data for D_n were computed using the algorithm and not measured directly (i.e. ijk data).

displacements within 5 μm of the LMSG measurements. A sensitivity study of the computer model displacements revealed that a variation of only 0.007° would reduce the difference between gage data and model data for the B_j component to 10 μm without creating any differences greater than 15 μm in the other eight displacement components. This angular variation is near the resolution of the MTS machine (±0.004°), and this, when coupled with the LVDT results indicates the acetabulum test setup accurately records displacements for general three-dimensional rigid-body motion. In addition, the data show that the algorithm accurately predicts displacements for general rigid-body

motion for the given gage configuration (resultant calculated micromotion was within 5% of the measured resultant micromotion for all three points and several points on a fictitious cup).

At this stage the validation tests suggested that excessive bony deformations and/or gage configuration were the only potential sources of error causing the unacceptable predictions of micromotion. The known displacement tests ruled out test apparatus/displacement measurement inaccuracies as sources of error. The computer point model analysis indicated that at least for rigid-body motion the algorithm accurately predicted micromotion of the cup.

To eliminate gage orientation as a source of error a new gage fixture was designed. This new fixture, named the "mega-fixture", enabled gage alignment identical to that used in the femur test, i.e. the local coordinate system at each measurement site would be parallel to the other sites and the vectors **AB** and **AC** lie along local coordinate system axes. The design was based on an L within an L. Displacements were measured between the two L's at the vertex and the two tips (Figure 35). The measurement plane and gage orientation with respect to the acetabulum coordinate system were defined by the location of the vertex and tips of mega-fixture frame (points MF_o, MF_i, and MF_j, Figure 35). The fixture allowed collection of data from seven, eight, or nine gages attached to both the cup and pelvis at only one point.

Using the mega-fixture, a specimen was tested and seven displacements were measured, three at the vertex, three at one tip, and one perpendicular to the measurement plane at the other tip. Calculated micromotion for the cup ranged from 700 μm at the rim to 350 μm near the fixation screw holes. The trend of decreasing motion from rim to fixation screw holes was an improvement in that this trend made physical sense.

However, the magnitudes of micromotion remained much higher than one would expect based on ingrowth studies.

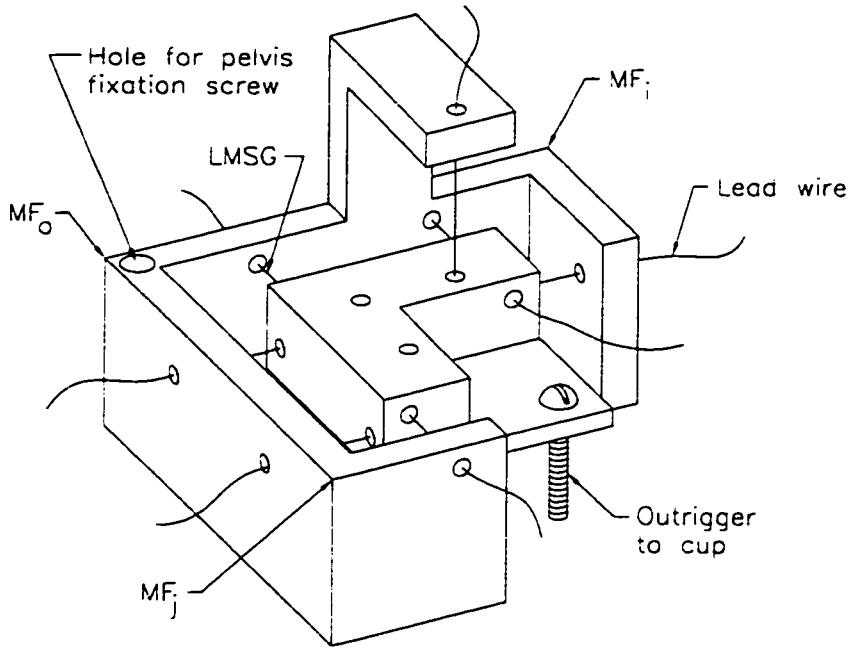

Figure 35. Schematic of acetabulum mega-gage fixture. For clarity, only one gage perpendicular to the measurement plane is shown.

To further investigate the estimate of micromotion using the mega-fixture, a subsequent test of the same specimen was run to record the micromotion at three locations around the cup rim, points 1, 2, and 3. These data were compared to the predicted micromotion at the same locations using the mega-fixture data (Table 8). Based on the measured micromotion the predicted micromotion at point 1 was acceptably accurate. However, point 1 was very close (less than 0.5 cm) away from the vertex measurement site of the mega-fixture. In light of this, points 2 and 3 offered a more independent comparison. The micromotion predicted at these two points differed from the measured micromotion by more than 200 μm. The pattern of micromotion predicted using the mega-fixture indicated gage configuration may affect estimates of micromotion

assuming rigid-body motion. However, the large magnitudes of micromotion and point to point comparisons suggested another source of error existed which contributed to the unacceptable estimations of micromotion from previous tests, namely bony deformations.

Table 8. Comparison of resultant micromotion measured at three points and that predicted from the mega-fixture test at the same three points (μm).

	Predicted	Measured
Point 1	313	295
Point 2	383	79
Point 3	349	92

In an attempt to more directly show the effect of bony deformations on the estimation of micromotion assuming rigid-body motion, a series of tests using one specimen were performed. For all tests in this series nine displacements were measured to allow direct comparison of the calculated non-measured displacements with measured displacements. Because the MTS machine can only record eight displacements simultaneously, two consecutive tests had to be run with one gage repositioned from its original position to the previously non-measured position (e.g. from C_k to C_j) to record all nine displacements. Examination of data from four consecutive tests proved repeatability and consequently the validity of recording nine displacements in this manner.

The effect of bony deformation was quantified by comparison of acetabulum data with femur data. The exact limit of (or even a parameter describing) bony deformations that permit an acceptable approximation of micromotion assuming rigid-body motion is unknown. Therefore the acetabulum data could not be compared to an absolute gold standard. Results from the femur test series indicate that the femoral prosthesis/femur

construct exhibited an acceptably small amount of bony deformation. Consequently, femur test data were used as a yardstick by which to judge the acetabulum data.

The first test was performed using the standard gage configuration, i.e. three gage fixtures positioned around the rim of the cup with no a priori knowledge of gage orientation between measurement sites. The first phase in analyzing the nine-gage test data compared extensional strains between the three measurement sites. Maximum strains were 0.7% and 1.1% for the femur and acetabulum respectively (Table 9). The relative value of strains for each specimen type makes sense if one attributes the majority of strain to bony deformation, rather than prosthesis deformation and gage inaccuracies. For the femur the maximum linear bone length, and hence bony deformation, between any two points was between points B and C and the minimum was between points A and C. For the acetabulum the largest strain occurs between points B and C, which span the cotyloid notch, the weakest region of the acetabulum. The similar peak strains do not support the explanation that bony deformations contributed to the unacceptable prediction of micromotion.

Table 9. Strains between measurement points for the femur and acetabulum tests.

Points	Femur	Acetabulum
AB	0.13%	0.18%
AC	0.70%	0.30%
BC	0.20%	1.12%

The second phase of analysis of the nine-gage test data compared parameters defining the rigid-body motion approximation of micromotion. Rigid-body motion theory states that the motion of a rigid body through space from an initial position to a final position can be completely described by a translation along and a rotation about a

screw displacement axis (SDA). In the current study this correlates to a SDA describing the motion of the prosthesis with respect to the specimen. The translation along the SDA is defined as δ, the rotation about the SDA as ϕ, and the orientation of the SDA in the acetabulum coordinate system as the unit vector $\mathbf{u}$. It can be shown that knowing the displacement in three directions at three points on the body enables the SDA parameters δ, ϕ, and $\mathbf{u}$ to be determined (Beggs 1983). In the derivation of the relationships between the displacement of three points on the body and the SDA parameters one of the points is used as a reference point, and the vector from that point to one of the remaining two as a reference vector.

For rigid-body motion there is a unique solution for the SDA parameters. This means that the solution is independent of the three points chosen for where displacements are measured, and subsequently the reference point and reference axis. If deformations occur the solution of SDA parameters is not unique and depends on the location of the points where displacement is measured. The solution also depends on the chosen reference point and reference axis. Therefore for three given points, e.g. points A, B, and C, a set of three solutions can be determined using each point in turn as the reference point and each side of the triangle defined by the three points as the reference axis. The more rigid a body is the more similar the three solutions will be, and vice versa.

The SDA parameters for the femur and acetabulum were compared at the instant of peak load since this instant correlates to peak deformation, assuming the stiffness of the prosthesis-specimen construct remains constant under the applied load regimen. By measuring three displacements at each measurement site it was possible to calculate a set of three unique rigid body approximations and the corresponding SDA parameters for the acetabulum. (A similar nine-gage test had been previously performed for a femur specimen). The solutions were defined by three reference point/reference axis cases:

Case 1 - reference point = point A, reference axis = **AB**; Case 2 - reference point = point B, reference axis = **BC**; Case 3 - reference point = point C, reference axis = **CA**. The rotation about the SDA and tranlsation along the SDA were compared directly from one case to the next. To compare the SDA orientation the angle between **u** for each case was calculated, e.g. α_{12} = the angle between **u** from case 1 and **u** from case 2. A similar set of solutions were calculated for the femur.

Comparison of the SDA parameters for the femur and acetabulum was inconclusive with respect to indicating bony deformations as causing the inaccurate estimation of micromotion. The case to case variation in δ and ϕ was similar for the femur and acetabulum (Table 10). However, the orientations of the SDA were more consistent for the femur than for the acetabulum. The small intercase variations observed for the femur were expected considering the micromotion data indicated the prosthesis/femur construct to be rigid enough to allow reasonable approximation of micromotion assuming rigid-body motion. The large variation of **u** for the acetabulum was consistent with the concept that bony deformations produce the unacceptable micromotion estimations. It was unclear why the variations in δ and ϕ observed for the acetabulum were small.

Table 10. SDA parameters for the femur and acetabulum at the instant of peak load.

		δ (μm)	ϕ (deg)	Angle between SDA's (deg)	
Acetabulum	Case 1	10	-0.10	α_{12}	42
	Case 2	14	0.05	α_{13}	37
	Case 3	7	0.12	α_{23}	71
Femur	Case 1	9	1.90	α_{12}	6
	Case 2	12	0.00	α_{13}	19
	Case 3	15	-0.50	α_{23}	23

The third phase of analysis of the nine-gage test data compared the calculated position of the point with non-measured displacements to the measured positon. From LMSG data the algorithms for both the femur and acetabulum directly calculated the location of points A and B at time t>0, denoted by the postion vectors **A′** and **B′**. An approximate location for point C , **C***, at time t was subsequently calculated by imposing quasi-rigid-body motion constraints (assuming the interpoint distance from point A to point C and from point B to point C remains constant, no constraint was imposed on the distance between point A and point B, Figure 36). The nine-gage test enabled the measured location of point C, **C′**, to be determined directly and compared to **C***. While point to point comparison between measured and estimated micromotion was the gold standard, the difference between **C′** and **C*** was also considered an important parameter regarding the validity of assuming rigid-body motion, for two reasons. First, **C*** was calculated imposing rigid body constraints. Second, recall the equation used to calculate the final position of a point on the cup, **D′**:

$$\mathbf{D'} = \mathbf{A'} + [R']\rho$$

where the rotation matrix [R′] is a function of **A′**, **B′**, and **C***. Consequently, the value of **C*** directly affects the calculation of micromotion for points on the cup.

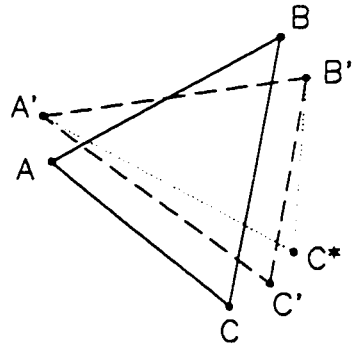

Figure 36. Schematic showing initial and final locations of points A, B, and C, and the approximated location of C, C*.

The stiffness of the prosthesis-specimen construct affects the magnitude of $\mathbf{C}^* - \mathbf{C}'$. For rigid-body motion the calculated position of the point with non-measured displacements and the measured position are identical, i.e. $\mathbf{C}^* = \mathbf{C}'$. As the stiffness of the prosthesis-specimen construct decreases the difference between $\mathbf{C}^*$ and $\mathbf{C}'$ will increase. Having measured three displacements at each measurement site, each point could be treated in turn as the point with non-measured displacements. This was done for the three reference point/reference axis cases outlined above. Since each measurement site was treated as the point with non-measured displacements the magnitude of the difference between the measured and calculated positions shall hereafter be referred to as r^*. An additional specimen test using the mega-fixture and measuring nine displacements was run to compare with the standard gage configuration for the acetabulum. The magnitude of r^* was very large for the acetabulum tests, for both the standard gage configuration and the mega-fixture configuration, for all three cases (Figures 37 and 38). This indicated a relatively flexible construct when compared to the femur data (Figure 39). The relatively small variation for r^* between each case for the mega-fixture compared to the standard configuration indicates that gage configuration may contribute to the inaccurate estimation of micromotion predicted by the acetabulum tests.

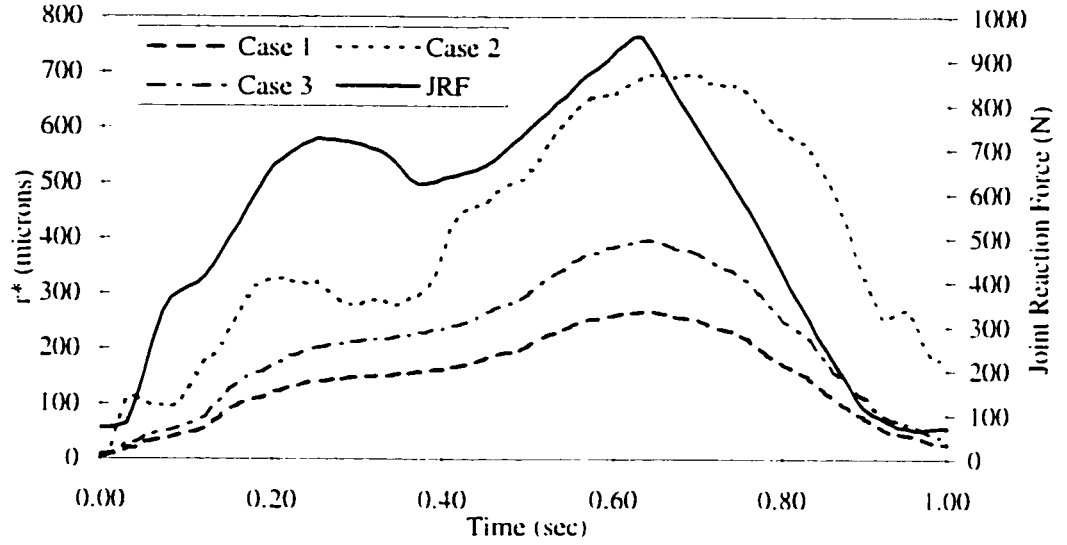

Figure 37. Difference between the calculated location and measured location for the point with non-measured displacements for three different reference point/axis cases. Data from acetabulum specimen using the standard gage configuration. Force curve shows progression during gait.

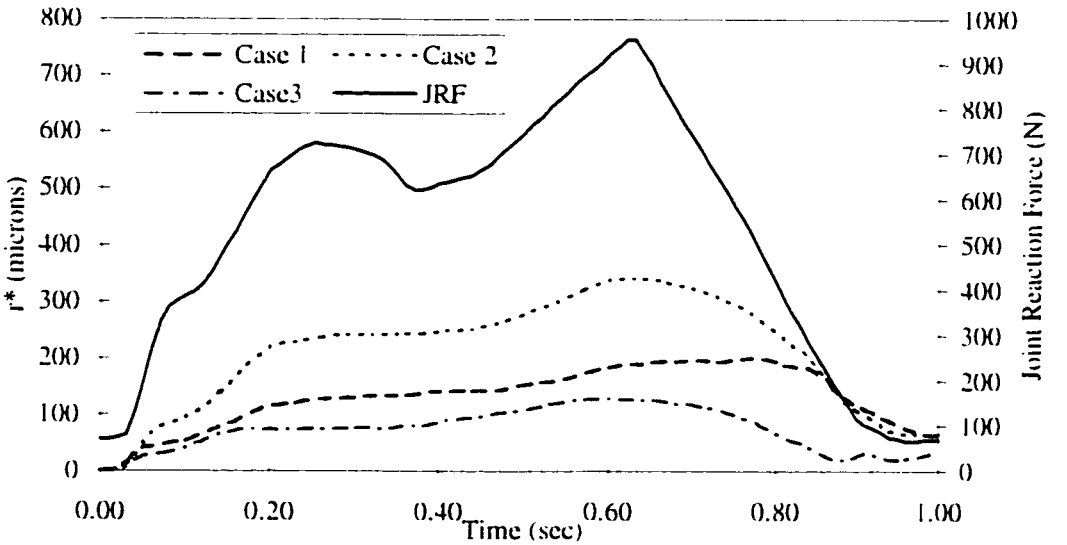

Figure 38. Difference between the calculated location and measured location for the point with non-measured displacements for three different reference point/axis cases. Data from acetabulum specimen using the mega-fixture gage configuration. Force curve shows progression during gait.

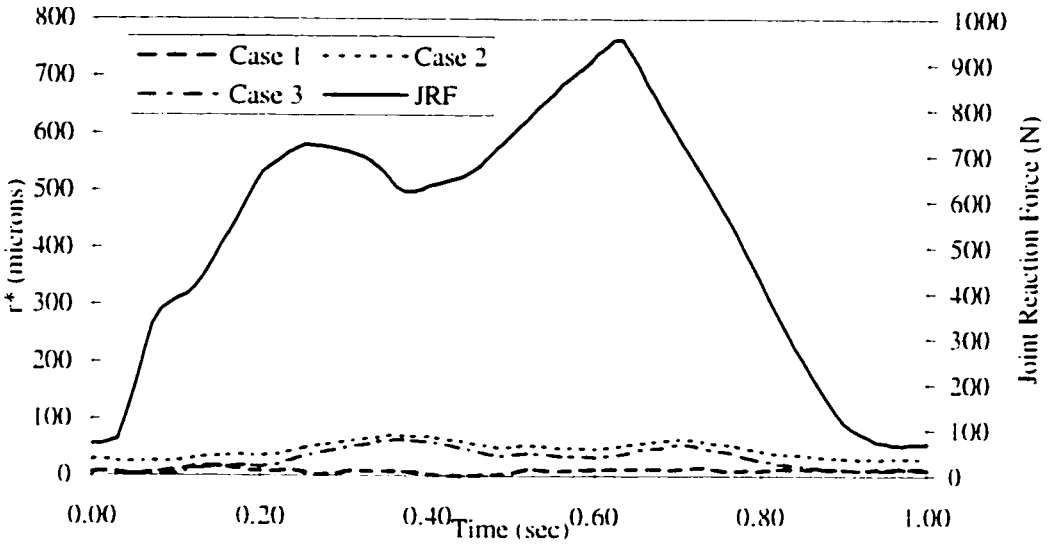

Figure 39. Difference between the calculated location and measured location for the point with non-measured displacements for three different reference point/axis cases. Data from femur using the standard gage configuration. Force curve shows progression during gait.

The series of nine-gage tests was completed by running three more tests with the goal of comparing a deformable acetabulum specimen to a rigid one. The first test was performed in the normal manner using the standard gage configuration. Following the test the specimen was potted in PMMA without removing the specimen from the MTS machine. The gage fixtures and gages were not disturbed during the potting. Because the rim of the acetabulum was not parallel to the ground the entire acetabulum could not be covered with PMMA without getting cement into the cup. For this reason only about 90% of the acetabulum was covered. A second test was performed after the PMMA cured. Gross motion of the specimen decreased significantly from the previous test (based on visual inspection) but some motion was still observed. Following the second test the specimen was removed from the MTS machine and more PMMA applied. Removal of the specimen allowed the cement to be applied up to the rim of the acetabulum. The gage fixtures were not moved during the second potting procedure. The

specimen was repositioned in the MTS machine in the same location as for the previous two tests and retested.

The data from the final three tests showed that bony deformations were the primary cause of the inaccurate estimations of micromotion calculated for the previous specimens. The addition of PMMA, i.e. reduction of bony deformations, decreased r* (case 1 plotted, cases 2 and 3 results were similar.Figure 40). The difference for 100% coverage was comparable to that for the femur.

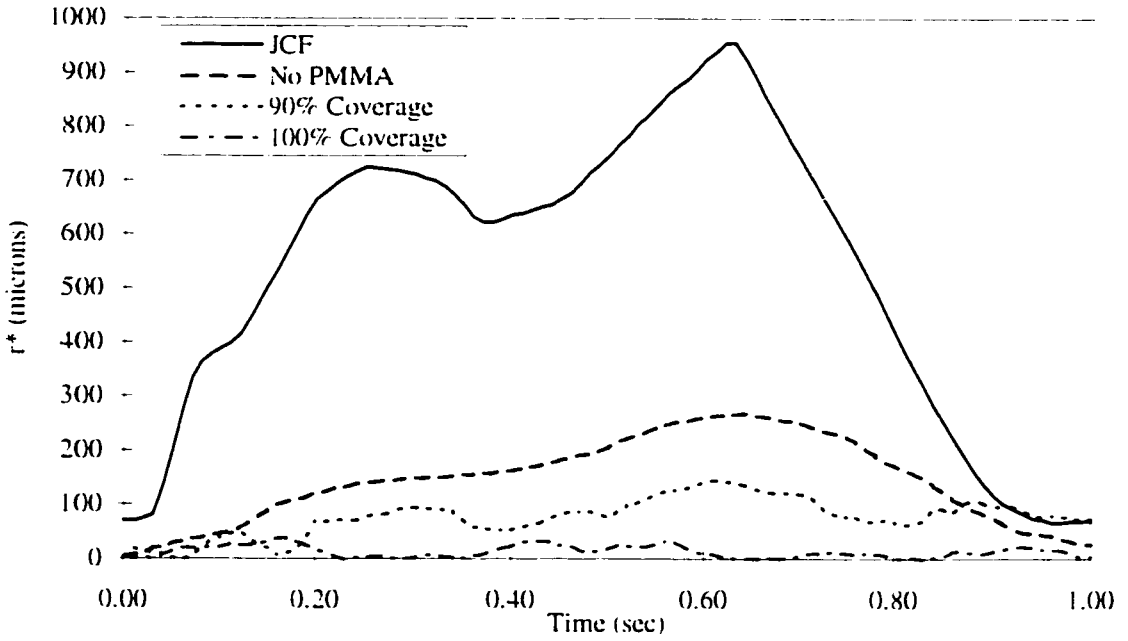

Figure 40. Difference between the calculated location and measured location for the point with non-measured displacements (case A) for three different specimen preparations using the standard gage configuration. Force curve shows progression during gait.

The pattern and magnitude of estimated micromotion was also affected by the addition of PMMA (Table 11). The addition of PMMA changed the pattern from the physically nonsensical pattern observed previously to the physically reasonable pattern of

the largest micromotion occurring near the rim and smallest near the fixation screws. For the 100% coverage test the estimated micromotion near the fixation screws was in the range favorable to bony ingrowth. Although the tests using the mega-fixture (thus removing gage orientation as a possible source of error) showed improved results compared to the estimated micromotion using the standard configuration, the absolute magnitudes were too large for even fibrous ingrowth. Therefore it was concluded that bony deformations were the primary source of error causing the inaccurate estimate of micromotion for the previously tested specimens.

Table 11. Estimated micromotion data for standard test and for a specimen potted in PMMA (μm).

Specimen Preparation	Range around rim of cup	Range near fixation screws
Normal	248-769	447-751
90% Coverage	155-295	97-151
100% Coverage	82-191	47-66

Despite the failure of the current technique for the acetabulum, the success with the femur prompted investigation of an alternative rigid-body motion analysis technique. The alternative technique, developed by Gilbert et al. (1992) had proven successful for the femur but had not been applied to the acetabulum. Gilbert et al.'s technique was considered a unique approach because while it measured seven displacements at three sites it did not calculate the non-measured displacements. Instead their technique used the seventh measured displacement to calculate the rotation about the line defined by the other two measurement sites. The technique required the seventh gage to measure the displacement normal to the measurement plane. Therefore data from a test using the mega-fixture configuration were used. Results for this technique were similar to that

from the current technique using the mega-fixture configuration. Estimated micromotion ranged from 156 μm to 365 μm around the cup rim and from 168 μm to 277 μm near the fixation screws.

The inability of several methods to accurately estimate micromotion of the cup called into question the assumption of rigid-body motion. The aim of mapping micromotion over the entire surface remained. Therefore, a micromotion calculation technique not dependent on assumed rigid-body motion was developed. This technique instead assumed homogenous deformation, which implies the final position of a point on a body is a linear function of its initial position (Boresi and Lynn 1974). To solve for the displacement of any point on the cup using this technique requires the displacement to be known at four locations. Data from a nine-gage test using the standard gage configuration were used for three points. The fourth point was chosen as a point near the fixation screws. The displacement could not be measured there but was assumed to be small. Analysis was performed using two approximations for the displacement at the fourth point: no displacement i.e. rigid fixation by the screws; and 30 μm of micromotion in all three directions, about equal to that estimated from the 100% coverage test. Estimated micromotion at the rim was exceedingly large, ranging from 52 μm to 509 μm (particularly since the largest magnitude of measured micromotion was 290 μm), but more reasonable near the fixation screws, ranging from 56 μm to 123 μm.

3.2.4 Measurement of the Relative Displacements to Evaluate Screw Fixation Configurations

Having attempted and failed with several techniques at calculating the micromotion over the entire cup this goal was therefore abandoned, but the test objective of determining the effect of screw configuration and different load cycles on cup motion remained. To address these remaining objectives, it was decided to measure the motion

at three points around the rim of the cup. Placement of the gages as near the rim as possible would effectively record micromotion at three locations on the cup. As stated previously, acetabulum geometry dictated gage fixture position. Due to the porous nature of the pelvic trabecular bone, few good sites existed where the gage fixtures could be attached. For consistency, the frames were attached to the ischium, iliac wing, and pubis, points A, B, and C, respectively, for every test (Figure 41). Three displacements were measured at points A and B and two displacements at point C.

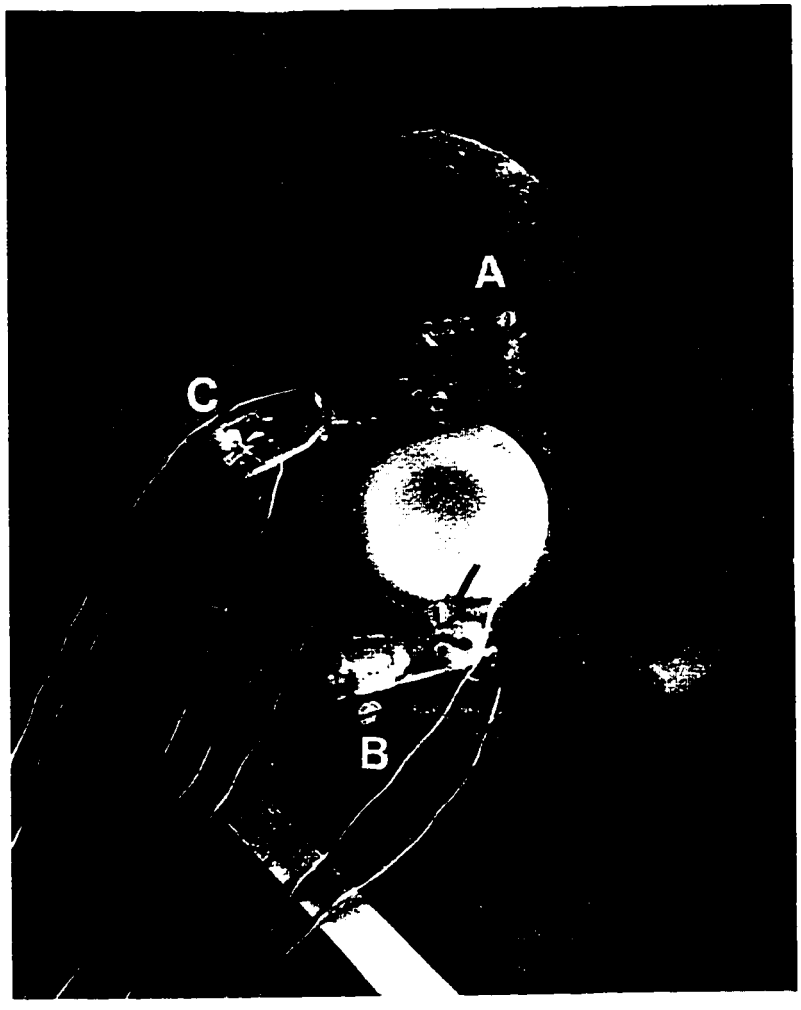

Figure 41. Photograph showing typical arrangement of gages used for acetabulum testing.

Cup outrigger location, with respect to the bony landmarks used to secure the gage fixtures, varied from specimen to specimen. To quantify subsequent variations in gage position, the angular location of the prosthesis outrigger and gage frame fixation screws were recorded (Table 12). The position angle was defined by rotation about an axis parallel to the SI axis passing through the center of the cup. The angle of rotation was defined by the right-hand rule.

Table 12. Angular location, with respect to an axis passing through the center of the cup oriented parallel to the SI axis, of the acetabulum cup outrigger and frame fixation screw {avg., (std. dev.), [range]}.

	Point A	Point B	Point C
Outrigger Screw	48° (24°) [22°-99°]	322° (12°) [301°-344°]	112° (42°) [58°-186°]
Frame Fixation Screw	52° (5°) [48°-60°]	327° (10°) [311°-345°]	147° (16°) [132°-168°]

3.2.5 Data Analysis

Reported micromotion is the Pythagorean resultant of all gage data measured at each point. Data smoothing and micromotion calculation from maxima and minima were the same as for the femur. To reduce the effect of varying gage fixture location, data were generally presented as a ratio of data from the same specimen. That is, micromotion from the various screw configurations were normalized with respect to the micromotion observed using configuration 1, and stair climbing micromotion was normalized with respect to level walking micromotion.

3.3 Statistical Analysis

Statistical analyses included the Wilcoxon Rank and Wilcoxon Ranked Sum tests to check for statistical significance. These correspond to normal and paired t-tests

respectively. The small number of specimens necessitated using the Wilcoxon tests because, unlike the t-tests, the Wilcoxon tests do not assume a Gaussian distribution. Results of the Wilcoxon tests report statistical significance in terms of a p-value in the same manner as a t-test, with $p<0.05$ generally indicating significantly different averages.

CHAPTER 4

RESULTS

4.1 Femur Results

Femur results are presented in two groups: general trends observed in all three fit categories; and fit-specific trends, which indicate the effect of fit on micromotion.

4.1.1 General Trends

All prostheses experienced more micromotion distally than proximally (porous-coated data is the average of eight points near the center of the coating, four on the anterior face and four on the posterior, Table 13). For specimens with a tight proximal fit the ratio of distal to proximal micromotion was approximately 4:1 ($p<0.05$). For the loose/tight specimens the ratio was 1.3:1 ($p<0.08$). No difference exists between level walking (LW) and stair climbing (SC) data ($p>0.35$).

Table 13. Proximal and distal resultant micromotion*.

	Tight-Tight		Tight-Loose		Loose-Tight	
Gait	PC[a]	DT[b]	PC	DT	PC	DT
LW	73 ±39	297 ±127	72 ±50	232 ±164	280 ±95	361 ±118
SC	68 ±30	246 ±85	83 ±54	280 ±125	295 ±74	390 ±195

*Series average±standard deviation (units = μm), [a]PC: porous-coated region.

[b]DT: distal tip.

Large spatial variations of micromotion were observed in the porous-coated region. Tight/tight and tight/loose specimens generally exhibited variations on the order

of 50 μm and occasionally up to 100 μm (Figure 42). Loose/tight specimens exhibited variations greater than 100 μm. All but one prosthesis showed less micromotion on the lateral aspect than on the medial aspect. Resultant micromotion was nearly identical on the anterior and posterior faces of the prostheses.

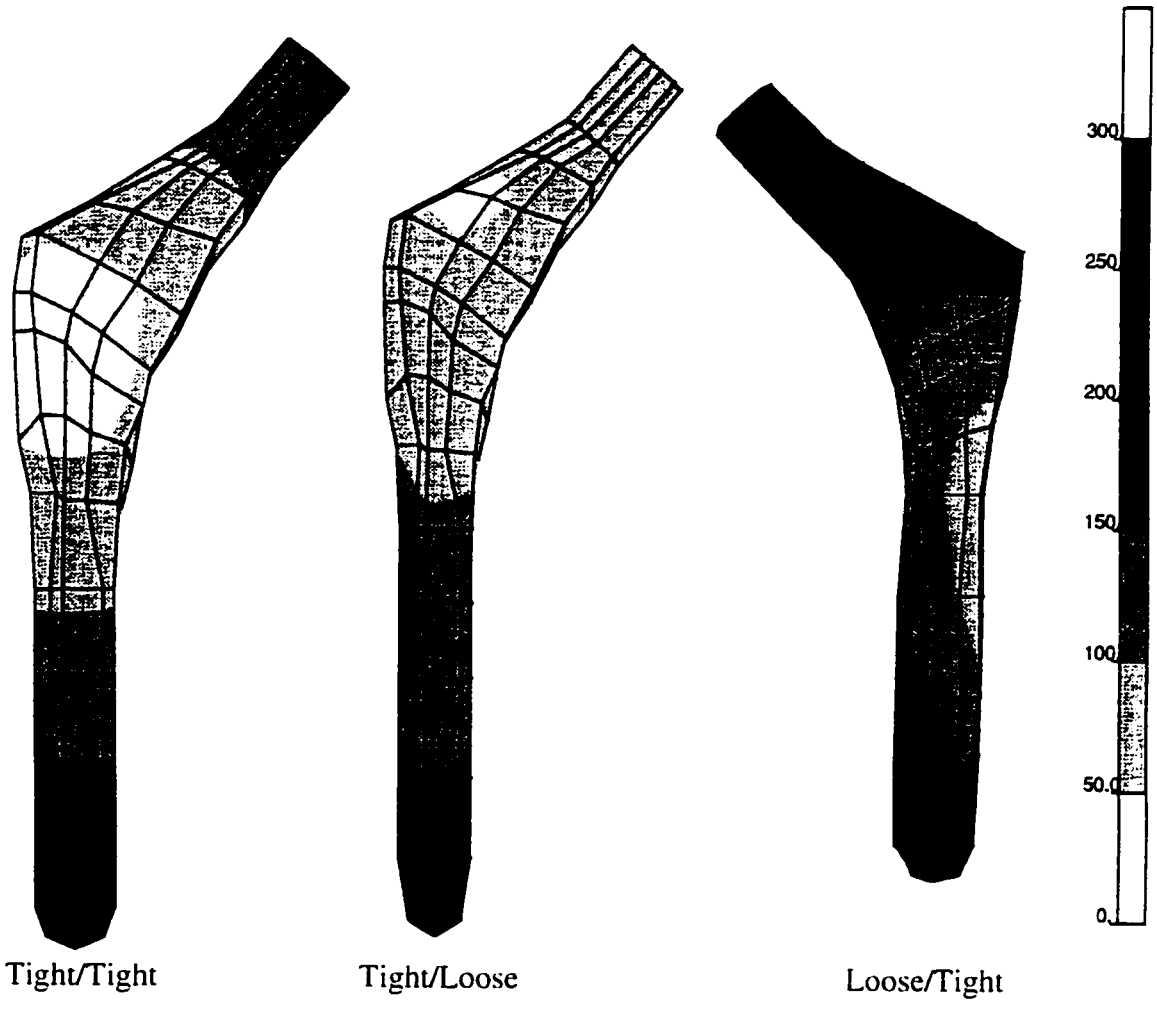

Figure 42. Contour mappings of the resultant micromotion for a typical specimen from each fit category, anterior view. The porous-coated region is outlined in bold.

Dominant directions of micromotion varied between proximal and distal regions and between the fit categories (Figures 43 and 44). Motion in the AP direction was

generally less than motion in the ML direction ($p<0.07$) and SI direction ($p<0.06$) for both load cycle types except in the porous-coated region for loose/tight specimens. Differences between ML and SI components were less consistent. In the porous-coated region motion in the AP direction was the smallest component of motion in all three fit categories. The AP component was also the smallest component of motion at the distal tip for tight proximal specimens, but it was the largest for loose/tight specimens. As with the resultant micromotion the data indicated no difference between level walking and stair climbing load cycles regarding individual components of micromotion ($p>0.43$).

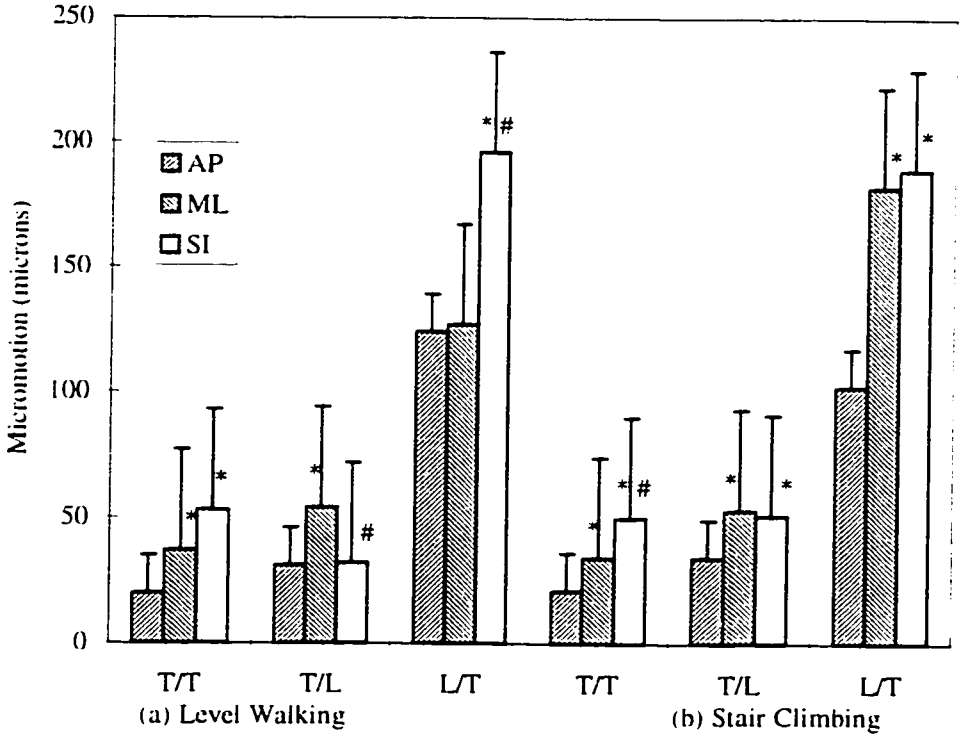

Figure 43. Directional components of micromotion in the geometrical center of the porous-coated region for each fit category, a) LW load cycle, b) SC load cycle.

Note: * and # denote a difference from AP ($p<0.07$) and ML components ($p<0.06$), respectively.

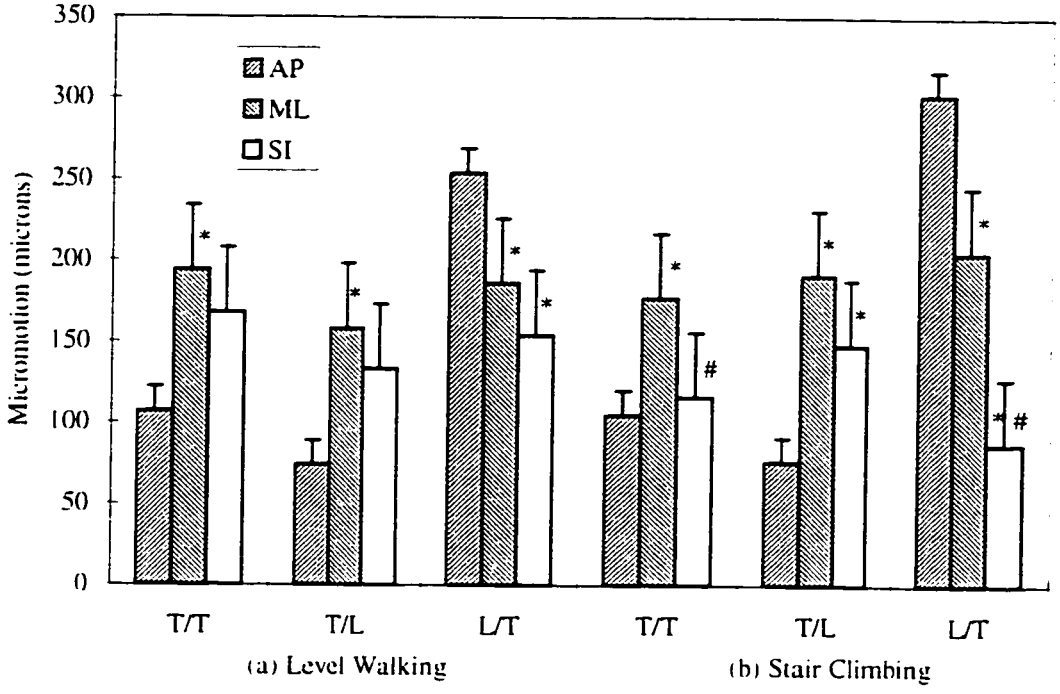

Figure 44. Directional components of micromotion at the distal tip for each fit category. a) LW load cycle. b) SC load cycle.

Note: * and # denote a difference from AP ($p<0.07$) and ML components ($p<0.06$), respectively.

4.1.2 Fit-Specific Trends

Previous studies (Bragdon et al., 1996; Engh et al., 1992; Pilliar et al., 1986) have shown bone ingrowth when micromotion of the prosthesis is less than 50 μm, and fibrous ingrowth when the micromotion is greater than 50 μm but less than 150 μm. When micromotion exceeds 150 μm ingrowth does not occur. Consequently, the areas of the porous-coated region experiencing these ranges of micromotion were determined and are presented as a percentage of the surface area of the entire porous-coated region (Figure 45). During level walking 22% (s.d. 26%) of the porous-coated region experienced less than 50 μm of micromotion for tight/tight specimens, versus 37% (s.d. 49%) for tight/loose specimens. No loose/tight specimens exhibited regions with less than 50 μm

of micromotion. The percentage of porous-coated region experiencing between 50 μm and 150 μm of micromotion was 74% (s.d. 24%) for tight/tight specimens, 63% (s.d. 49%) for tight/loose specimens, and 37% (s.d. 51%) for loose/tight specimens. Only one tight/tight specimen and one tight/loose specimen (for level walking and stair climbing load cycles respectively) contained areas in the porous-coated region with greater than 150 μm. In this regard, the trends were again the same for the stair climbing load cycle as for the level walking load cycle, with no statistically significant differences between the two load cycles in any of the three ranges of motion magnitude.

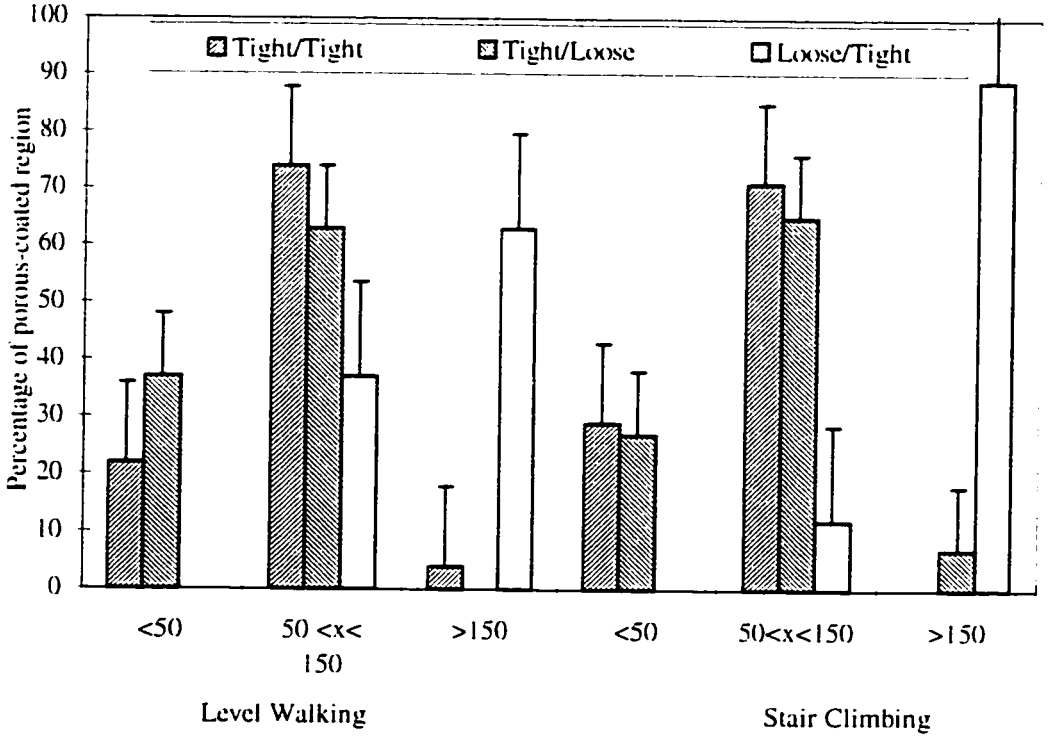

Figure 45. Percentage of the porous-coated region experiencing plausibly ingrowth-permissive levels of micromotion.

The tight/tight and tight/loose specimens experienced much less subsidence than loose/tight specimens ($p<0.01$, Figure 46). Tight/tight specimens averaged approximately 130 μm of subsidence, tight/loose specimens 140 μm, and loose/tight specimens 879 μm. There was no significant difference between tight/tight and tight/loose specimens or between the porous-coated region and the distal tip. Subsidence ceased at between 10 and 150 cycles, with the loose proximal/tight distal fit specimens needing the largest number of cycles before cessation of subsidence.

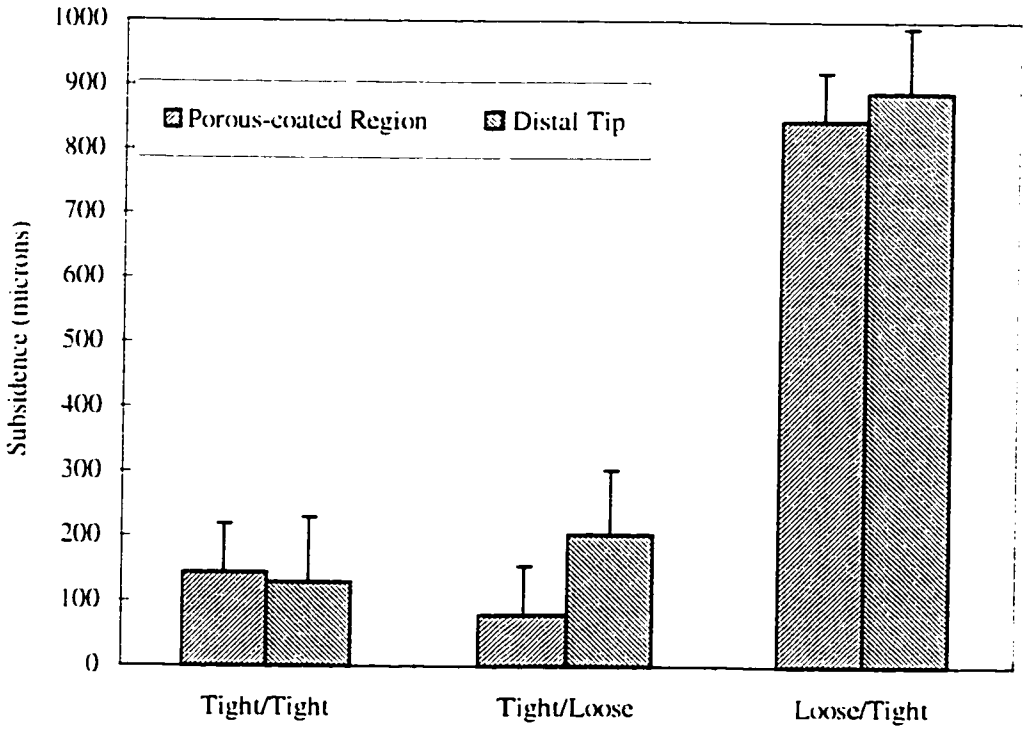

Figure 46. Average subsidence in the porous-coated region and at the distal tip. Dispersion bars signify variance.

4.2 Acetabulum Results

The aim of the acetabulum study was to examine the effects of screw configuration and various load cycles on cup micromotion. To successfully complete this task, screw fixation and measurement of micromotion needed to be comparable between specimens.

Screw fixation, quantified by screw insertion torque, was consistent from specimen to specimen (Table 14). Hereafter, the term screw A refers to the screw inserted into screw hole A; screw B and screw C are similarly defined. For torque less than 0.5 N-m, the screw could be continuously turned. Torque in the range from 0.6-1.0 N-m produced a good snug fit and would be considered adequate during surgery. Torques greater than 1.0 N-m felt extremely tight and would be considered excellent surgically. Uni-cortical and bi-cortical purchase (determined by visual inspection) showed no difference on insertion torque during loading protocol 1, including the removal and re-insertion of screw B. However, preliminary tests indicated that after approximately 300 cycles, or for a second removal/re-insertion, uni-cortical insertion torque declined sharply, whereas bi-cortical did not. Evidence of this was shown in loading protocol 2, where for two of the three uni-cortical screws, no appreciable insertion torque could be achieved.

Table 14. Average initial screw torque {units=N-m, avg. ± std. dev.}

	Uni-cortical	Bi-cortical	Uni/Bi Combined	Reinsertion	Protocol 2
Screw A	1.4 ± 0.2	1.5 ± 0.1	1.4 ± 0.2	n.a.	1.0 ± 0.5
Screw B	1.0 ± 0.6	1.5 ± 0.2	1.3 ± 0.5	1.1 ± 0.5	0.7 ± 0.9
Screw C	n.a.	0.5 ± 0.2	0.5 ± 0.2	n.a.	0.2 ± 0.3

The relative insertion torque between screws A and B and screw C justify the clinical priority afforded these locations. Screw direction and design explain why screw

C did not achieve meaningful torque. Screw hole C directs the screw through a thin section of the acetabulum with very little distance between the subchondral plate and the outer cortex, leaving minimal thread purchase. Exacerbating this effect was the Duraloc screw design, which has a large shank length to thread length ratio, especially for the shortest screw (20 mm total length, Figure 47).

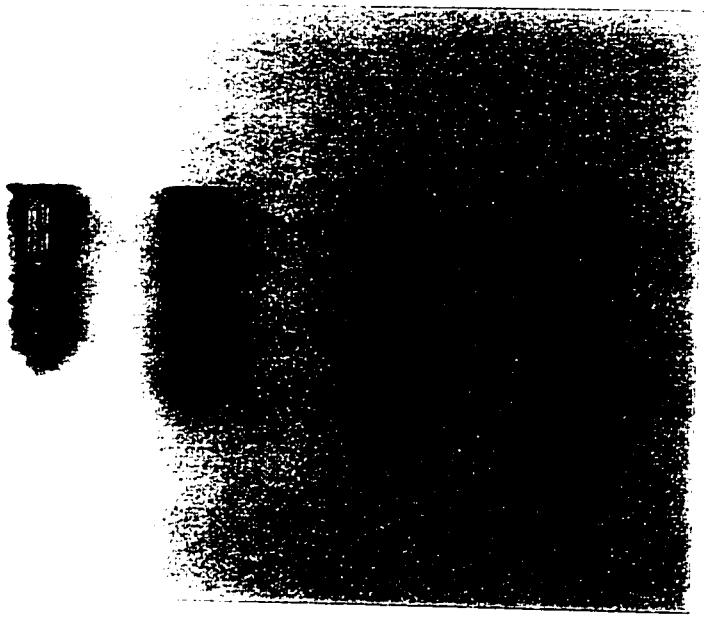

Figure 47. Fixation screws for Duraloc acetabular cup. Lengths range from 20 mm to 35 mm in 5 mm increments.

To reduce inter-specimen measurement variability resulting from different pelvic geometries, the cup rim screw holes, and consequently the gage fixture outriggers, were positioned near the same bony structures for each specimen. Evaluation of the data showed that no correlation existed between angular location of the outrigger screw (or the gage frame fixation screw) and the magnitude of micromotion. The low linear correlation coefficients, 0.05 to 0.46 (Figures 48-50), were indicative of other correlations

investigated, namely polynomial (second, third, and fourth order), exponential, logarithmic, and power series. The distance between the outrigger and gage frame fixation screws was constant for each gage fixture.

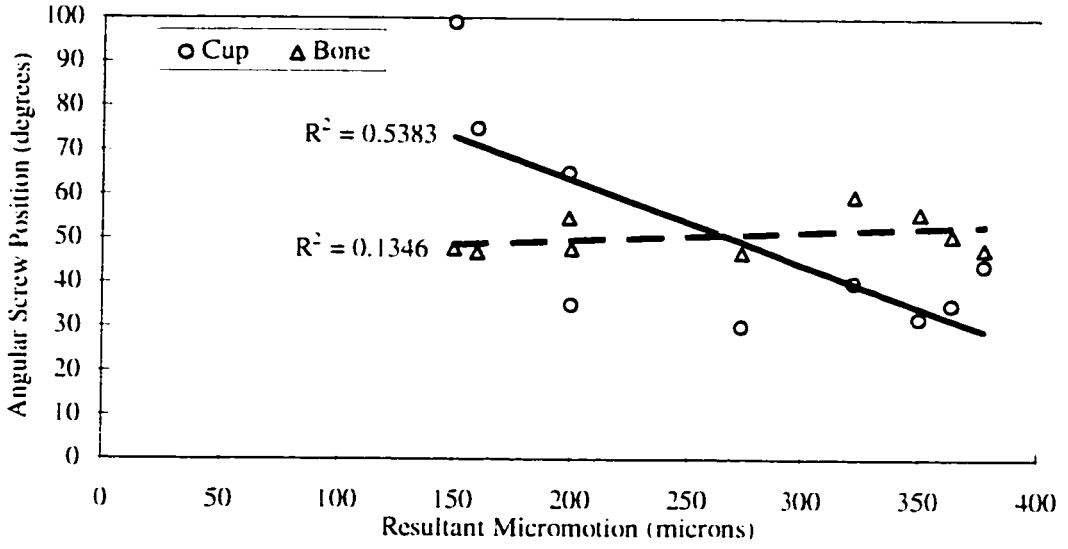

Figure 48. Linear correlation between micromotion measured at the ischium and the angular positions of the outrigger and gage frame fixation screws.

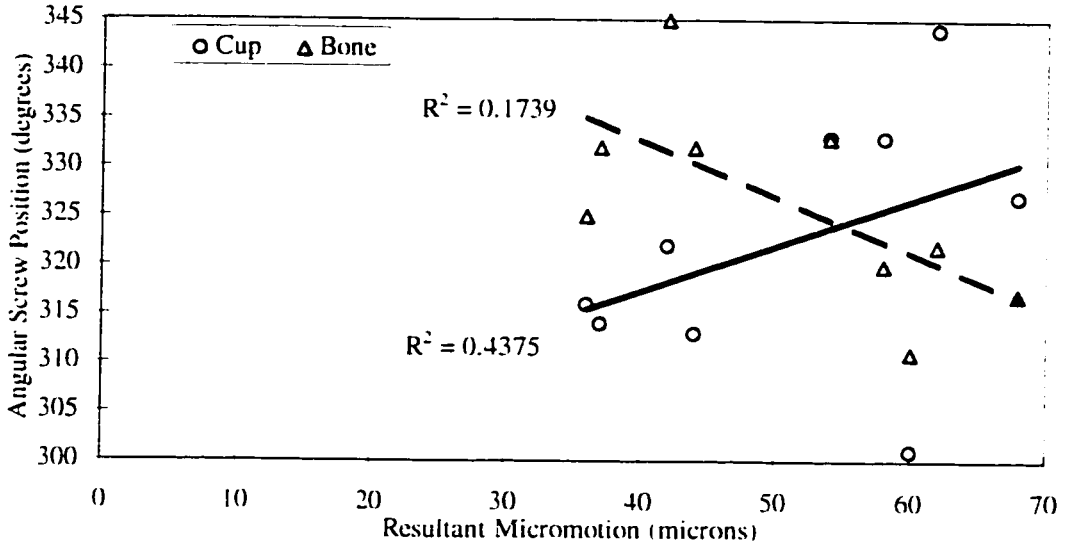

Figure 49. Linear correlation between micromotion measured at the ilium and the angular positions of the outrigger and gage frame fixation screws.

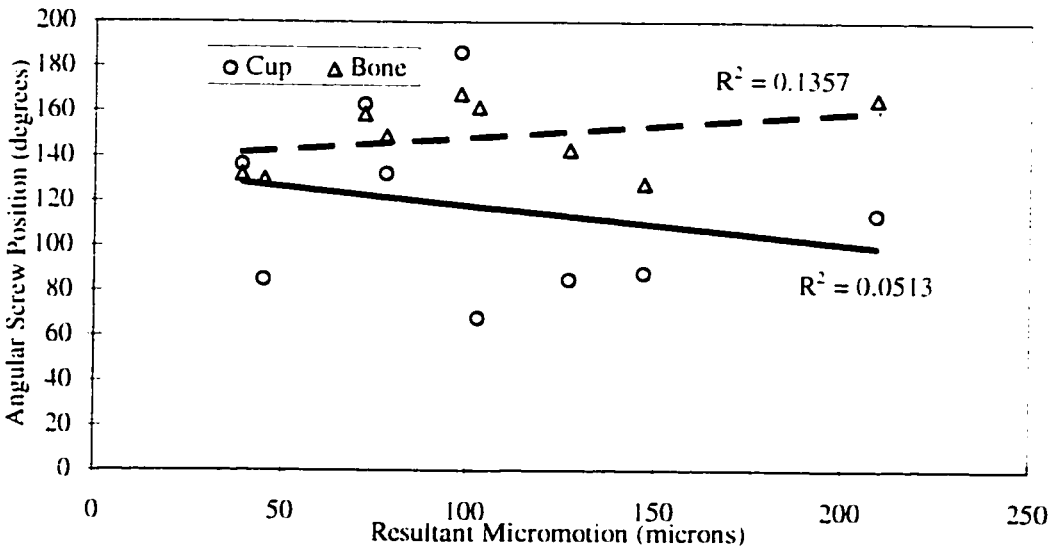

Figure 50. Linear correlation between micromotion measured at the pubis and the angular positions of the outrigger and gage frame fixation screws.

4.2.1 Loading Protocol 1

Micromotion varied from specimen to specimen as well as around the rim of the cup for any given specimen. The largest magnitudes of micromotion were observed near the ischium (gage site A), with the least near the ilium (gage site B), and with motion near the pubis (gage site C) generally in between (Table 15).

Table 15. Average (range) of micromotion at the three gage sites (units=μm).

Gage Site	Screw Configuration						
	1	2	3	4	5	6	7
Ischium	266 (160-377)	221 (111-310)	231 (132-329)	257 (165-365)	271 (189-394)	232 (132-322)	218 (99-304)
Ilium	51 (36-68)	37 (25-61)	36 (22-64)	46 (26-67)	64 (40-112)	48 (29-110)	52 (34-112)
Pubis	102 (39-209)	76 (39-128)	71 (38-127)	87 (54-165)	99 (45-183)	77 (43-124)	77 (49-114)

4.2.1.1 Screw Configuration

Screw configuration affected micromotion in roughly the same manner at all three measurement sites (Figure 51). Data from all three gage sites indicated addition of screw B reduced micromotion compared to the initial configuration ($p<0.05$). Micromotion with screw B alone was not different from either screw A alone or screw A and B combined ($p>0.29$). Not surprisingly, based on screw insertion torque, micromotion was largest for the configuration with only screw C inserted. Though not statistically significant ($p=0.42$), the data showed that the insertion of screw C to the configuration already containing screws A and B consistently increased micromotion at the ischium, and did so as well for several individual specimens at the ilium and pubis.

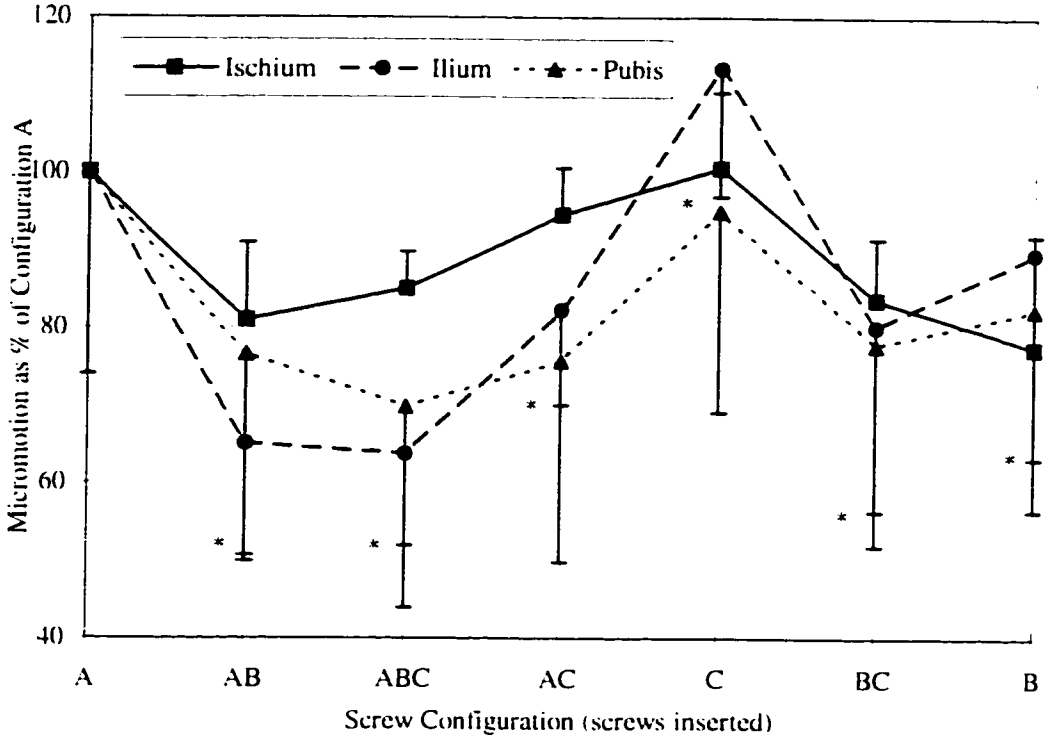

Figure 51. Micromotion for the level walking loading cycle around the acetabulum for the seven screw configurations.

Note: The * denotes the dispersion bars for the ilium data.

4.2.1.2 Vari-directional vs. Uni-directional Loading

The difference in micromotion between the level walking load cycle (directionally variant) and the uni-directional load cycle was not significant. At all measurement sites the individual components of motion were within 10 μm of each other and the resultant was within 15 μm. The level walking motion waveform did exhibit a wrinkle (Figure 52) which was attributed to the dual-peak loading waveform. In some specimens the peak motion did not occur simultaneously in all measured directions. A "lag" of up to 0.2 seconds was observed (out of a gait cycle of approximately 1.0 seconds).

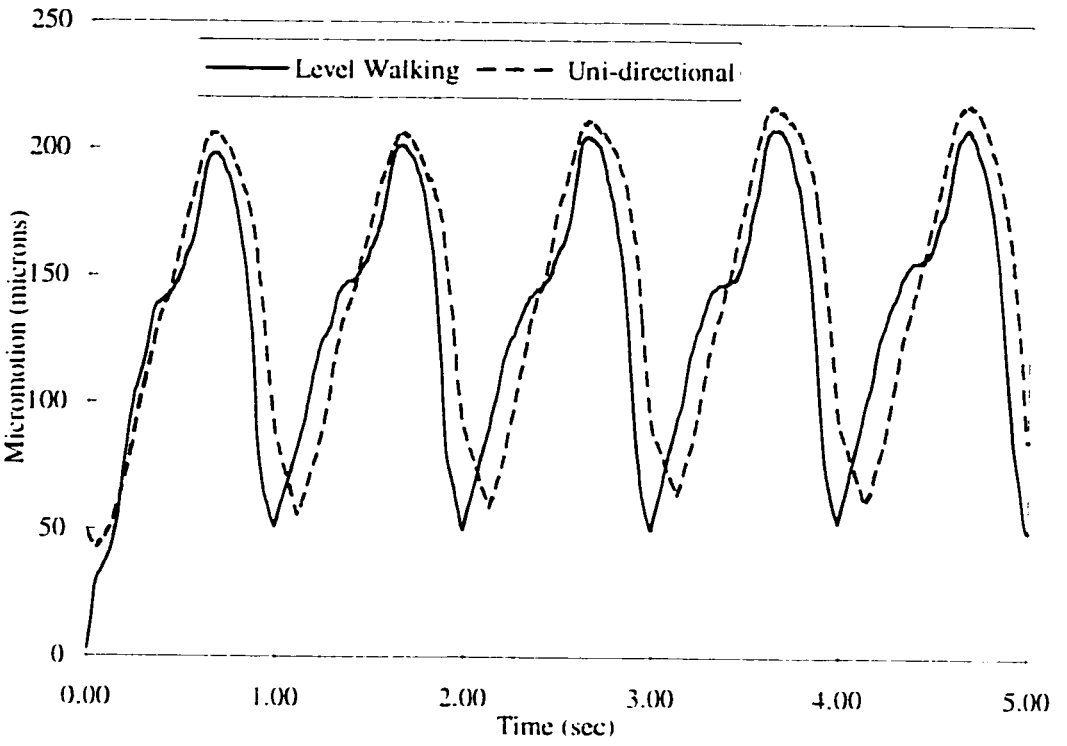

Figure 52. Plot of the resultant micromotion measured at the ischium, as an example of motion patterns created by vari- and uni-directional level walking load cycles. This effect was consistent for all screw configurations for the three specimens tested in this manner.

4.2.1.3 Independence of Screw Configuration Order

Tests of three specimens indicated that screw configuration order had no effect on micromotion results (Figure 33, page 82). The difference between micromotion for the first and second applications of loading protocol 1 was generally less than ten percent. There were two instances of change greater than 20%. However, for both of these cases the change in absolute resultant micromotion was less than 17 μm, well within the range of measurement error.

4.2.2 Loading Protocol 2

For loading protocol 2, only the first three screw configurations were used for all five specimens. Omission of the other configurations resulted from not being able to attain more than 50% of the loading protocol 1 screw insertion torque for either screw B or screw C. One specimen did achieve over 75% of loading protocol 1 screw insertion torque with both screws B and C, so this specimen was tested using six (all but the screw C-only) different screw configurations. To assure good comparison between level walking and stair climbing data (i.e., under similar screw fixation conditions), level walking data were re-recorded.

Micromotion during stair climbing differed from micromotion during level walking at all three measurement locations (Figure 53). The motion at the ischium and pubis decreased between fifty and sixty percent ($p<0.05$). Motion at the ilium increased slightly ($p<0.05$). Insertion of screw B reduced micromotion during stair climbing, as it

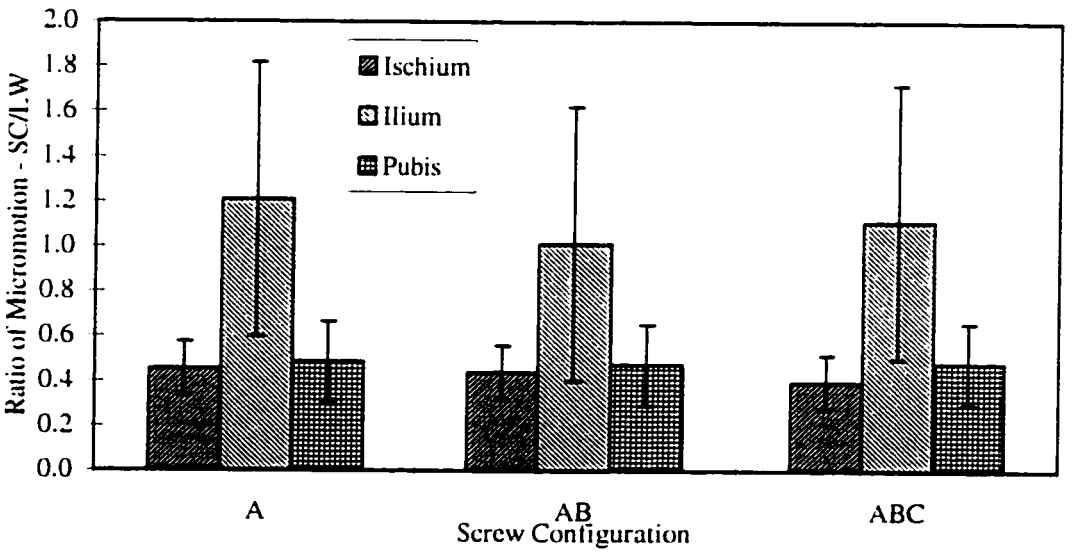

Figure 53. Micromotion during stair climbing normalized to micromotion during level walking.

had during level walking in protocol 1. From visual observation it was apparent that the entire pelvis moved more during stair climbing than level walking despite the reinforced support at the sacrum and sacro-iliac joints.

Level walking data did not change from loading protocol 1 to loading protocol 2 ($p>0.23$), indicating that the differences observed between the stair climbing and level walking loading cycles resulted from the different load cycles and not from specimen variability or screw purchase degradation. Micromotion relative to that for configuration A, during the level walking portion of loading protocol 2, showed similar trends to that observed during loading protocol 1 for screw configurations AB and ABC (Figure 54). Comparison of the average micromotion at each location indicated no significant difference between loading protocols near the ischium and the pubis (Table 16). The ilium and pubis exhibited greater micromotion ($p<0.08$) for configurations AB and ABC. However, the absolute change in motion, <23 μm, approached the limit of system accuracy for resultant micromotion.

Table 16. Comparison of motion during the level walking load cycle applied in loading protocol 1 (LP1) and loading protocol 2 (LP2). (avg. ± std.dev., units=μm)

	Configuration A		Configuration AB		Configuration ABC	
	LP1	LP2	LP1	LP2	LP1	LP2
Ischium	266 ± 91	288 ± 63	221 ± 69	281 ± 73	231 ±71	278 ± 82
Ilium	51 ± 12	67 ± 30	37 ± 13	60 ± 27	36 ±13	53 ± 23
Pubis	102 ± 53	108 ± 63	76 ± 34	98 ± 64	71 ± 33	86 ± 41

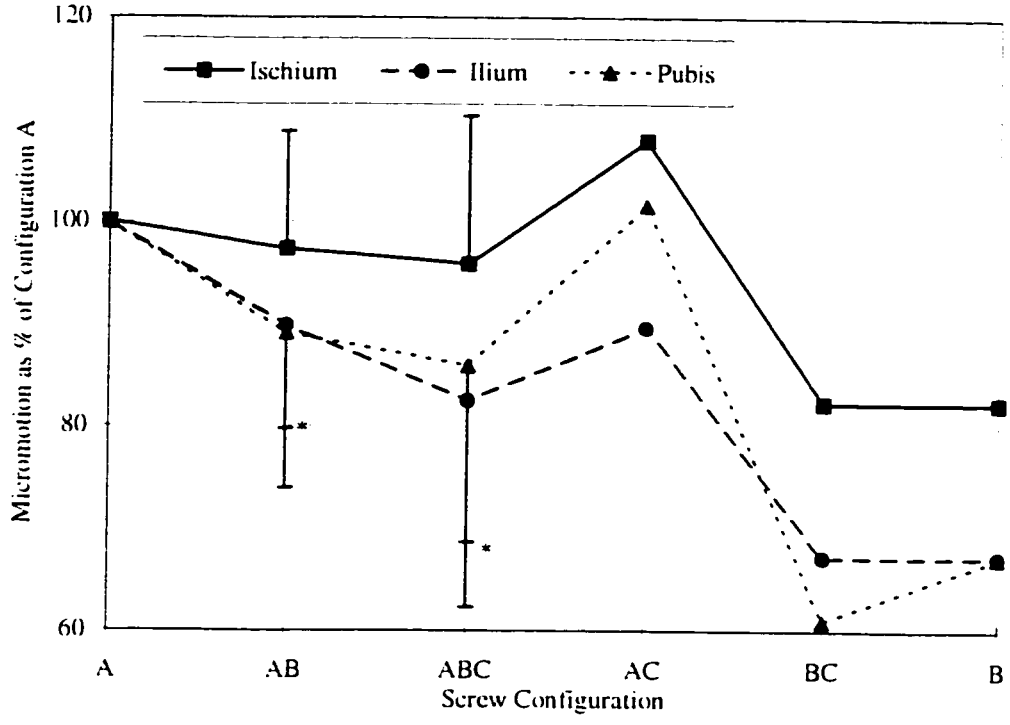

Figure 54. Micromotion for the level walking load cycle from loading protocol 2. Data for configurations A, AB, and ABC were averaged from all five specimens. Data for configurations AC, BC, and B were taken from only one specimen.

Note: The * denotes dispersion bars for the ilium data.

4.2.3 Cup-to-Bone Gaps

Cup-to-bone gaps varied over the surface of the acetabulum and throughout the experiment. Initial gap size ranged from 0.90 mm to 1.15 mm at the inner ring of screw holes (Figure 55). The initial gaps at the outer ring of screw holes were very close to 1.00 mm, except near the medial wall, where the gap averaged 1.45 mm (Figure 56). The cotyloid notch strongly influenced results for the gap near the medial wall. There were no significant differences in gaps around an individual ring, for either the inner or outer ring of screw holes. The average change in gap size was approximately the same (~0.30 mm) for the inner ring and outer ring of screw holes although screw A was located off center from the dome of the cup.

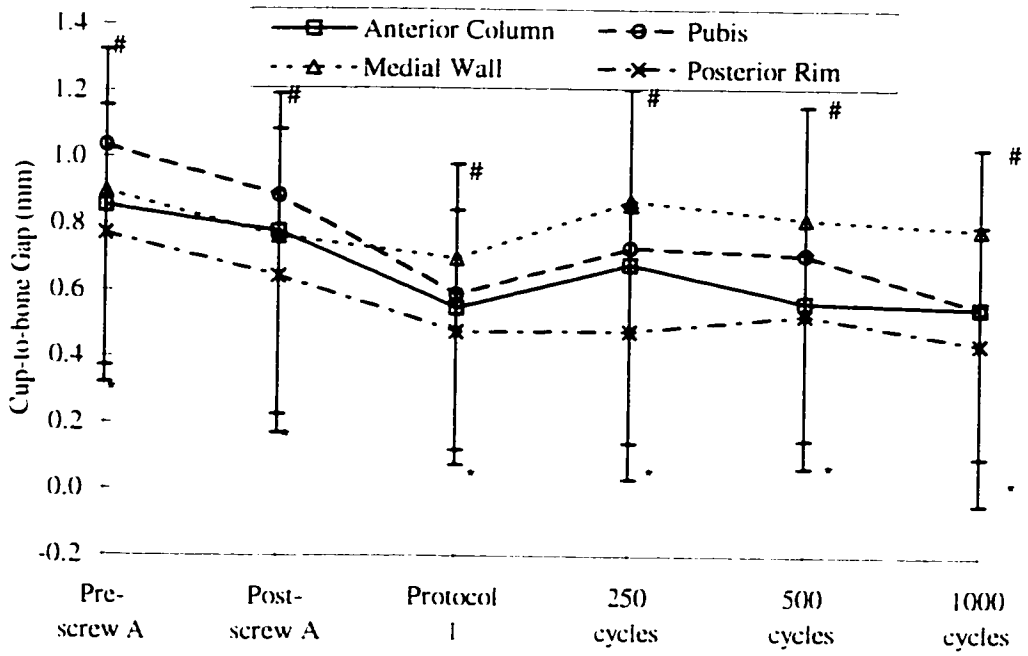

Figure 55. Average cup-to-bone gaps after each significant phase of the experimental procedure for the inner ring of screw holes.
The * and # denote dispersion bars for the anterior column and pubis respectively.

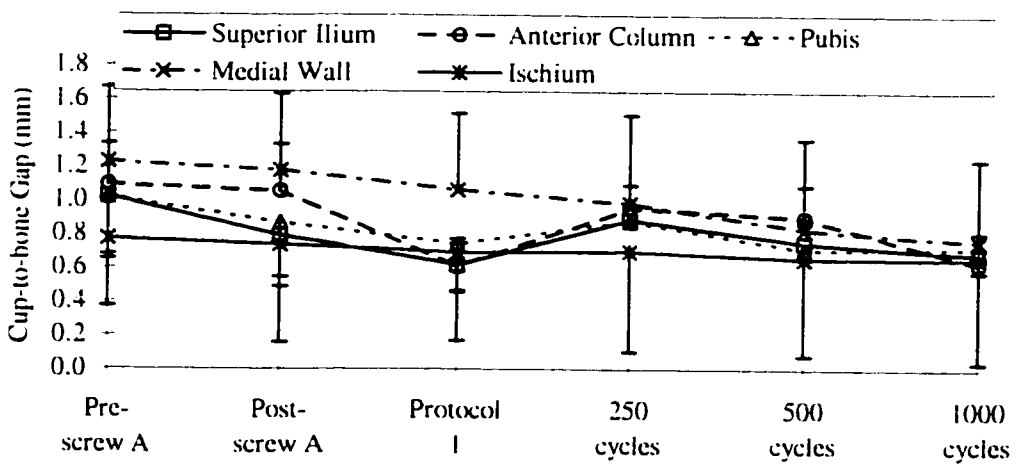

Figure 56. Average cup-to-bone gaps after each significant phase of the experimental procedure for the outer ring of screw holes.

A comparison between the inner and outer ring average screw hole gaps exhibited a consistent (but not statistically significant) difference (Figure 57). There was a decrease in the ring average gap after insertion of screw A and after loading protocol 1 ($p<0.05$). The additional level walking load cycles did not change the gap sizes ($p>0.40$).

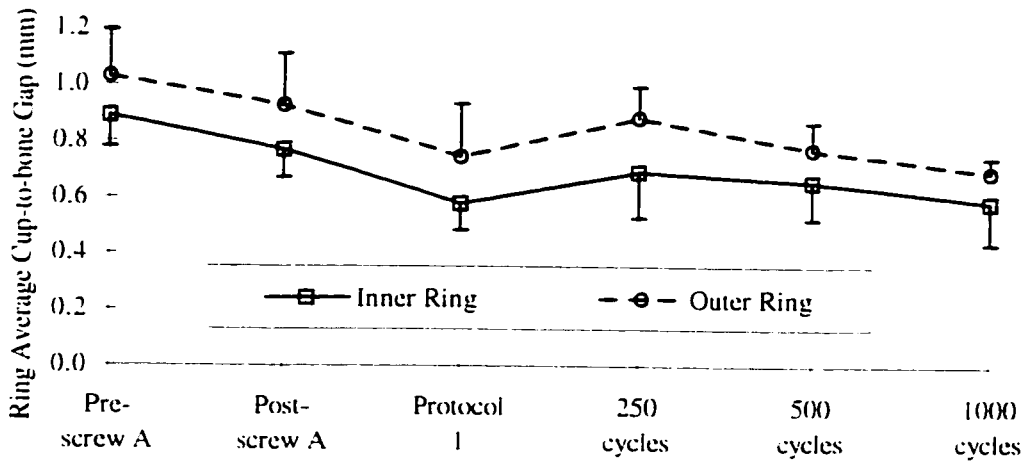

Figure 57. Ring average cup-to-bone gaps after each significant phase of the experimental procedure for the inner and outer ring of screw holes.

Cup size affected the initial and post-screw configuration 1 gap size (variation in specimen size required several different cup sizes to achieve the clinically optimal fit). As the diameter of the cup increased, the gaps at the inner of of screw holes increased, and eventually surpassed those near at the outer ring of screw holes (Table 17). The reduction of gap size achieved by inserting screw A increased with increasing cup size. However, gap sizes after insertion still increased because the difference in the initial gap size could not be overcome by the greater gap reduction.

Table 17. Gaps as a function of cup size (units=mm).

	Cup Size (No. tested)	50 mm (4)	52 mm (5)	54 mm (5)	56 mm (2)
Initial	Inner Ring	0.56	0.68	0.73	1.59
	Outer Ring	0.83	0.67	0.75	1.17
Screw Configuration 1	Inner Ring	0.54	0.51	0.47	1.22
	Outer Ring	0.75	0.71	0.69	0.93

CHAPTER 5
DISCUSSION

Interest in the use of noncemented prostheses in THA remains high due to the long-term failure rates of cemented components. The success of noncemented prostheses initially depends on achieving bone ingrowth into the porous-coating on the surface of the prosthesis. Excessive micromotion of the prosthesis reduces the amount of ingrowth and consequently the likelihood of adequate fixation. The goals of this study were twofold: to develop test procedures for both the femur and acetabulum which would enable prediction of *in vivo* performance based on calculated micromotion of the porous-coated regions, and to use the procedures to evaluate various fixation parameters for femoral and acetabular prostheses.

5.1 Applied Loads

The objective of the loading regimen was to apply loads to the components in such a manner as to match the JRF observed *in vivo* by Kotzar et al. (1991). To accomplish this the JRF was decomposed into three orthogonal components directed along the AP, ML, and SI axes. Frictional torque at the femoral head/cup liner interface was not considered because of its small magnitude (peak value of 1 N-m, Ma et al., 1983; Andersson et al., 1972) compared to stem torque resulting from the hip contact force component acting on the head of the femur (22 N-m to 35 N-m).

5.1.1 Femur Loading

The applied actuator axial loads generated coronal plane forces that accurately approximated the corresponding hip contact force components observed *in vivo*, but the

applied actuator torsional load did not generate the corresponding AP force component. The test apparatus transferred the applied actuator torque from the MTS machine directly to the prosthesis as torque about the SI axis, instead of generating the desired AP force component at the head of the prosthesis. This aspect of the test apparatus was demonstrated by removing the torsional constraint of the specimen support fixture at the base of the MTS machine after which applied torque rotated the test apparatus despite specimen constraint in the AP direction. For an AP force the reaction loads consist of moments about the ML and SI axes and an AP force in the opposite direction (Figure 58). Studies applying only an AP force to femoral prostheses show that the failure results from the moment generated about the stem (Nunn et al., 1989; Phillips et al., 1991; Sugiyama et al., 1989). Ryd et al. (1995) observed *in vivo* micromotion was dominant vertically with motion in the transverse plane only occurring severe cases, which is similar to results from the current study. Based on these results the applied torque generated the critical, though less than ideal, out-of-plane load.

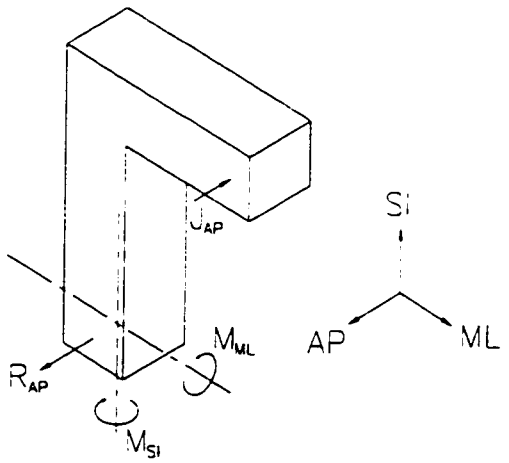

Figure 58. Schematic of reactions at the prosthesis/femur interface generated by a posteriorly directed force at the head of the prosthesis.

Simulation of the abductor muscle group force was considered important because of the large estimated magnitude attributed to these muscles during normal gait, up to 1.4 BW (McLeish and Charnely, 1970). Hazelwood (1996), using a finite element model, reported that inclusion of abductor muscle forces can increase strain in the proximal region by 17%. The load analysis of the current study estimated an abductor muscle force of 1.2 BW at peak JRF during the level walking load cycle.

5.1.2 Acetabulum Loading

The three hip contact force components observed *in vivo* were accurately reproduced for the acetabulum test. The level of complexity required to accurately simulate the large number of muscle groups acting on the pelvis did not warrant muscle simulation at this time.

5.1.3 Three-dimensional, Directionally-Variant Loading

The application of two-dimensional (i.e., generation of force components parallel to the ML and SI axes) uni-directional loads (primarily a result of only single-actuator test machines being available) limited previous studies. Studies applying three-dimensional (i.e., generation of force components parallel to all three anatomic reference frame axes) uni-directional loads reported micromotion magnitudes three to six times the magnitude observed when applying two-dimensional uni-directional loads to the same test configuration (Burke et al., 1991; Callaghan et al., 1992; Walker et al., 1987). The importance of applying a directionally variant JRF versus a uni-directional JRF has not previously been addressed.

The uni-directional and vari-directional load cycles applied to the acetabulum generated essentially the same amount of micromotion at all measurement sites. This is perhaps attributable to the cup being well fixed to the acetabulum. Attachment of the cup

to the acetabulum can be thought of as making the two bodies one. Recoverable relative motion can then be likened to elastic strain, implying that the same peak load will produce the same relative motions, independent of the intermediate load path. The fact that the only time the two load cycles were identical was at the maximum JRF suggests that peak micromotion depends only on the maximum applied load. The linear relationship between applied load and micromotion reported by Stiehl et al. (1991) supports this conclusion.

The relationships between forces acting at the head of the prosthesis and the resulting reaction loads at the femur prosthesis interface are complex. Clinical studies reporting thigh pain during stair climbing and rising from a chair suggest that the large posterior force generated during these activities may be the cause (Engh et al., 1987; Kotzar et al., 1995). As stated above, a posterior force at the head of the prosthesis creates several components of load in the femur, the apparently critical one being stem torque. However, Kotzar et al. (1995) reported that while the absolute values of stem torque were sometimes less during stair climbing and rising from a chair than during level walking, the ratio of stem torque to SI force at the femoral head increased during these activities. This complex interaction between SI forces and stem torque, and the potential effects of other as-yet-undetermined relationships, indicate that application of the complex patterns of the JRF observed *in vivo*, while possibly not so for the acetabulum, may be necessary to accurately determine the stability of femoral components.

5.2 Micromotion Calculation and the Assumption of Rigid-body Motion

The largest assumption made in developing a technique to calculate micromotion over the entire surface of the prosthesis was that the prostheses and specimens behaved as rigid bodies. This implied that strains in the specimens were small enough that rigid-

body motion analysis would provide a reasonable approximation of the actual relative motion at the prosthesis-bone interface. Specimen strain effects were divided into two categories: local effects, defined as those effects directly influencing displacement measurements, and global effects resulting from the overall strain distribution. Local effects are somewhat quantifiable and can be reduced by test procedures. Global effects cannot be directly estimated and must be accounted for by independent validation.

5.2.1 Consideration of the Assumption of Rigid-body Motion for the Femur

Local strain effects arise from the fact that strains in the femur may influence measurements by displacing the gage fixture block with respect to the gage fixture frame, even if no relative motion between the prosthesis and bone occurred, tending to overestimate measured motion. Axial strains in a femur with an implanted prosthesis have been reported at 1000 με (where $\mu\varepsilon = 10^{-6}$) near the distal tip, and range from 250 με to 620 με proximally (Holmberg et al., 1986; Walker et al., 1987). The femur test apparatus for the current study located the clamp supporting the proximal gage fixture frame within 1 cm of the outrigger attached to the porous-coated region, and the distal frame clamp within 5 mm of the distal outrigger. The artifactual displacements due to local strain effects were approximated as 620 με * 1 cm = 6.2 μm proximally, and as 1000 με * 5 mm = 5μm distally. These artifactual displacements of course only account for axial strains. Circumferential strains may also affect measurement displacement, but even if of the same magnitude as the axial displacements (which seems unlikely) the total artifact would be within the range of artificial perturbations used to test the rigid-body algorithm. Thus local strain effects do not appreciably influence the current micromotion calculations.

The overall strain distribution of the femur produces changes in the shape of the femur due to bending, twisting, and compression, i.e., global effects. Changes in shape occur regardless of the test apparatus, and depending on the measurement sites, may or may not influence the measured displacememts. Even without directly influencing the measured displacements, global effects can influence the accuracy of calculated displacements by overestimating or underestimating the motion (Figure 59).

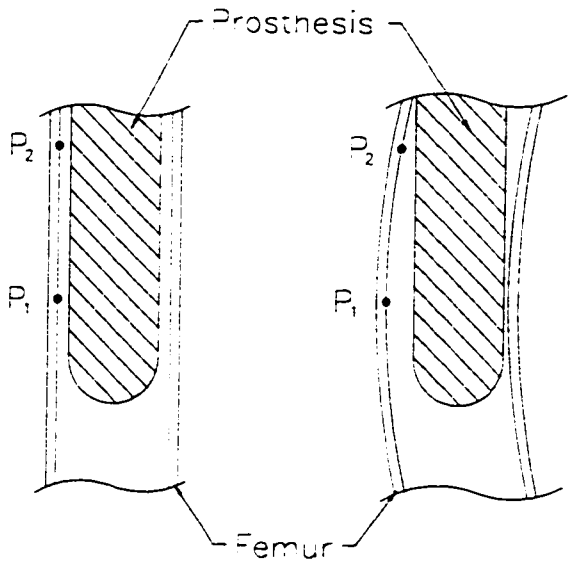

Figure 59. Graphical representation of the potential affects of the strain distribution in the femur on the calculated displacements at two points. Left is the unloaded specimen, center is the rigid-body approximation of displacement, and right is the true displacements. In this example the motion at point P_1 is overestimated and the motion at point P_2 is underestimated.

Stiffness of the prosthesis and contact between the prosthesis and femur may reduce the influence of global effects. Gilbert et al. (1992) reasoned that separating the measurement locations proximally and distally reduces the artifact generated by these effects. Previous investigators assuming rigid-body motion (Gilbert et al., 1992; Elder 1992) have not quantitatively shown that the global effects do not appreciably affect

micromotion calculations. In addition, the interaction between local and global effects (do shape changes magnify local effects?) has not previously been addressed.

Comparison between measured and calculated displacements validated the current micromotion calculation technique. First, comparisons were made at the locations where measurements were normally recorded, i.e., points A, B, and C (the ends of the prosthesis outriggers). Agreement between measured and calculated displacements at these points, including the two normally nonmeasured displacements at point C, was excellent, differing by less than 5 μm. As a more rigorous validation, a similar comparison was made at a point independent from the normal measurement locations. Results for this independent point were nearly as good. Differences in measured and calculated micromotion were 10 μm in the AP and ML directions, and 35 μm in the SI direction. The cause for the relatively large overestimation in the SI direction could not determined. However, since the error only created a 14 μm difference between the calculated resultant micromotion and the measured resultant micromotion, it was deemed acceptable. (The small effect of the SI component error stems from the fact that motion at the distal tip, where the independent displacements were recorded, was dominated by motion in the AP or ML directions.)

5.2.2 Consideration of the Assumption of Rigid-body Motion for the Acetabulum

The assumption of rigid-body motion proved invalid for the acetabulum test. Failure of all of the rigid-body motion analyses to accurately estimate micromotion of the cup was attributed to global strain effects (i.e., deformations), not local strain effects. Reported extensional strains are only slightly larger for the acetabulum than for the femur but still within reported physiologic ranges, i.e., <3000 με (Table 18). These strain data, coupled with the distance from the cup outrigger to the gage frame fixation screw

(ranging from 1.0 cm to 1.4 cm), indicated larger local strain effect artifact. Based on site-specific data from Noble et al. (1995), the estimated local strain effect artifactual displacement was 1.4 cm * 747 με = 10 μm at the ilium and 1.4 cm * 1642 με = 23 μm at the pubis. Though larger than the femur, these artifacts were still within the range of artificial perturbations used to verify the various calculation techniques used for the acetabulum, and consequently do no seem large enough to generate the observed errors.

Table 18. Reported bony strain after implantation of noncemented prostheses (units=με).

Femur		Acetabulum	
		Massin (1995)	100 - 400
Walker (1987)	620	Lionberger (1985)	400 - 1000
Holmberg (1986)	250/1000	Noble (1995)	120 - 1920

Note: Acetabulum strains shown are the range reported around the acetabulum, femur strains are axial for the proximal region except for Holmberg which are the proximal/distal strains.

It is believed that the relatively compliant cup/acetabulum experimental construct generated global strains which invalidated the assumption of rigid-body motion. The suspected difference in global strain effects between the femur and acetabulum lies in the different prosthesis/specimen constructs. The femur is basically a thick-walled cylinder loaded slightly asymmetrically at one end and directly supported at the other. In contrast, the acetabulum is a thin-walled hemisphere loaded symmetrically but supported asymmetrically by three irregular members, the ilium, the ischium, and the pubis. Global deformations of the pelves were quite large, with visually observed translations ranging from 2 cm to 3 cm at the symphysis, an order of magnitude larger than translations measured *in vivo* at the same location (Walheim and Selvik, 1989). Large deformations were also observed at the sacro-iliac joint. Reinforcement of the pelvis for the stair climbing loads reduced flexion of the sacro-iliac joint, but relative motions were still visible.

The final evidence indicating global effects as the source of the inaccurate micromotion calculations came from the "mega-fixture" test. This test removed any differences between the femur test (which proved to accurately estimate micromotion) and the acetabulum test with respect to data capture and analysis. The only remaining difference between the two tests was the prosthesis/specimen construct. In light of the fact that the "mega-fixture" test did not accurately estimate the nonmeasured displacement at point C or the micromotion at independent measurement sites around the cup, it is reasonable to conclude that global effects are the source of the inaccurate micromotion calculations based on the assumption of rigid-body motion.

A linear correction to rigid-body motion analysis does not appear to be a likely solution to the problem of acetabulum deformations using the current test apparatus. Maps generated using the homogenous deformation analysis of Boresi and Lynn (1974) were reasonable for two cases (micromotion of 20 μm near the screws to 200 μm near the rim, all values less than the measured displacements). Four other specimens had widely varying results with inaccuracies in the estimation of micromotion comparable to those observed using the assumption of rigid-body motion. The inaccuracies of the homogeneous deformation approximation lie in assumptions made when deriving the formulation. In deriving the equations it is assumed that the body undergoing deformation is isotropic and that finite straight lines remain straight, a concession to Saint-Venant's principle. However, the bony architecture of cancellous bone sandwiched between cortical plates is anisotropic (not to mention variations in the cancellous bone itself). Saint-Venant's principle states that stresses, and consequently strains, cannot be computed in the immediate vicinity of the application of point loads. Yet in this experiment we attempt to measure deformations at the site of point loads generated by screw fixation. In short, the homogeneous deformation analysis is a linear approximation

of a non-linear system that in this case proves to be unreliable.

5.3 Femur Data

Micromotion magnitudes from the present study are in reasonable agreement with previous studies (Table 19). The slightly higher distal micromotion could be attributed to larger applied loads and measurement of three-dimensional motion but it is suspected to reflect prosthesis design. Results from the present study, and several earlier studies, indicate that more micromotion occurs distally than proximally. Studies that applied torsional loads about the stem of the prosthesis observed larger magnitudes of motion than those where only coronal plane forces were applied.

The current data indicate that proximal fit was critical in reducing micromotion, and that tight distal fit minimally influenced micromotion. This is in direct contrast to two early studies. Whiteside and Easley (1989b) compared distal fit to proximal fit, defining tight proximal fit by impingement of the prosthesis collar on the calcar femorale. They concluded that micromotion over the entire prosthesis depended on distal fit, with proximal fit having no effect. In another study, Noble et al. (1989) examined three distal fit conditions: tight, 1 mm undersize in stem diameter (the same as this study), and 2 mm undersize, with nominal proximal fit for all cases. Data from their study also indicated that distal fit was essential in limiting micromotion. The difference in conclusions for the early studies and for the present study plausibly result from prosthesis shape and the applied loads. Both early studies used a straight-stemmed, collared prosthesis with proximal wedging in only the ML direction. This is unlike the Ranawat/Burstein prosthesis, which has proximal wedging in the ML and AP directions as well as anteversion. Also, in these earlier studies only axial loads were applied to the head of the prosthesis. Proximal wedging resists not only translation of the prosthesis down the diaphysis but also torsion about the stem. Both an AP and ML wedge makes the

Table 19. Femoral micromotion reported in previous studies (units=μm).

Study	Loading	Fit Proximal/Distal	Data Site	Micromotion	
				Proximal	Distal
Present	Quasi-physiologic JRF =2.8 BW/ 22 N-m	T/T* T/L L/T	Global	69 64 182	234 217 391
Berzins (1996)	Quasi-physiologic 5 BW	Standard	Local 6 d.o.f.	n.a.	104
Bühler (1995)	Level Walking 3 BW	Standard	3D[§] Local	90	106
Burke (1991)	SLS[†] SC 1 BW	Standard	2D local	15 108	n.a. n.a.
Callaghan (1992)	Axial ~3 BW Axial/torsional ~2.2 BW/22 N-m	Curve Stem Curve/straight stem	2D local	31/11 20/35	14/13 48/96
Dujardin (1996)	SLS 3 BW	Custom fit/ Anatomic	3D local	73/55	98/104
Gilbert (1992)	Axial - 2000 N	Standard	Global	70	120
Hayes (1992)	Axial/torsional 1500 N/±10 N-m	Custom	Global	Peak 314 - 517	
Noble (1989)	Axial 2000 N	T/T T/0.5 mm gap T/1.0 mm gap	3D Local	n.a. n.a. n.a.	75 130 150
Schneider (1989 a,b)	Axial/torsional 4 BW/8 N-m	Standard	2D Local	210	111
Sugiyama (1992)	Torsional 20 N-m	Under-reamed Line-to-Line	1D Local	50 260	n.a. n.a.
Walker (1987)	Axial - 1000 N Axial/torsional 1000 N/100 N AP	Exact fit/ Loose proximal	1D Local	28/42 52/78	n.a. n.a.
Whiteside (1989)	Axial - 1500 N	Collar/tight Collar/loose No collar/tight	3D Local	21 22 40	10 207 8

Note: T/T*=Tight proximal/tight distal fit

SLS[†]=Single leg stance, coronal plane loading

3D[§]=measurement of displacement in three dimensions.

proximal region wider, and consequently more resistant to stem torque, than the prosthesis stem. Failure to apply an AP force (or stem torque directly) would therefore underestimate the relative contribution of proximal fit to femoral prosthesis stability.

More recent studies report data supporting the current study regarding proximal fit as more essential in reducing micromotion than distal fit. Callaghan et al. (1992) reported that a curved stem experienced less micromotion than a straight stem, especially for loading with torsion about the stem. The curved stem afforded better fixation proximally and the straight stem afforded better fixation distally. While studying custom-made components, Dujardin et al. (1996) observed that increasing proximal fit reduced vertical translation and rotation about the stem. No correlation between distal fit and prosthesis motion was observed. Walker et al. (1987) reported results similar to Dujardin et al., in that as proximal fit was reduced micromotion increased up to 50%. In a study using a modular component that allowed independent fit proximally and distally, Whiteside et al. (1994) obtained results indicating that proximal support at the base of the femoral neck was the most important factor in reducing micromotion. The results also showed significant contribution of the prosthesis stem. The increased importance of proximal fit to prosthesis stability arose from two important differences from the earlier studies: torsional loads were combined with axial loads, and the proximal portion of the prosthesis was much wider in the AP direction than was the stem. The earlier studies indicating the importance of distal fit over proximal fit differ from the present study in the same fashion. The fact that studies applying stem torque as well as axial loads (hence more physiologic loads) indicate that proximal fit is more important than distal fit in reducing prosthesis micromotion, suggests that proximal fit may also be more important clinically.

While proximal fit may play the more important role in reducing micromotion, it should be noted that distal fit may still provide an important contribution to clinical performance. Specifically, good distal fit judged radiographically has been shown to reduce thigh pain (Callaghan et al., 1992; Whiteside, 1989a) and potentially to reduce disuse resorption of bone by keeping femoral strains nearer normal than press-fit or loose stems (Jasty et al., 1994).

Knowledge of the micromotion over the entire prosthesis is critical in predicting the amount of bone ingrowth into porous surfaces. Many studies have shown significant differences between micromotion in the proximal and distal regions. However, the current data reveal that large, physiologically significant variations (greater than 50 μm) may occur even in the proximal region alone.

The results from the present study indicate that a tight proximal fit ensures that 22% to 37% of the surface of the porous-coated region will experience micromotion small enough to be conducive to bone ingrowth. In a retrieval study of AML femoral prostheses, Engh et al. (1994) reported that an average of 57% of the sampled areas demonstrated bone ingrowth. From a mechanical viewpoint, some of the difference likely results from the fact that the studies involved different prostheses. Also, the current study used loads observed 58 days postoperatively. Loads during the first month are lower (Kotzar et al., 1991) suggesting more of the porous-coated region would experience levels of micromotion conducive to bone ingrowth *in vivo*.

Biological factors invariably effect the amount of ingrowth. During healing, woven bone forms in the porous-coated region as early as one week after surgery, and begins to remodel into lamellar bone within four weeks (Galante, 1985). The remodeling process would most likely add stability to the prosthesis, reducing micromotion and rendering more of the porous-coated region conducive to bone ingrowth. This cycle of

increased stability leading to increased ingrowth may repeat until an equilibrium is reached. This is the ideal situation. The healing process which leads to mature lamellar bone is complicated. The events include migration of neutrophils and macrophages, bone resorption, cell differentiation and proliferation. Early resorption of necrotic bone occurs prior to bone ingrowth and may therefore reduce initial fixation. In addition, any condition which decreases bone formation with respect to bone resorption (e.g., decreased estrogen, age, increased interleukin 1, low calcium levels) may lengthen the time before bone ingrowth occurs. Indeed, it is at least possible that in some patients the resorptive aspect of the normal healing process may lead to component loosening.

Mapping micromotion over the entire surface may also prove beneficial in modifying designs to show the areas where the largest motions occur. The present prosthesis exhibited its least amount of micromotion on the lateral aspect for all but one loose/tight specimen. Collier et al. (1988), reporting on retrieved AML and PCA components, stated bone ingrowth was most likely to occur on the lateral quadrant of the prosthesis.

5.4 Acetabulum Data

5.4.1 Micromotion

The minimum amount of resultant micromotion occurred with two screws inserted near the dome of the cup. Addition of a third screw had no significant effect on micromotion at any of the three measurement locations. Removal of either central screw increased micromotion, independent of insertion of the third screw.

Comparison with data from previous studies indicates that insertion of two screws minimizes micromotion for 2 mm and 3 mm over-sized cups, as well as for on-line reamed cups (Table 20). Interestingly, two studies of 1 mm press-fit cups showed no

effect on micromotion from the insertion of one or two screws (Kwong et al., 1994, Won et al., 1995). The effect of screws may have been underestimated in these studies, however, since motion was only measured in one direction.

Table 20. Acetabular micromotion reported in previous studies (units=μm).

Study	Load	Fixation	Data Type	Micromotion		
				Ilium	Ischium	Pubis
Current	Quasi-physiologic 3.14 BW	1 Screws 2 Screws 3 Screws	3D[§] at ilium and ischium 2D at pubis	266 221 231	51 37 36	102 76 71
Hadjari (1994)	Scaled 1000N Coronal Plane	OL - 3S rim OL - 3S central	2D	150 250	n.a. n.a.	n.a. n.a.
Kwong (1994)	Uni-directional 1100N SLS (ischium = dome)	OL - 1S OL - 2S OL - 3S 1mm PF/1S/2S 2mm PF/1S/2S	1D	62 54 40 22/20/20 35/31/31	83 33 32 15/17/12 38/36/25	n.a. n.a. n.a. n.a. n.a.
Lachiewicz (1989)	1000N SLS	OL - 3S OL - 2Peg OL - 3 Spikes	1D	570 970 690	n.a. n.a. n.a.	n.a. n.a. n.a.
Perona (1992)	Uni-directional 2300N SLS*	2 mm PF[^] PF 1 Screw PF 2 Screws	1D	162 134 126	54 51 52	96 93 80
Pfleiderer (1996)	Uni-directional 3BW SLS	2 Peg 2 Peg - 3S	3D	91 46	90 40	80 36
Noble (1996)	Uni-directional 2000N SLS	1mm PF	3D	Dome 19	Notch 51	Floor 24
Stiehl (1991)	Coronal/cyclic 3000 N	OL - 3S[+] 1mm PF - 2S 1 mm Pf 5 Pegs 1.5 mm PF	3D	120 60 105 130	110 60 110 115	n.a. n.a. n.a. n.a.
Won (1995)	Coronal Plane 1500N	OL - 2S OL - 3S 1mm PF	1D	47 34 17	38 32 64	51 33 42

SLS*=single leg stance, PF[^]=press-fit, OL-2S[+]=on-line ream 2 screws.

3D[§]=measurement of displacement in three dimensions.

Almost all previous studies indicate that centrally located screws offer the best fixation. The one exception was the study by Hadjari et al. (1994). The screw locations for that study were unique, in that for both the central and rim configurations, the screws were placed at 120° intervals. This eliminates the possibility of directing two screws into the posterior column region (which general clinical consensus considers to be the best location) and opens the possibility of screw penetration through the medial wall into critical soft tissue structures.

Screw location may also have an effect on toggle of the cup. All studies that compared configurations of two, three, and four screws observed increased micromotion on the side of the cup opposite from the insertion site of the third and fourth screws. The effect was observed in both on-line and press-fit cups. Perona et al. (1992) observed this toggle effect in individual cases at the pubis and ischium, with insertion of only two screws. The current data do not indicate a toggling effect from insertion of the first two screws. Insertion of screw C into the posterior wall did, however, increase the motion observed at the ischium (approximately 180° around the rim from the insertion site) for four of the nine specimens tested with loading protocol 1.

Micromotion at the ischium and pubis during stair climbing was significantly less than during level walking. This reduction was attributed to the large difference in the JRF: 3.14 BW for level walking and 2.04 BW for stair climbing. As stated above, when comparing vari-directional loading to uni-directional loading, the micromotion depends primarily on the resultant magnitude of the JRF (Stiehl et al., 1991). To the author's knowledge, no previous data exist for comparing level walking and stair climbing motion for the acetabulum.

5.4.2 Gaps

Gaps between the cup and bone averaged approximately 1 mm for gaps measured through the inner ring of screw holes (approximately 30° from the pole of the cup) and for gaps measured through the outer ring of screw holes (approximately 60° from the pole of the cup). Insertion of screw A into the posterior column, and completion of loading protocol 1 (which applied both vari-directional and uni-directional level walking load cycles), reduced both inner ring and outer ring gaps by approximately the same amount. Initial and final gaps increased with increasing cup size.

The relatively even distribution of gap sizes at both screw hole rings indicates that the majority of apposition between the cup and the acetabulum occurred near the cup rim. This has been observed for both press-fit and on-line reamed cups (Kim et al., 1995a and b; MacKenzie et al., 1994; Schwartz et al., 1993), and was attributed to the acetabular surface being less than spherical after reaming. Kim et al. (1995a) reported that for cups up to 56 mm in diameter (the maximum size used in the current study), spherical reaming left a shallow, less-than-hemispherical surface. The effect was more pronounced for smaller diameter reamers, implying that smaller cups would exhibit narrower gaps at the inner ring than at the outer ring, and that the ratio of inner ring to outer ring gap thickness would increase with increasing cup size. Both trends were observed in the current study. In fact, for the largest cup (56 mm diameter), the inner ring gaps were larger than the outer ring gaps. The fact that increasing cup size increases gap width my be due to the larger acetabula providing more resistance to cup insertion than the smaller acetabula.

Press-fit cups often exhibit gaps larger than 1.5 mm, the upper limit in gap size that new bone can bridge. The failure of loading cycles to advance the cup in the current study suggests that press-fit cups may require screws to reduce gaps. The decrease in gaps measured after loading protocol 1 was attributed to the insertion of screw B into the

superior wall, not to the applied load cycles. Average gap decrease due to loading protocol 1 was only 0.11 mm, except for the two cases where screw B achieved such a tight fit that screw A had to be retightened. The gap decrease for these two cases was 0.36 mm and 0.42 mm. After removing all screws, several hundred level walking load cycles failed to reduce gaps anywhere on the cup. Failure to advance an on-line reamed cup without screws suggests that normal postoperative gait does not seat cups *in vivo*.

There was concern that screw A may increase gaps due to the fact that it was not located in the cup dome. This proved an unfounded concern. The average change in gaps was consistent for all locations on both the inner and outer rings of screw holes. In only two cases did insertion of screw A increase gap size. Both cases occurred at the medial wall site of the inner ring, but the magnitude of the increase was only 0.05 mm, which was within the error of the depth gage.

5.5 Conclusions

5.5.1 Experimental

The introduction of low-friction components and cement fixation by Sir John Charnley truly revolutionized THA. Subsequent improvements in cementing techniques have led to clinical success rates of 95% up to eight years post-operatively (Madey et al., 1997). Long term results remain less successful. Short term results, and one long term study (Engh et al., 1994) of noncemented prostheses, indicate biological fixation may provide the solution to long term clinical difficulties. However, clinical results of cement fixation require that new designs undergo long term trials (up to ten years) to show useful improvement. Before putting a large number of patients at risk, *in vitro* testing of new designs must indicate a high probability of improved clinical results.

Prediction of clinical performance of noncemented prostheses rests in part on predicting bone ingrowth. Prediction of bone ingrowth from *in vitro* tests requires two criteria be met. First, apply three-dimensional load patterns that adequately match the load patterns of the JRF observed *in vivo*. For the acetabulum this may only mean matching the peak JRF and its appropriate direction, whereas for the femur it may entail matching the complex waveform observed from instrumented prostheses (Kotzar, et al., 1995). Second, estimate with sufficient accuracy three-dimensional micromotion over the entire surface of the porous-coated region of the prosthesis.

The experimental procedure for the femur met both criteria. Quasi-physiologic load application was achieved using a dual-actuator testing machine and a specially designed test apparatus. Seven relative displacements between the prosthesis and specimen were measured and incorporated into a rigid-body motion analysis, enabling a reasonably accurate estimation of the micromotion anywhere on the surface of the prosthesis. Results of the femur test predicted amounts of bone ingrowth in the porous-coated region comparable to those observed clinically.

The acetabulum experimental procedure met only the loading criterion. Failure to accurately estimate micromotion over the cup surface was attributed to the nature of deformations in the acetabulum. To accurately estimate micromotion over the cup surface one could change the test setup or the analysis. Changing the test setup would require increasing the stiffness of the acetabulum and consequently decreasing the similarity with the *in vivo* environment. The current data suggest that modification of the displacement analysis may require a non-linear correction to the rigid-body motion analysis or a deformable body solution. While these analyses may more accurately represent the true deformation pattern of the pelvis in this instance they are both complex open-ended undertakings.

Whether using new test procedures on the acetabulum or measuring displacements at another joint it would be advantageous to have a parameter to guide the investigator in determining the feasibility of assuming rigid-body motion. Current data suggest that local and extensional strains are not effective in differentiating between a feasible specimen test setup and a non-feasible one. Global deformations, as the source of error in the acetabulum testing, may be useful in predicting the validity of assuming rigid-body motion. Possible guidelines using global deformations include the maximum deformation of the specimen and a predicted r* (the difference between the measured position and the position calculated assuming rigid-body motion).

To estimate the maximum deformation of a specimen and avoid the complexity of a complete test setup the specimen can be modeled by a geometrically simple system under a representative load. For example, in modeling the femur as a thick-walled cylinder, pinned at both ends, with a compressive load (the test setup restricts translation), the predicted peak deformation was approximately 27 μm. Predicting acetabular deformations proves more complicated. Modeling the acetabulum as a hemisphere requires simplification of the boundary conditions (e.g., evenly distributed load, continuous support around the rim) to obtain a closed form solution (Roark, 1989). The resulting calculated deformations were on the order 100 μm. These data suggest that an upper limit of maximum specimen deformation may exist and prove useful in predicting whether rigid-body motion is a reasonable assumption. This guideline is limited by the simple fact that the maximum deformation may not occur in the region of the prosthesis.

The current study suggests r* is useful in determining whether rigid-body motion is a reasonable assumption. However, to predict r* requires knowledge of the strain field of the specimen. The strain field may be estimated analytically or may necessitate creating a finite element model (either method should use a geometrically simplified

model). From the strain field, relative displacements between the specimen and a rigid prosthesis could be computed at prospective measurement sites. One could then use the displacements and a rigid body analysis to calculate "non-measured" displacements and subsequently r*. The value of r* could be used as an absolute discriminant, i.e., by comparing it to r^*_{femur} and $r^*_{acetabulum}$ from the current study. It may also prove useful to compare r* values calculated at numerous measurement sites, since the simplified analysis may introduce an error which, if consistent at each measurement site, could be accounted for.

5.5.2 Clinical

Stability of the Ranawat/Burstein femoral prosthesis was found to depend heavily on proximal fit. The minimal effect of distal fit on the stability of the prosthesis was somewhat surprising, based on the results of previous studies. Nonetheless, current data suggest that to achieve fixation conducive to bone ingrowth in the porous-coated region, a tight proximal fit must be achieved.

The acetabulum data indicate that two central screws are the best configuration for cup stability. The lack of cup advancement from cyclic loading suggests that surgeons using press-fit fixation may want to use dual-radius cups or screws to reduce polar gaps.

REFERENCES

Andersson, G.B.J., Freeman, M.A.R., and Swanson, S.A.V., Loosening of the cemented acetabular cup in total hip replacement. J. Bone and Joint Surg., 54B:590, 1972.

Bachus, K.N., Jensen, J.W., Bloebaum, R.D., and Hofmann, A.A., Postmortem analysis of tibial components. p. 215, Trans. 42nd Ann. Mtg. of Ortho. Res. Soc., Atlanta, GA, 1996.

Ballard, W.T., Callaghan, J.J., Sullivan, P.M., and Johnston, R.C., The results of improved cementing techniques for total hip arthroplasty in patients less than fifty years old: A ten-year follow-up study. J. Bone & Joint Surg., 76A:959, 1994.

Bauer, T.W., Stulberg, B.N., Ming, J., and Geesink, R.G., Uncemented acetabular components - histologic analysis of retrieved hydroxyapatite-coated and porous implants. J. Arthro., 8:167, 1993.

Bechtold, J.E., Bianco, P.T., Kyle, R.G., and Gustilo, R.B., Experimental evaluation of strain and stability for short stem and long curved stem uncemented femoral prostheses in torsion and stance loading. Trans. of 34th Annual Mtg. of ORS, Atlanta, GA, 1988.

Beckenbaugh, R.D. and Ilstrup, D.M., Total hip arthroplasty: a review of three hundred and thirty-three cases with long follow-up. J. Bone and Joint Surg., 60A:306, 1978.

Beggs, J.S., Kinematics, Hemisphere Publishing Corp., Washington D.C., 1983.

Bergmann, G., Graichen, F., and Rohlmann, A., Hip joint loading during walking and running, measured in two patients. J. Biomech. 26:969, 1993.

Bergmann, G., Graichen, F., and Rohlmann, A., Is staircase walking a risk for the fixation of hip implants?, J. Biomech., 28:535-553, 1995.

Berzins, A., Sumner, D.R., Wasielewski, R.C., and Galante, J.O., Impacted particulate allograft for femoral revision total hip arthroplasty - *in vitro* mechanical stability and effects of cement pressurization. J. Arthro., 5:500, 1996.

Bobyn, J.D., Pilliar, R.M., Cameron, H.U., and Weatherly, G.C., The optimum pore size for the fixation of porous-surfaced metal implants by the ingrowth of bone. Clin. Ortho. and Rel. Res., 150:263, 1980.

Bobyn, J.D., Pilliar, R.M., Cameron, H.U., and Weatherly, G.C., Osteogenic phenomena across endosteal bone-implant spaces with porous surfaced intramedullary implants. ACTA Ortho. Scand., 52:145, 1981.

Boehler, M., Knahr, K., Plenk Jr., H., Walter, A., Salzer, M., Schreiger, V., Long-term results of uncemented alumina acetabular implants. J. Bone & Joint Surg., 76B:53, 1994.

Boresi, A.P. and Lynn, P.P., Elasticity in Engineering Mechanics, Prentice-Hall, New York, 1974.

Bragdon, C.R., Burke, D., Lowenstein, J.D., O'Connor, D.O., Ramamurti, B., Jasty, M., and Harris, W.H., Different stiffness of the interface between a cementless porous implant and cancellous bone *in vivo* in dogs with varying amounts of implant motion. p. 156, Trans. 42nd Ann. Mtg. of Ortho. Res. Soc., Atlanta, GA, 1996.

Brand, R.A., Pedersen, D.R., Davy, D.T., Kotzar, G.M., Heiple, K.G., and Goldberg, V.M., Comparison of hip force calculations and measurements in the same patient. J. Arthro., 9:45, 1994.

Brown, T.D., Sigal, L., Njus, G.O., Njus, N.M., Singerman, R.J., and Brand, R.A., Dynamic performance characteristics of the liquid metal strain gage. J. Biomech., 19:165, 1986.

Bühler, D.W., Berlemenn, U., Frei, H.-P., and Nolte, L.-P., Three-dimensional motion of femoral prosthetic stems: an *in vitro* evaluation of a novel measuring concept, Trans. of 41st Annual Mtg. of ORS, Orlando, FL, 1995.

Burke, D.W., Bragdon, D.R., O'Connor, D.O., Jasty, M., Haire, T., and Harris, W.H., Dynamic measurement of interface mechanics *in vivo* and the effect of micromotionon bone ingrowth into a porous surface device under controlled loads *in vivo*. p. 103, Trans. 37th Ann. Mtg. of Orhto. Res. Soc., Anaheim, CA, 1991.

Calderale, P.M. and Scelfo, G., A mathematical model of the locomotor apparatus. Engr. in Medicine, 16:147, 1987.

Callaghan, J.J., Dysart, S.H., and Savory, C.G., The Uncemented Porous-coated Anatomic Total Hip Prosthesis, J. Bone and Joint Surg., 70A:337-346, 1988.

Callaghan, J.J., Fulghum, C.S., Glisson, R.R., and Stranne, S.K., The effect of femoral stem geometry on interface motion in uncemented porous-coated total hip prostheses: Comparison of straight-stem and curved-stem designs. J. Bone and Joint Surg., 74A:839, 1992.

Cameron, H.U., Pilliar, R.M., and MacNab, I., The effect of movement on the bonding of porous metal to bone. J. Biomed. Mater. Res., 7:301, 1973.

Cameron, H.U., Pilliar, R.M., and MacNab, I., The rate of bone ingrowth into porous metal. J. Biomed. Mater. Res., 10:295, 1976.

Chandler, H.P., Reineck, F.T., Wixson, R.L., and McCarthy, J.C., Total hip replacement in patients younger than thirty years old. J. Bone and Joint Surg., 63A:1426, 1981.

Charnley, J., Anchorage of the femoral head prosthesis to the shaft of the femur. J. Bone and Joint Surg., 42B:28, 1960.

Charnley, J. and Kettlewell, J., The elimination of slip between prosthesis and femur. J. Bone and Joint Surg., 47B:56, 1965.

Cheal, E.J., Spector, M., and Hayes, W.C., Role of loads and material properties on the mechanics of the proximal femur after total hip arthroplasty. Trans. of 37th Annual Mtg. of ORS, Anaheim, CA, 1991.

Chmell, M.J., Scott, R.D., Thomas, W.H., and Sledge, C.B., Total hip arthroplasty with cement for juvenile rheumatoid arthritis. J. Bone and Joint Surg., 79A:44, 1997.

Clarke, H.J., Jinnah, R.H., Warden, K.E., Cox, Q.G., and Curtis, M.J., Evaluation of acetabular stability in uncemented prostheses. J. Arthro., 6:335, 1991.

Collier, J.P., Mayor, M.B., Chae, J.C., Surprenant, V.A., Surprenant, H.P., and Dauphinais, L.A., Macroscopic and microscopic evidence of prosthetic fixation with porous-coated materials. Clin. Ortho. and Rel. Res., 235:173, 1988.

Collis, D.K., Cemented total hip replacement in patients who are less than fifty years old. J. Bone and Joint Surg., 66A:353, 1984.

Cook, S.D., Barrack, R.L., Thomas, K.A., and Haddad, R.J., Quantitative analysis of tissue growth into human porous total hip components. J. Arthro. 3:249, 1988a.

Cook, S.D., Thomas, D.A., and Haddad, Jr., R.J., Histologic Analysis of Retrieved Human Porous-Coated Total Joint Components. Clin. Ortho. and Rel. Res., 234:90, 1988b.

Cornell, C.N. and Ranawat, C.S., The Impact of Modern Cement Techniques on Acetabular Fixation in Cemented Total Hip Replacement. J. Arthro., 1:197-202, 1986.

Crowninshield, R.D., Johnston, R.C., Andrews, J.G., and Brand, R.A., A biomechanical investigation of the human hip. J.Biomech., 11:75, 1978.

Curtis, M.J., Jinnah, R.H., Wilson, V.D., and Hungerford, D.S., The initial stability of uncemented acetabular components. J. Bone and Joint Surg., 74B:372, 1992.

Dall, D.M., Learmonth, I.D., Solomon, M.I., Miles, A.W., and Davenport, J.M., Fracture and loosening of Charnley femoral stems - Comparison between first-generation and subsequent designs. J. Bone & Joint Surg., 75B:259, 1993.

Dalton, J.E., Cook, S.D., Thomas, K.A., and Kay, J.F., The effect of operative fit and hydroxyapatite coating on the mechanical and biological response to porous implants. J. Bone and Joint Surg., 77A:97, 1995.

D'Antonio, J.A., Capello, W.N., and Manley, M.T., Remodeling of bone around hydroxyapatite-coated femoral stems. J. Bone and Joint Surg., 78A:1226, 1996.

DeLee, J.G. and Charnley, J., Radiological Demarcation of Cemented Sockets in Total Hip Replacement. Clin. Orth. Rel. Res., 121:20, 1976.

Dujardin, F.H., Mollard, R., Toupin, J.M., Coblentz, A., and Thomine, J.M., Micromotion, fit, and fill of custom made femoral stems designed with an automated process. Clin. Ortho. & Rel. Res., 325:276, 1996

Elder, S., Experimental studies of three dimensional micromotion of hip prostheses relative to bone, Master's Thesis, University of Iowa, August 1992.

Engh, C.A. and Bobyn, J.D., Biological Fixation in Total Hip Arthroplasty, p. 5, Slack Inc., New Jersey, 1985.

Engh, C.A., and Bobyn, J.D., The influence of stem size and extent of porous coating on femoral bone resorption after primary cementless hip arthroplasty. Clin. Ortho. & Rel. Res., 231:7, 1988.

Engh, C.A., Bobyn, J.D., and Glassman, A.H., Porous-coated hip replacement: the factors governing bone ingrowth, stress shielding, and clinical results. J. Bone and Joint Surg., 69B:45, 1987.

Engh, C.A., Griffin, W.L., and Marx, C.L., Cementless acetabular components. J. Bone and Joint Surg., 72B:53, 1990a.

Engh, C.A., Hooten Jr., J.P., Zettl-Schaffer, K.F., Ghaffarpour, M., McGovern, T.F., Macalino, G.E., and Zicat, B.A., Porous-coated total hip replacement, Clin. Ortho. & Rel. Res., 298:89, 1994.

Engh, C.A., Massin, P., and Suthers, K.E., Roentgenographic assessment of the biologic fixation of porous-surfaced femoral components. Clin. Ortho. and Rel. Res., 257:107, 1990b.

Engh, C.A., O;Connor, D., Jasty, M., McGovern, T.F., Bobyn, J.D., and Harris, W.H., Quantification of implant micromotion, strain shielding, and bone resorption with porous-coated anatomic medullary locking femoral prostheses. Clin. Ortho. and Rel. Res., 285:13, 1992.

Engh, C.A., Zettl-Schaffer, K.F., Kukita, Y., Sweet, D., Jasty, M., and Bragdon, C., Histological and radiographic assessment of well functioning porous-coated acetabular components. J. Bone and Joint Surg., 75A:814, 1993.

English, T.A. and Kilvington, M., *In vivo* records of hip loads using a femoral implant with telemetric output (a preliminary study). J. Biomed. Engr., 1:111 1979.

Freeman, M.A.R., and Plant-Bordeneuve, P., Early migration and late aseptic failure of proximal femoral prostheses. J. Bone & Joint Surg., 76B:432, 1994.

Galante, J., Rostoker, W., Lueck, R., and Ray, R.D., Sintered fiber metal composites as a basis for attachment of implants to bone. J. Bone and Joint Surg., 53A:101, 1971.

Galante, J.O., Acetabular fixation: clinical problems and possible solutions. Hip 187, 1985.

Galante, J.O., Overview of current attempts to eliminate methylmethacrylate. *New Developments in Hip Arthroplasty*, Chapter 9, 1983.

Geesink, R.G.T., and Hoefnagels, N.H.M., Six-year results of hydroxyapatite-coated total hip replacement. J. Bone & Joint Surg., 77B:534, 1995.

Gilbert, J.L., Bloomfeld, R.S., Lautenschlager, E.P., and Wixson, R.L., A Computer-based biomechanical analysis of the three-dimensional motion of cementless hip prostheses. J. Biomech., 25:329, 1992.

Goetz, D.D., Smith, E.J., and Harris, W.H., The prevalence of femoral osteolysis associated with components inserted with or without cement in total hip replacements. J. Bone & Joint Surg., 76A:1121, 1994.

Goldring, S.R., Clark, C.R., and Wright, T.M., The problem in total joint arthroplasty: Aseptic loosening. Editorial J. Bone & Joint Surg., 65A:1134, 1983.

Green, E.L., Bahniuk, E., Liebelt, R.A., Fender, E., and Mirkov, P., Biplane radiographic measurements of reversible displacement (including clinical loosening) and migration of total joint repleacements. J. Bone & Joint Surg., 75A:961, 1993.

Greenwood, D.T., Principles of Dynamics, 18th edition, Prentice-Hall, Inc., Englewood Cliffs, New Jersey, 1983.

Gruen, T.A., McNeice, G.M., and Amstutz, H.C., "Modes of Failure" of cemented stem-type femoral components: A radiographic analysis of loosening. Clin. Ortho. & Rel. Res., 141:17, 1979.

Gustilo, R.B., Bechtold, J.E., Giacchetto, J., and Kyle, R.F., Rationale, experience, and results of long-stem femoral prosthesis. Clin. Ortho. and Rel. Res., 249:159, 1989.

Gustilo, R.B., Mendoza, R.M., and Burnham, W.H., Long term results of total hip arthroplasty in younger age group. Comparative analysis with young resurfacing arthroplasty patients. Orthopedics, 6:60, 1983.

Haddad, R.J., Cook, S.D., and Thomas, K.A., Biological fixation of porous-coated implants. J. Bone and Joint Surg., 69A:1459, 1987.

Hadjari, M.H., Hollis, J.M., Hofmann, O.E., Flahiff, C.M., and Nelson, C.L., Initial stability of porous coated acetabular implants. Clin. Ortho. and Rel. Res., 307:117, 1994.

Harper, G.D., Bull, T., Cobb, A.G., and Bentley, G., Failure of the Ring polyethylene uncemented acetabular cup. J. Bone & Joint Surg., 77B:557, 1995.

Harris, W.H. and Maloney, W.J., Hybrid Total Hip Arthroplasty. Clin. Ortho. & Rel. Res., 249:21, 1989.

Harris, W.H., McCarthy Jr., J.C., and O'Neill, D.A., Femoral component loosening using contemporary techniques of femoral cement fixation. J. Bone & Joint Surg., 64A:1063, 1982.

Harris, W.H., White Jr., R.E., McCarthy, J.C., Walker, P.S., and Weinberg, E.H., Bony ingrowth fixation of the acetabular component in canine hip joint arthroplasty. Clin. Ortho. and Rel. Res, 176:7, 1983.

Havelin, L.E., Espehaug, B., Vollset, S.E., and Engesaeter, L.B., Early aseptic loosening of uncemented femoral components in primary total hip replacement - A review based on the Norwegian arthroplasty register. J. Bone & Joint Surg., 77B:11, 1995.

Hayes, Jr., D.E.E., Bargar, W.L., Paul, H.A., and Taylor, J.K., Three dimensional micromotion of femoral prostheses. Trans. of 38th Annual Mtg. of ORS. Washington, D.C., 1992.

Hazelwood, S.J., A finite element analysis on the importance of abductor muscle forces in comparative femoral strain gage studies. p. 409, Trans. 42nd Ann. Mtg. of Ortho. Res. Soc., Atlanta, GA, 1996.

Hedley, A.K., Kabo, M., Kim, W., Coster, I., and Amstutz, H.C., Bony ingrowth fixation of newly designed acetabular components in a canine model. Clin. Ortho. and Rel. Res., 176:12, 1983.

Heekin, R.D., Callaghan, J.J., Hopkinson, W.J., Savory, C.G., and Xenos, J.S., The porous-coated anatomic total hip prosthesis, inserted without cement. J. Bone and Joint Surg., 75A:77, 1993.

Heiner, J.P., Manley, P., Kohles, S., Ulm, M., Bogart, L., and Vanderby Jr., R., Ingrowth reduces implant-to-bone relative displacements in canine acetabular prostheses. J.Ortho. Res., 12:657, 1994.

Hofman, A.A., Bachus, K.N., and Bloebaum, R.D., Comparative study of human cancellous bone remodeling to titanium and hydroxyapatite-coated implants. J. Arthro., 8:157, 1993.

Holmberg, P.D., Bechtold, J.E., Sun, B.N., Kyle, R.F., and Gustilo, R.B., Strain analysis of a femur with long stem press fit prosthesis, Trans. of 32nd Annual Mtg. of ORS, New Orleans, LA, 1986.

Horowitz, S.M., Doty, S.B., Lane, J.M., and Burstein, A.H., Studies of the mechanism by which the mechanical failure of polymethylmethacrylate leads to bone resorption. J. Bone & Joint Surg., 75A:802, 1993.

Jasty, M., Henshaw, R.M., O'Connor, D.O., Harrigan, R.P., and Harris, W.H., Strain alterations in the proximal femur with an uncemented femoral prosthesis, emphasizing the effect of component fit, an experimental in vitro strain study. Trans. 34th Annual Mtg. of ORS, Atlanta, GA, 1988.

Jasty, M., Jiranek, W., and Harris, W.H., Acrylic fragmentation in total hip replacements and its biological consequences. Clin. Ortho. and Rel. Res., 285:116, 1992.

Jasty, M., O'Connor, D.O., Henshaw, R.M., Harrigan, T.P., and Harris, W.H., Fit of the uncemented femoral component and the use of cement influence the strain transfer to the femoral cortex. J. Ortho. Res., 12:648, 1994.

Johnsson, R., Franzén, H., and Nilsson, L.T., Combined survivorship and multivariate analyses of revisions in 799 hip prostheses. J. Bone & Joint Surg., 76B:439, 1994.

Joshi, A.B., Porter, M.L., Trail, I.A., Hunt, L.P., Murphy, J.C.M., and Hardinge, K., Long-term results of Charnley low-friction arthroplasty in young patients. J. Bone & Joint Surg., 75B:616, 1993.

Kamaric, E., Noble, P.C., Alexander, J.W., Collier, M., and Paravic, V., The distribution of micromotion at the cementless acetabular interface. p. 528, Trans. 42nd Ann. Mtg. of Ortho. Res. Soc., Atlanta, GA, 1996b.

Kamaric, E., Noble, P.S., and Alexander, J.W., Are cadaveric femora essential for measuring interface micromotion of cementless femoral stems? p. 529, Trans. 42nd Ann. Mtg. of Ortho. Res. Soc., Atlanta, GA, 1996a.

Kärrholm, J., Borssén, B., Löwenhielm, G., and Snorrason, F., Does early micromotion of femoral stem prostheses matter? - 4-7 year steroradiographic follow-up of 84 cemented prostheses. J. Bone & Joint Surg., 76B:912, 1994a.

Kärrholm, J., Malchau, H., Snorrason, F., and Herberts, P., Micromotion of femoral stems in total hip arthroplasty. J. Bone & Joint Surg.,76A:1692, 1994b.

Keaveny, T.M., and Bartel, D.L., Effects of porous coating, with and without collar support, on early relative motion for a cementless hip prosthesis. J. Biomech., 26:1355, 1993.

Kim, K.J., Chiba, J., and Rubash, H.E., *In vivo* and *in vitro* analysis of membranes from hip prostheses inserted without cement. J. Bone & Joint Surg., 76A:172, 1994.

Kim, Y-H., and Kim, V.E.M., Uncemented porous-coated anatomic total hip replacement - Results at six years in a consecutive series. J. Bone & Joint Surg., 75B:6, 1993.

Kim, Y.S., Brown, T.D., Pedersen, D., Callaghan, J.J., Reamed surface topography and component seating in press-fit cementless acetabular fixation. J. Arthro. Suppl., 10:S14, 1995a.

Kim, Y.S., Callaghan, J.J., Ahn, P., Brown, T.D., Fracture of the acetabulum during insertion of an oversized hemispherical component. J. Bone and Joint Surg., 77A:111, 1995b.

Kotzar, G.M., Davy, D.T., Berilla, J., and Goldberg, V.M., Torsional loads in the early postoperative period following total hip replacement. J. Ortho. Res., 13:945, 1995.

Kotzar, G.M., Davy, D.T., Goldberg, V.M., Heiple, K.G., Berilla, J., Heiple Jr., K.G., Brown, R.H., and Burstein, A.H., Telemeterized in vivo hip joint force data: a report on two patients after total hip surgery. J. Ortho. Res., 9:621, 1991.

Kwong, L.M., O'Connor, D.O., Sedlacek, R.C., Krushell, R.J., Maloney, W.J., and Harris, W.H., A quantitative *in vitro* assessment of fit and screw fixation on the stability of a cementless hemispherical acetabular component. J. Arthro., 9:163, 1994.

Lachiewicz, P.F., Suh, P.B., and Gilbert, J.A., In vitro initial fixation of porous-coated acetabular total hip components - a biomechanical comparative study. J. Arthro., 4:201, 1989.

Latimer, H.A. and Lachiewicz, P.F., Porous-coated acetabular components with screw fixation. J. Bone and Joint Surg., 78A:975, 1996.

Lewis, C.G., Nowak, M.D., and Leone, D.J., Uncemented hip implants: effects of stem modulus and length variations via an orthotropic finite element model. Trans. of Annual Bioeng. Conf. of ASME, 1993.

Lionberger, D., Walker, P.S., and Granholm, J., Effects of prosthetic acetabular replacement on strains in the pelvis, J. Ortho. Res., 3:372, 1985.

Ma, S.M., Kabo, J.M., and Amstutz, H.C., Frictional torque in surface and conventional hip replacement. J. Bone and Joint Surg., 65A:366, 1983.

MacKenzie, J.R., Callaghan, J.J., Pedersen, D.R., and Brown, T.D., Areas of contact and extent of gaps with implantation of oversized acetabular components in total hip arthroplasty. Clin. Ortho. & Rel. Res., 298:127, 1994.

Madey, S.M., Callaghan, J.J., Olejniczak, J.P., Goetz, D.D., and Johnston, R.C., Charnley total hip arthroplasty with use of improved techniques of cementing - the results after a minimum of fifteen years of follow-up. J. Bone and Joint Surg., 79A:53, 1997.

Malkani, A.L., Settecerri, J.J., Sim, F.H., Chao, E.Y.S., and Wallrichs, S.L., Long-term results of proximal femoral replacement for non-neoplastic disorders. J. Bone & Joint Surg., 77B:351, 1995.

Maloney, W.J., Jasty, M., Burke, D.W., O'Connor, D.O., Zalenski, E.B., Bragdon, C., and Harris, W.H., Biomechanical and histologic investigation of cemented total hip arthroplasties; a study of autopsy-retrieved femurs after in vivo cycling, Clin. Ortho. and Rel. Res. 249:129-140, 1989.

Markholf, K.L., Amstutz, H.C., and Hirschowitz, D.L., The effect of calcar contact on femoral component micromovement. J. Bone and Joint Surg., 62A:1315, 1980.

Martell, J.M., Pierson III, R.H., Jacobs, J.J., Rosenberg, A.G., Maley, M., and Galante, J.O., Primary total hip reconstruction with a titanium fiber-coated prosthesis inserted without cement. J. Bone & Joint Surg., 75A:554, 1993.

Massin, P., Vandenbussche, E., Landjerit, B., and Augereau, B., Experimental study of periacetabular deformations before and after implantation of hip prostheses. J. Biomech., 29:53, 1995.

McLeish, R.D. and Charnley, J., Abduction forces in the one-legged stance. J.Biomech., 3:191, 1970.

Mjöberg, B., Hansson, L.I., and Selvik, G., Instability of total hip prostheses at rotational stress. Acta. Orthop. Scand., 55:504, 1984.

Mohler, C.G., Callaghan, J.J., Collis, D.K., and Johnston, R.C., Early loosening of the femoral component at the cement-prosthesis interface after total hip replacement. J. Bone and Joint Surg., 77A:1315, 1995.

Mohler, C.G., Kull, L.R., Martell, J.M., Rosenberg, A.G., and Galante, J.O., Total hip replacement with insertion of an acetabular component without cement and a femoral component with cement. J. Bone & Joint Surg., 77A:86, 1995.

Mont, M.A., Maar, D.C., Krackow, K.A., Jacobs, M.A., Jones, L.C., and Hungerford, D.S., Total hip replacement without cement for non-inflammatory osteoarthrosis in patients who are less than forty-five years old. J. Bone & Joint Surg., 75A:740, 1993.

Morscher, E.W., Current Status of Acetabular Fixation in Primary Total Hip Arthroplasty, Clin. Ortho. and Rel. Res., 274:172, 1992.

Morscher, E.W. and Dick, W., Cementless fixation of "isoelastic" hip endoprostheses manufactured from plastic materials. Clin. Ortho. and Rel. Res., 176:77, 1983.

Mulroy, Jr., R.D. and Harris, W.H., The Effect of Improved Cementing Techniques on Component Loosening in Total Hip Replacement - An 11-year Radiographic Review. J. Bone and Joint Surg., 72B:757, 1990.

Natarajan, R.N., Andriacchi, T.P., Freeman, P.M., and Galante, J.O., A relationship between the extent of porous coating and micromotion in a cementless femoral stem of a total hip replacment. Trans. 37th Annual Mtg. of ORS, Anaheim, CA, 1991.

Neumann, L., Freund, K.G., Sørenson, K.H., Long-term results of Charnley total hip replacement - Review of 92 patients at 15 to 20 years. J. Bone & Joint Surg., 76B:245, 1994.

Neumann, L., Freund, K.G., Sørenson, K.H., Total hip arthroplasty with the Charnley prosthesis in patients fifty-five years old and less. J. Bone & Joint Surg., 78A:73, 1996.

Nilsson, L.T., Franzén, H., Carlsson, Å.S., and Önnerfält, R., Early radiographic loosening impairs the function of total hip replacement - The Nottingham health profile of 49 patients at five years. J. Bone & Joint Surg., 76B:235, 1994.

Nistor, L., Blaha, J.D., Kjellström, U., and Selvik, G., In vivo measurement of relative motion between an uncemented femoral total hip component and the femur by roentgen stereophotogrammetric analysis. Clin. Ortho. and Rel. Res, 269:220, 1991.

Noble, P.C., Kamaric, E., and Alexander, J.W., Distal stem centralization critically affects the acute fixation of cementless femoral stems. Trans. 35th Annual Mtg. of ORS, Las Vegas, NV, 1989.

Noble, P.C., and Paul, J.P., The deformation of the acetabulum during walking. Trans. of 41st Ann. Mtg. of Ortho. Res. Soc., Orlando, FL., 1995.

Nunn, D., Freeman, M.A.R., Tanner, K.E., and Bonfield, W. Torsional stability of the femoral component of hip arthroplasty. J. Bone and Joint Surg., 71B:452, 1989.

Oishi, C.S., Walker, R.H., and Colwell Jr., C.W., The femoral component in total hip arthroplasty, six to eight-year follow-up of one hundred consecutive patients after use of a third-generation cementing technique. J. Bone & Joint Surg., 76A:1130, 1994.

Otani, T., et al, Strain Distribution Changes in the Proximal Femur Caused by Metallic and Flexible Composite Femoral Components Under Torsional Load, 37th ORS, Anaheim, CA, 1991.

Paul J.P., Force actions transmitted by joints in the human body. Proc. Royal Soc. fo London - Series B: Biological Sciences, 192:163, 1976.

Pedersen, D.R., Brand, R.A., and Davy, D.T., Pelvic muscle and acetabular contact forces during gait. Submitted to J. Biomech., 1995.

Perona, P.G., Lawrence, J., Paprosky, W.G., Patwardhan, A.G., and Sartori, M., Acetabular micromotion as a measure of initial implant stability in primary hip arthroplasty - an *in vitro* comparison of different methods of initial acetabular component fixation. J. Arthro., 7:537, 1992.

Pfleiderer, M., Knecht, M., Peters, C., and Schneider, E., The effect of screw fixation on initial stability of cementless acetabular cups and on bone deformation. p. 421, Trans. 42nd Ann. Mtg. of Ortho. Res. Soc., Atlanta, GA, 1996.

Phillips, T.W., Nguyen, L.T., and Munro, S.D., Loosening of cementless femoral stems: a biomechanical analysis of immediate fixation with loading vertical, femur horizontal. J. Biomech., 24:37, 1991.

Pidhorz, L.E., Urban, R.M., Jacobs, J.J., Sumner, D.R., and Galante, J.O., A quantitative study of bone and soft tissues in cementless porous-coated acetabular components retrieved at autopsy. J. Arthro., 8:213, 1993.

Pilliar, R.M., Powder metal-made orthopedic implants with porous surface for fixation by tissue ingrowth, Clin. Ortho. and Rel. Res., 176:42, 1983.

Pilliar, R.M., Lee, J.M. and Maniatopoulos, C., Observations on the effect of movement on bone ingrowth into porous-surfaced implants. Clin. Ortho. and Rel. Res., 208:109, 1986.

Ramamurti, B.X., Ladin, Z., Spector, M., and Cheal, E.J., Effect of prosthetic material properties on the optimal bonding distribution for a femoral component of THA. Trans. 39th Annual Mtg of ORS, San Francisco, CA, 1993.

Ranawat, C.S., Atkinson, R.E., Salvati, E.A., and Wilson Jr., P.D., Conventional total hip arthroplasty for degenerative joint disease in patients between the ages of forty and sixty years. J. Bone and Joint Surg., 66A:745, 1984.

Rapperport, D.J., Carter, D.R., and Schurman, D.J., Contact finite element stress analysis of porous ingrowth acetabular cup implantation, ingrowth, and loosening. J. Ortho. Res., 5:548, 1987.

Roarke, R.J., Formulas for Stress and Strain, 3rd edition, McGraw-Hill, New York, 1954.

Rockborn, P., and Olsson, S.S., Loosening and bone resoprtion in Exeter hip arthroplasties - Review at a minimum of five years. J. Bone & Joint Surg., 75B:865, 1993.

Rohlmann, A., Mössner, U., Bergmann, G., Hees, G., and Kölbelt, Effects of stem design and material properties on stresses in hip endoprostheses. J. Biomed. Eng., 9:77, 1987.

Röhrle, H., Scholten, R., Sigolotto, C., Sollbach, W., Kellner, H., Joint forces in the human pelvis-leg skeleton during walking. J. Biomech 17:409, 1984.

Rothman, R.H., Hozack, W.J., Ranawat, A., and Moriarty, L., Hydroxyapatite-coated femoral stems - a matched-pair analysis of coated and uncoated implants. J. Bone & Joint Surg., 78A:319, 1996

Russotti, G.M., Coventry, M.B., and Stauffer, R.N., Cemented total hip arthroplasty with contemporary techniques: a five-year minimum follow-up study. Clin. Ortho. and Rel. Res., 235:141, 1988.

Ryd, L., Albrektsson, B.E.J., Carlsson, L., Dansgård, F., Herberts, P., Lindstrand, A., Regnér, L., and Toksvig-Larsen, S., Roentgen stereophotogrammetric analysis as a predictor of mechanical loosening of knee prosthesses. J. Bone & Joint Surg., 77B:377, 1995.

Rydell 1966 Acta Orth. Scand 1966:37 Supplemental 88 p. 37

Schmalzried, T.P., Kwong, L.M., Jasty, M., Sedlacek, R.C., Haire, T.C., O'Connor, D.O., Bragdon, C.R., Kabo, J.M., Malcolm, A.J., Path, M.R., and Harris, W.H., The mechanism of loosening of cemented acetabular components in total hip arthroplasty, CORR, 274:60, 1992c.

Schneider, E., Eulenberger, J., Steiner, W., Wyder, D., Friedman, R.J., and Perren, S.M., Experimental method for the *in vitro* testing of the initial stability of cementless hip prostheses. J. Biomech., 22:735, 1989a.

Schneider, E., Kinast, C., Eulenberger, J., Wyder, D., Eskillsson, G., and Perren, S.M., A Comparative study of the initial stability of cementless hip prostheses. Clin. Ortho. and Rel. Res., 248:200, 1989b.

Schulte, K.R., Callaghan, J.J., Kelley, S.S., and Johnston, R.C., The outcome of Charnley total hip arthroplasty with cement after a minimum twenty-year follow-up. J. Bone & Joint Surg., 75A:961, 1993.

Schwartz, J.T. Jr., Engh, C.A., Forte, M.R., Kikita, Y., and Grandia, S.K., Evaluation of initial surface apposition in porous-coated acetabular components. Clin. Ortho. and Rel. Res., 293:174, 1993.

Seireg, A., and Arvikar, R.J., The prediction of muscular load sharing and joint forces in the lower extremities during walking. J. Biomech. 8:89, 1975.

Stauffer, R.N., Ten-year follow-up study of total hip replacement: With particular reference to roentgenographic loosening of the components. J. Bone & Joint Surg., 64A:983, 1982.

Stiehl, J.B., MacMillan, E., and Scrade, D.A., Mechanical stability of porous-coated acetabular components in total hip arthroplasty. J. Arthro., 6:295, 1991.

Sugano, N., Nishii, T., Nakata, K., Masuhara, K., and Takaoka, K., Polyethylene sockets and alumina ceramic heads in cemented total hip arthroplasty - A ten-year study. J. Bone & Joint Surg., 77B:548, 1995.

Sugiyama, H., Whiteside, L.A., and Engh, C.A., Torsional fixation of the femoral component in total hip arthroplasty, the effect of surgical press-fit technique. Clin. Ortho. and Rel. Res., 275:187, 1992.

Sugiyama, H., Whiteside, L.A., and Kaiser, A.D., Examination of rotational fixation of the femoral component in total hip arthroplasty. Clin. Ortho. and Rel. Res., 249:122, 1989.

Sullivan, P.M., MacKenzie, J.R., Callaghan, J.J., and Johnston, R.C., Total hip arthroplasty with cement in patients who are less than fifty years old. J. Bone & Joint Surg., 76-A:863-869, 1994.

Sumner, D.R., Jasty, M., Jacobs, J.J., Urban, R.M., Bragdon, C.R., Harris, W.H., and Glante, J.O., Histology of porous-coated acetabular components - 25 cementless cups retrieved after arthroplasty. Acta. Orthop. Scand. 64:619, 1993.

Sutherland, C.J., Wilde, A.H., Borden, L.S., and Marks, K.E., A ten-year follow-up of one hundred consecutive Müller curved-stem total hip-replacement arthroplasties. J. Bone and Joint Surg., 64A:970, 1982.

Takedani, H., Whiteside, L.A., White, S.E., and Otani, T., The effect of screws and pegs on cementless acetabular fixation. Trans. 37th Annual Mtg. of ORS, Anaheim, CA, 1991.

Tisdel, C.L., Goldberg, V.M., Parr, J.A., Bensusan, J.S., Staikoff, L.S., and Stevenson, S., The influence of a hydroxyapatite and tricalcium-phosphate coating on bone growth into titanium fiber-metal implants. J. Bone & Joint Surg., 76A:159, 1994.

Tompkins, G.S., Jacobs, J.J., Kull, L.R., Rosenberg, A.G., and Galante, J.O., Primary total hip arthroplasty with a porous-coated acetabular component - seven-to-ten year results. J. Bone & Joint Surg., 79A:169, 1997.

Tooke, S.M., Nugent, P.J., Chotivichit, A., Goodman, W., and Kabo, J.M., Comparison of *In Vivo* Cementless Acetabular Fixation. Clin. Ortho. and Rel. Res., 235:253, 1988.

Torchia, M.E., Klassen, R.A., and Bianco, A.J., Total hip arthroplasty with cement in patients less than twenty years old - long-term results. J. Bone & Joint Surg., 78A:995, 1996.

Walheim, G.G. and Selvik, G., Mobility of the pubic symphysis. *In vivo* measurements with an electromechanic method and a Roentgen stereophotogrammetric method. Clin. Ortho. and Rel. Res., 191:129, 1984.

Walker, P.S., Schneeweis, D., Murphy, S., and Nelson, P., Strains and micromotion of press-fit femoral stem prostheses. J. Biomech., 20:693, 1987.

Whiteside, L.A., The effect of stem fit on bone hypertrophy and pain relief in cementless total hip arthroplasty. Clin. Ortho. and Rel. Res., 247:138, 1989a.

Whiteside, L.A., Amador, D., and Russell, K., The effects of the collar on total hip femoral component subsidence. Clin. Ortho. and Rel. Res., 231:120, 1988.

Whiteside, L.A., Arima, J., White, S.E., Branam, L., and McCarthy, D.S., Fixation of the modular total hip femoral component in cementless total hip arthroplasty. Clin. Ortho. and Rel. Res., 298:184, 1994.

Whiteside, L.A. and Easley, J.C., The effect of collar and distal stem fixation on micromotion of the femoral stem in uncemented total hip arthroplasty. Clin. Ortho. and Rel. Res., 239:145, 1989b.

Whiteside, L.A., White, S.E., Engh, C.A., and Head, W., Mechanical evaluation of cadaver retrieval specimens of cementless bone-ingrown total hip arthroplasty femoral components. J. Arthro., 8:147, 1993.

Won, C.H., Hearn, T.C., and Tile, M., Micromotion of cementless hemispherical acetabular components. J. Bone and Joint Surg., 77B:484, 1995.

Wroblewski, B.M., 15-21-year results of the Charnley low-friction arthroplasty. Clin. Ortho. and Rel. Res., 211:30, 1986.

IMAGE EVALUATION
TEST TARGET (QA-3)

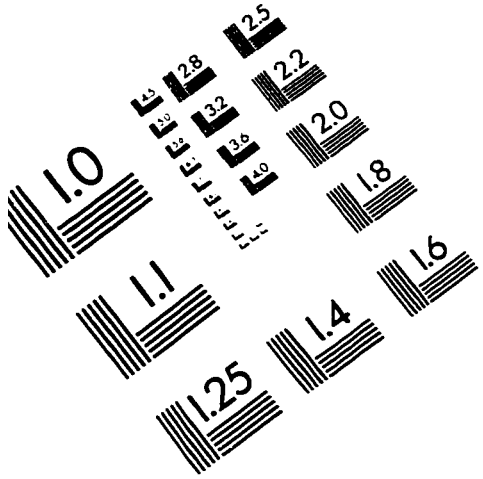

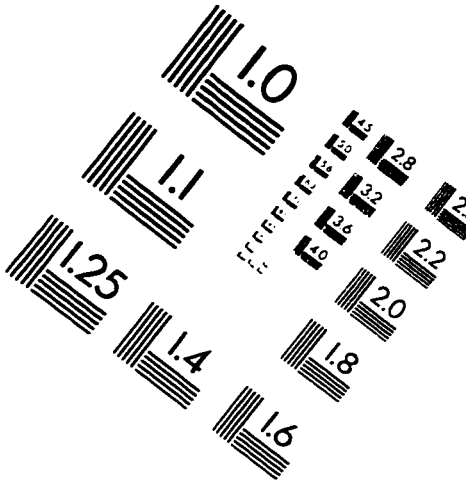

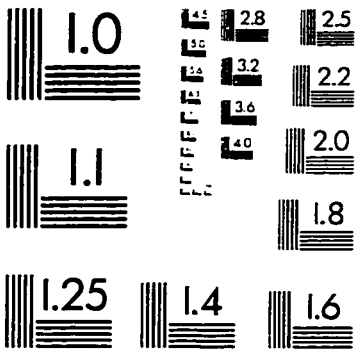

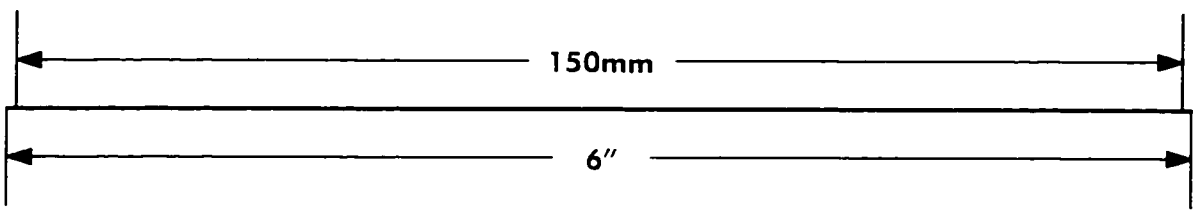

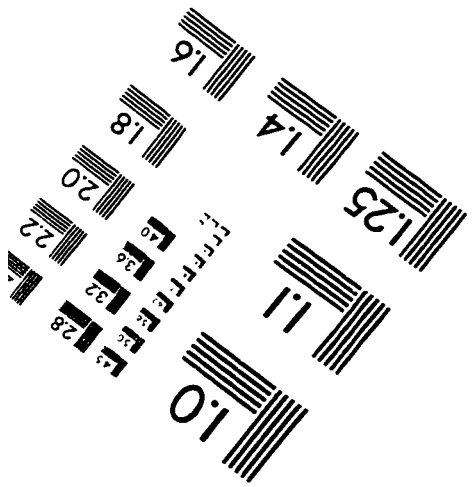

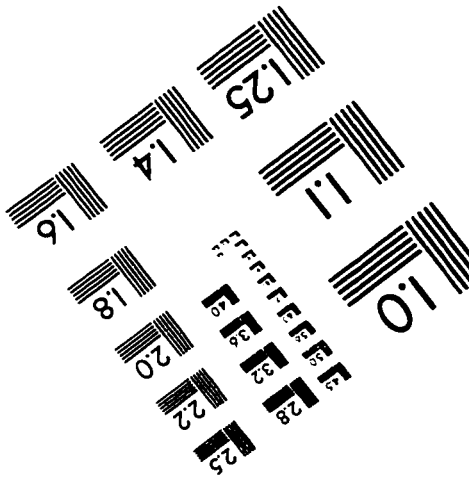

APPLIED IMAGE, Inc
1653 East Main Street
Rochester, NY 14609 USA
Phone: 716/482-0300
Fax: 716/288-5989